Experience-dependent functional plasticity of thalamocortical axons

Juliane Jäpel-Schael

München 2017

Experience-dependent functional plasticity of thalamocortical axons

Dissertation
zur Erlangung des Grades
eines Doktors der Naturwissenschaften

an der Fakultät für Biologie
der Ludwig–Maximilians–Universität

vorgelegt von
Juliane Jäpel-Schael
München, den 27.06.2017

Erstgutachter: Prof. Dr. Mark Hübener
Zweitgutachter: Prof. Dr. Laura Busse
Promotionsgesuch eingereicht am: 27.06.2017
Tag der mündlichen Prüfung: 25.09.2017

Eidesstattliche Erklärung

Ich versichere hiermit an Eides statt, dass die vorgelegte Dissertation mit dem Titel "Experience-dependent functional plasticity of thalamocortical axons" von mir selbstständig und ohne unerlaubte Hilfe angefertigt ist.

München, 27.06.2017

Juliane Jäpel-Schael

Erklärung

Hiermit erkläre ich,

dass die Dissertation **nicht** ganz oder in wesentlichen Teilen einer anderen Prüfungskommission vorgelegt worden ist.

dass ich mich anderweitig einer Doktorprüfung ohne Erfolg **nicht** unterzogen habe.

München, 27.06.2017

Juliane Jäpel-Schael

Contents

List of Figures

List of Tables

Summary

Ocular dominance (OD) plasticity, the shift in eye-specific responsiveness after chronic closure of one eye, is a widely studied model of experience-dependent plasticity. Most theories of OD plasticity assume that the synaptic changes in response to monocular deprivation (MD) are exclusively cortical. This assumption is largely based on early cross-sectional recordings from cells in the dorsal lateral geniculate nucleus (dLGN) that did not reveal prominent functional changes. Yet, none of the subcortical measurements so far have been performed chronically with single-cell resolution, leaving the possibility that subtle changes may have been overlooked.

Additionally, recent studies show that a significant fraction of dLGN cells responds robustly to stimulation of both eyes in rodents and primates, potentially providing the basis for competitive plasticity.

In this thesis, I readdress the question of subcortical experience-dependent plasticity in the dLGN by chronically following the activity of the same thalamocortical afferents in layer I of the binocular visual cortex of adult mice during OD plasticity. Additionally, I provide a general functional characterization of the visual response characteristics of thalamocortical boutons in comparison to layer II/III cells of the binocular visual cortex.

I repeatedly measured the visual responses of thalamocortical boutons in layer I of the visual binocular cortex, both before and after MD, using chronic two-photon Ca^{2+} imaging of the genetically encoded Ca^{2+} indicator GCaMP6m.

With this minimally-invasive longitudinal readout for the activity of dLGN neurons, I could indeed observe responses to both eyes in a subset of boutons, but dLGN boutons were significantly less binocular than cortical neurons.

I observed that dLGN boutons surprisingly show prominent OD plasticity after MD. Similar to the changes that we previously observed in visual cortex, a large fraction of in-

dividual boutons reduced their response to deprived eye stimulation and increased their responsiveness to open eye stimuli. However, very different from cortex, initially monocular contralateral boutons also showed the most prominent increase in ipsilateral-eye responsiveness. This effect was reversible after 1-2 weeks of binocular recovery.

In summary, eye-specific responses of dLGN neurons are not rigid, but undergo substantial functional OD plasticity and which is likely to contribute to cortical OD shifts.

Abbreviations

A	anterior area
AAV	adeno-associated virus
AL	anterolateral area
ACSF	artificial cerebrospinal fluid
AMPA	α-amino-3-hydroxy-5-methyl-4-isoxazolepropioic acid
BDNF	brain-derived neurotrophic growth factor
dLGN	dorsal lateral geniculate nucleus
DREADD	designer receptors exclusively activated by designer drugs
DSI	direction selectivity index
GABA	γ-aminobutyric acid
GAD-67	glutamic acid decarboxylase 67
GFP	green fluorescent protein
GeCI	genetically encoded calcium indicators
gDSI	global direction selectivity index
gOSI	global orientation selectivity index
LP	lateral posterior thalamic nucleus
LTP	long-term potentiation
LTD	long-term depression
MD	monocular deprivation
MI	monocularity index
NA	numerical aperture
NMDA	N-methly-D-asparate
OD	ocular dominance
ODI	ocular dominance index
OSI	orientation selectivity index
PoM	posteromedial thalamic nucleus
PV	parvalbumin
RF	receptive field

RL	rostrolateral area
RGC	retinal ganglion cells
ROI	region of interest
SC	superior colliculus
SD	standard deviation
SEM	standard error of the mean
TRC	thalamic relay cell
v/v	volume per volume
V1	primary visual cortex
VPM	ventral posteriomedial thalamic nucleus
w/v	weight per volume

1 Introduction

One of the leading questions in the field of neuroscience is how information is stored in the brain. Already in 1893, Ramón y Cajal proposed that the contact sites between neurons - the synapses - could be involved in information storage. Half a century later, Donald Hebb suggested a synaptic mechanism for memory formation, in which connections are strengthened by coincident pre- and postsynaptic firing (Hebb, 1949). In the following decades, such reorganization of neural networks by correlated and uncorrelated activity was discovered *in vitro*. These Hebbian mechanisms, known as long-term potentiation (LTP, Bliss and Lomo, 1973) and long-term depression (LTD, Dudek and Bear, 1992), are dependent on glutamatergic NMDA receptors, which act as coincidence detectors of pre- and postsynaptic activity. Next to modifications at already existing synapses, activity-dependent formation and elimination of synapses is probably also involved in strengthening and weakening of specific connections (Engert and Bonhoeffer, 1999). The activity-dependence and biochemical origins of LTP and LTD have been studied *in vitro* for decades. Yet, it is still unclear how well suited these mechanisms are for storing specific memories *in vivo*.

Sensory systems are well suited to investigate how experience changes neuronal circuits *in vivo*. Already more than fifty years ago, David Hubel and Torsten Wiesel dedicated their research to answer this question by studying experience-dependent plasticity in the mammalian visual system. Many studies have described anatomical, physiological and biochemical changes occuring in the cortex following experience-dependent plasticity (e.g. Wiesel and Hubel, 1963b; Antonini and Stryker, 1993; Gordon and Stryker, 1996; Rittenhouse et al., 1999; Sawtell et al., 2003). Much less is known about the input to the cortex, particularly about the dorsal lateral geniculate nucleus (dLGN). For a long time, the dLGN has been considered a simple relay station between the periphery and the cortex. But more and more studies suggest some further important processing in the mouse dLGN, which prompted us to re-examine some of its visual properties and its role during experience-dependent plasticity.

1.1 The visual system

1.1.1 The mouse visual system

Most of our knowledge about visual processing originates from work in carnivorans, like cats and ferrets, and primates. However, due to recent developments in genetics and imaging methods in the last two decades, mice have become a widely used model organism despite their poor visual abilities. The visual acuity of mice is relatively low with 0.5 to 0.6 cycles/degree (Gianfranceschi et al., 1999; Sinex et al., 1979) in comparison to 60 cycles/degree in humans (Campbell and Green, 1965). Similarly, the receptive fields (RFs) are larger in mice (average: 14 deg, Métin et al., 1988) in comparison to, for example, cats (1 deg, Wilson and Sherman, 1976). However, they can perform visual tasks (Prusky and Douglas, 2003) such as the popular Morris water maze (Morris, 1984) that is used to study memory function in mice.

As their eyes are more laterally positioned, mice have a reduced binocular field of 30-40 deg (Dräger, 1978; Dräger and Olsen, 1980), which corresponds to the central 30 % of the visual field. Overall, the extent of their lateral visual field is increased. Nevertheless, the main stages of visual processing show many similar features to what has been described for cats (Fig. 1.1 A).

1.1.1.1 The retina

Visible light is detected by rod- and cone photoreceptors located in the retina. As a nocturnal animal, the mouse retina is strongly dominated by rods (97 %, Carter-Dawson and LaVail, 1979). In contrast to primates, mice do not have a fovea, a region in the center of the retina with the highest density of cones. Still, the density of photoreceptors is not equal in all parts of the retina. It peaks in the *area centralis* and decreases more peripherally (Volland et al., 2015). The photoreceptors excite and inhibit, directly and indirectly, a network of several cell types (bipolar, amacrine and horizontal neurons), which pass signals to the retinal ganglion cells (RGCs).

Classically, RGCs respond either to increases (ON-center) or decreases (OFF-center) in stimulus luminescence in a small clearly localized regions of the visual space and stimuli of the opposite polarity in the region immediately surrounding these centers (cats: Kuffler, 1953; Limulus: Hartline, 1969). In the literature, this is referred to as a center-surround RF. Other RGCs selectively respond to more specialized RFs like edges or direction of movement (Barlow et al., 1964). It is estimated that there are more than 32

functional types of RGCs (Baden et al., 2016) that project to more than 50 different brain regions (Lawrence and Studholme, 2014; Martersteck et al., 2017). While some RGC types are already well defined in their structural, molecular and physiological properties, many are still incompletely characterized (see Sanes and Masland, 2014 for review).

1.1.1.2 Retinal projections

The axons of the RGCs are bundled in the optical nerve and most of the projections cross over to the contralateral hemisphere at the optic chiasm. A minority (3 - 5 %, Williams et al., 2003) project ipsilaterally and virtually all of the corresponding RGCs are located in the peripheral ventrotemporal region of the retina (Dräger and Olsen, 1980).

The major projections areas are the superior colliculus (SC) and the dorsal lateral geniculate nucleus (dLGN, see also 1.1.2). Other retinal projections are, e. g., the suprachiasmatic nucleus of the hypothalamus, the optic tract nuclei and the ventral thalamus, which are associated with circadian responses to light and the pupilary light reflex (Moore and Eichler, 1972; Pickard et al., 1987; Hattar et al., 2002).

The SC is a phylogenetically old structure, where the majority of axons from the mouse RGCs terminate (Hofbauer and Dräger, 1985). In cats and primates, it is considered to be involved in the generation of sacchades, attention and visual target selection (see Krauzlis et al., 2013 for review; Inoue et al., 2015). Recent studies in rodents showed its role in visual processing (Feinberg and Meister, 2014; Ahmadlou and Heimel, 2015). It is also considered to integrate information from several modalities (mice: Dräger and Hubel, 1975; cats: Ghose et al., 2014) and to control eye-movements involved in tracking moving stimuli (Douglas et al., 2005).

1.1.1.3 Primary visual cortex (V1)

Like most other areas of the neocortex, V1 consists of six layers. Around 70 - 80 % of the neurons are excitatory (Markram et al., 2004), while the rest are inhibitory interneurons of diverse cell types.

Layer I consists mostly of dendrites and axons, with only a few inhibitory cells. The majority of dLGN axons project to layer IV, but there is also strong input to layer I and few thalamocortical axons are also present in layer II/III and VI (Hubel and Wiesel, 1972; Lund, 1988; Cruz-Martín et al., 2014). Cells in layer IV then project mainly onto basal dendrites of cells in layer II/III, which then connect to layer V (Thomson et al., 2002) and send out other cortico-cortical projections (Gilbert and Wiesel, 1979; Gilbert and Kelly,

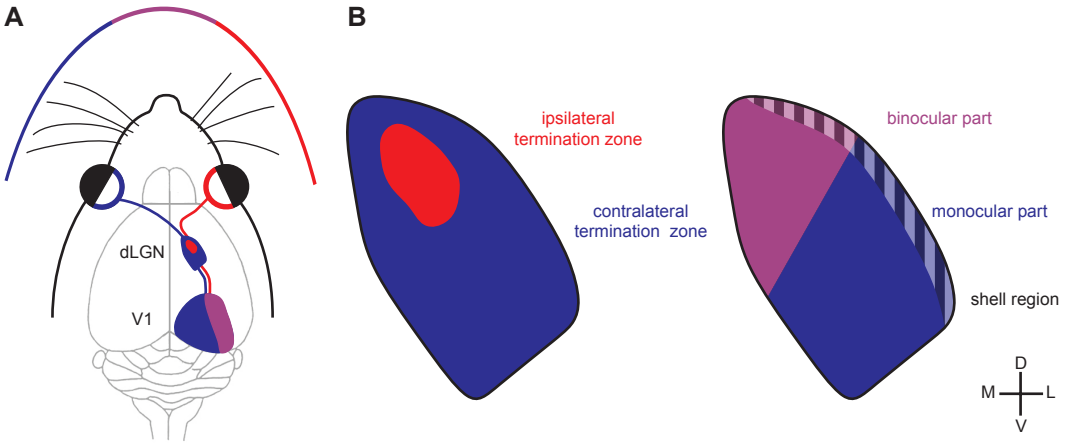

Figure 1.1: **Schematic of the mouse visual system and structure of the dLGN. A** Retinal ganglion cells (RGCs) project to the primary visual cortex (V1) via the dorsal lateral geniculate nucleus (dLGN). The majority of RGC axons (blue) cross the midline at the optic chiasm, but a small part of RGCs from the ventrotemporal retina (red) send their projections to the ipsilateral hemispere. These ipsilateral projections end in the dorsomedial part of the dLGN. V1 is subdivided into a monocular (blue) and a binocular (purple) region. While the monocular V1 processes information only from the contralateral eye, binocular V1 receives input from both eyes. **B** Left: RGC axon termination zones from contralateral (blue) and ipsilateral (red) retinas. Right: The dorsomedial tip of the dLGN (purple) receives input from the binocular visual field. The shell region is thought to be a biochemically and functionally distinguished sub region.

1975). Layer V neurons project to layer VI, subcortical regions (for example to the SC), and via the corpus callosum to the contralateral hemisphere (Swadlow, 1983; Kasper et al., 1994). Cortical feedback to the dLGN is provided by projections from cells in layer VI (Vastola, 1967; Marrocco et al., 1982; Alitto and Usrey, 2003).

In the mouse, V1 is separated into two parts: the bigger monocular region processes information only from the contralateral eye, whereas cells in the binocular regions receive input from both eyes. Although only 3-5 % of the RGCs project ipsilaterally (Williams et al., 2003), the binocular region occupies the lateral third of V1 (Dräger, 1975; Gordon and Stryker, 1996). There are two reasons for the cortical expansion of the ipsilateral input: First, there is a 1:1 numerical ratio of RGCs to thalamic relay cells (TRCs) along the ipsilateral pathway, whereas it is 3:1 along the contralateral pathway, indicating that three contralaterally projecting RGCs contact one TRC. Second, only half of the contralateral projecting RGCs terminate in the dLGN, while all ipsilateral RGCs project to the dLGN (Coleman et al., 2009).

1.1.1.4 Higher visual areas

The visual cortex projects to up to 15 higher cortical areas, from which at least nine show an orderly representation of the visual hemifield (Wang and Burkhalter, 2007) and are considered to be higher visual areas. These projections seem to be functionally target specific, meaning that the properties of the axons from V1 terminating in different areas are matching the average preferences of the recipient neurons (Glickfeld et al., 2013).

While the precise visual feature selectivity of the different higher areas is still unknown, it seems that each area prefers different combinations of spatio-temporal features (Andermann et al., 2011; Marshel et al., 2011).

1.1.2 Dorsal lateral geniculate nucleus (dLGN)

The dLGN is a nucleus of the thalamus that is located at its posterior-lateral end. It is classically considered to be a relay station, where visual information from the retina is passed on to the cortex. However, recent studies are changing this view.

1.1.2.1 Cell types

Two main categories of neurons are present in the mouse dLGN (Rafols and Valverde, 1973): excitatory thalamic relay cells (TRCs) and inhibitory neurons. The latter comprises 15-20 % of the neural population (Arcelli et al., 1997). Based on anatomical and physiological properties such as cell size and RF properties, TRCs can be further distinguished into different cell types in many species.

In the monkey, TRCs are distinguished into M, P and K cells that are comparable to Y, X and W cells of the cat, which have been defined based on both electrophysiological and morphological characteristica (Friedlander et al., 1981). X cells have a smaller cell body and a dendritic tree that is oriented perpendicular to the border of the layer and stays within a single layer. In contrast, the dendritic tree of a Y cell is wider with peripheral dendrites crossing layers. Functionally, the RFs of X cells are smaller and inputs summate more linearly. The two types also vary in their spatiotemporal properties. W cells show poor spatial and temporal resolution, contrast sensitivity and many lack a center/surround RF organization. They are localized to a specific layer in the dLGN (Sherman and Spear, 1982; Friedlander et al., 1981).

In the mouse, TRCs appear to be functionally very homogeneous and resemble X cells (Grubb and Thompson, 2003), whereas morphologically there is some evidence of X-, Y-

and W-like cells (Krahe et al., 2011).

1.1.2.2 Structure

In most mammals, the dLGN is comprised of different layers, but the individual number of layers and distinct functional types of retinal projections to these layer vary between species. But characteristically, each layer gets input only from one eye (Tigges and Tigges, 1970; Jeffries et al., 2014). In the monkey, the dLGN is comprised of six layers. P and M cells are restricted to parvo- or magnocellular layers, respectively, while K cells are present ventrally in between magnocellular and parvocellular layers. Their dendrites overlap with those of M and P cells. In the cat, W cells project exclusively to laminae C1 and C2, while X and Y cells are intermingled in laminae A and A1 and Y cells are also found in lamina C (Sherman and Spear, 1982).

In the mouse, by contrast, no discrete cellular layers can be distinguished (Rafols and Valverde, 1973). However, the dLGN can be biochemically divided into two subregions, the core and the dorsolaterally located shell (Grubb and Thompson, 2004), which seems to coincide with a direction-selective RGC type with known molecular identity (Kim et al., 2010; Huberman et al., 2009). Additionally, the collicular projection is strongest in the shell, but not completely restricted to it (Grubb and Thompson, 2004; Bickford et al., 2015).

Furthermore, based on the RGC termination zones, the dLGN can be divided into eye-specific domains. The ipsilateral projection from the RGCs terminate in the dorsomedial region of the nucleus, which is considered the binocular part of the dLGN that is projecting to the binocular visual cortex (Coleman et al., 2009, see Fig. 1.1 B), suggesting a “hidden lamination” (Reese, 1988). Different cell types seem to show regional preferences: X-like cell are typically located within the monocular part, whereas Y-like cells preferably reside in the binocular part. Furthermore, W-like cells show a preference for the shell region (Krahe et al., 2011).

1.1.2.3 Retinogeniculate input

There are two categories of thalamic afferents: drivers and modulators (Sherman and Guillery, 1998, Bickford et al., 2015). The retinogeniculate afferents serve as the drivers as they determine the qualitative receptive field properties of the TRCs. Although it comprises only roughly 7 % of all the input to the dLGN (Sherman and Guillery, 1998), mouse TRCs resemble their RGC inputs extremely closely (Grubb and Thompson, 2003). This input is most often organized in triade synapses: a single RGC monosynaptically contacts

both a TRC and a local inhibitory neuron, which in return contacts the same TRC (Rafols and Valverde, 1973), although other RGC axons terminals also form simple contacts onto dendrites of TRCs. It is speculated that this organization is important for contrast gain control (Sherman, 2004).

The dLGN gets input from at least two different classes of RGC cells: direction selective RGCs (possibly comprising 8 different types, Baden et al., 2016) and non-direction selective RGCs (Dhande and Huberman, 2014). Two recent connectomics studies show that individual TRCs are innervated by many RGCs and revealed a complex network that does not show a structural division of RGCs and TRCs into distinct pathways (Morgan et al., 2016; Hammer et al., 2015). Additionally, Rompani et al., 2017 performed a transsynaptic tracing study, in which tracing is initiated from a single TRC in the binocular part of the dLGN. The number of presynaptic RGCs ranges from 1 to 91, but overall three distinct types of RGC integration modes are present: 1. Relay mode: a TRC receiving input from one or two closely-related RGC types, 2. Combinational mode: a TRC integrating input from a variety of different RGC types and 3. Binocular mode: a TRC receiving input from both retinas.

1.1.2.4 Development of retinogeniculate axons

Directly after birth, projections from the ipsilateral and the contralateral eye partly share a termination zone. Only afterwards, they start segregating into eye-specific domains (Linden et al., 1981; Shatz, 1983). In mice, projections from the contralateral eye first start innervating the dLGN at embryonic day 16 followed by ipsilateral axons five days later at birth. At the age of one week, eye segregation begins and is finished by the time of eye-opening (Godement et al., 1984; Jaubert-Miazza et al., 2005). However, there is a continuation of growing and elaborating of axonal arbours in the correct dLGN termination zones (Sretavan and Shatz, 1986; Sur et al., 1984; Dhande et al., 2011).

These structural changes are accompanied and followed by functional changes: In the first postnatal week, the fraction of binocular cells is very high (roughly 50 %), whereas after the second postnatal week no binocular responses were observed in the dLGN (Jaubert-Miazza et al., 2005; Ziburkus and Guido, 2006). Additionally, there is a decrease in RGC input convergence onto single dLGN cells during this period: from more than ten inputs from either eye to one to three inputs from only one eye (Chen and Regehr, 2000; Ziburkus and Guido, 2006). Simultaneously, AMPA receptor currents increase, suggesting an unsilencing of synapses through insertion of AMPA receptors (Chen and Regehr, 2000). Furthermore, remaining inputs are strengthened (Chen and Regehr, 2000) and

tend to cluster (Hong et al., 2014). After the critical period, the total number of boutons is decreasing and axons are refined (Hong et al., 2014).

Both, molecular and activity-dependent mechanisms are important for eye-specific segregation (Huberman et al., 2005; Pfeiffenberger et al., 2005; Penn et al., 1998). Whereas before eye-opening spontaneous retinal activity in the form of retinal waves (Meister et al., 1991; Mooney et al., 1996) is important for synapse remodeling, visual experience is driving synaptic strengthening and pruning afterwards (Hooks and Chen, 2006).

1.1.2.5 Non-retinal input

The majority of thalamic afferents belong to the second class of inputs - the modulators. They affect response properties like overall firing rate and size and strength of the receptive field. This modulating input to the dLGN is provided by layer VI of the visual cortex, the thalamic reticular nucleus (McCormick and Bal, 1997; Alitto and Usrey, 2003), and the brainstem (Erisir et al., 1997b; Erisir et al., 1997a).

Of all those modulatory inputs, the corticothalamic feedback is the most studied. Feedback from layer VI is retinotopically organized and it seem to influence spatial properties of dLGN cell receptive fields as well as dLGN firing patterns (reviewed in Alitto and Usrey, 2003 and Sillito et al., 2006). Further theories involve an enhancement of specific features by egocentric selection: e.g. enhancement of orientation selectivity by recurrent activation of the dLGN and a limited region of the cortex that is selective for this orientation. There is evidence both for and against these theories (e.g. Sillito et al., 1994; Brody, 1998).

It has been long known in several species that the SC projects to the dLGN (Harting et al., 1991). In mice, these projections are mostly confined to the dorsolateral shell (see Fig. 1.1 B, Grubb and Thompson, 2004). There is some evidence that these projections preferentially target W-like cells and coincide with input from direction-selective RGCs (Huberman et al., 2009; Cruz-Martín et al., 2014) to not only modulate but actually drive those cells (Bickford et al., 2015).

1.1.2.6 Modulation of response properties

Most of the input to the dLGN modulates its response properties (e.g. Sherman and Guillery, 1996; Guillery and Sherman, 2002). One way to modulate the response properties is to change the firing mode of TRCs. Typically, two firing modes exist, burst and tonic, which are controlled by a T-type calcium channel. Usually, at membrane potentials

around > 60 mV, this channel is inactivated and depolarizing inputs produce tonic action potentials. However, after hyperpolarization for more than 100 ms, the channel changes to a state, where it can be activated. Depolarizing inputs are then prolonged by the additional influx of calcium ions and produce a depolarizing waveform, the low-threshold calcium spike (Jahnsen and Llinas, 1984).

Not only is the switch between these firing modes important for the transition between sleep and wakefuleness (Livingstone and Hubel, 1981; Weyand et al., 2001), but the two firing modes might also carry specific types of visual information. While they encode very similar spatial information, they are significantly different in their temporal characteristics. For example, bursting is more phase advanced and is associated with better stimulus detection (Grubb and Thompson, 2005).

While an earlier study did not find an effect on locomotion on response properties of dLGN neurons (Niell and Stryker, 2010), two recent studies showed that locomotion transiently increased responses, both during spontaneous and visually-driven activity (Erisken et al., 2014; Roth et al., 2016). Whether this is due to corticothalamic feedback, neuromodulatory influences or input from other subcortical pathways is debated (see also 1.1.2.5).

1.1.3 Characteristic visual properties

1.1.3.1 Binocularity

In primates and cats, dLGN projections from the two eyes are segregated into eye-specific patches or stripes in layer IV in V1, which form the anatomical basis for the ocular dominance columns (Wiesel et al., 1974; Shatz et al., 1977). In monkeys, binocular processing starts with the convergence of layer IV inputs onto layer II/III neurons (Wiesel, 1968), while feline layer IV neurons are already binocular (Shatz and Stryker, 1978). In mice, this columnar organization is absent (Gordon and Stryker, 1996; Mrsic-Flogel et al., 2007) and thalamic inputs from different eyes converge onto layer IV neurons (Métin et al., 1988). In the binocular region of V1, about one third of cells can be driven by both eyes (Dräger, 1975). Cells in the monocular zone respond only to stimulation of the contralateral eye.

There is considerable debate about binocularity in individual TRCs in adult mice (see 1.1.2.4 for binocularity during development). Earlier studies assessing ocularity *ex vivo* using slice electrophysiology exclusively find monocularly driven cells beyond postnatal day 18 (Grubb et al., 2003; Ziburkus and Guido, 2006; Zhao et al., 2013). However,

in vivo studies in rodents (Grieve, 2005; Howarth et al., 2014) and also in marmosets (Zeater et al., 2015) demonstrate that some cells in the dLGN react to visual stimulation of both eyes. This is supported by the transsynaptic tracing study of (Rompani et al., 2017), in which a single TRC receives input from both retinas.

In mice, these binocular cells are found in the zone of binocular retinotopic convergence (compare 1.1.2.2). Interestingly, in this area Howarth et al., 2014 do not observe cells responding exclusively to stimulation of one eye. Similarly, TRCs integrate input either from only the contralateral retina or from both eyes (Rompani et al., 2017). In marmosets, these binocular cells reside in the koniocellular layers (43 % of cells, Zeater et al., 2015), which have been shown to convey short wavelength-sensitive (S or "blue") cone information.

There are several possible sources of binocularity: 1. Retinogeniculate convergence: TRCs receiving direct input from RGCs from both retinas. 2. Corticothalamic feedback: Binocularity is inherited from the cortex via feedback connections from layer VI. 3. Colliculothalamic feedback: In cats and monkeys, a high percentage of cells in the SC are binocular (Sherk, 1979; Tailby et al., 2012) and the SC is projecting exclusively to the koniocellular layer (Harting et al., 1991; Casagrande, 1994), hence binocular cells in the koniocellular layer could inherit binocularity from projection from the SC. In mice, inputs from the SC to the shell region of mouse dLGN are also know to drive responses in TRCs (Bickford et al., 2015). However, SC neurons in the mouse appear to be mostly monocular (Dräger and Hubel, 1975). 4. Parabigeminal feedback: Neurons in the parabigeminal nucleus are mostly binocular in cats (Sherk, 1979) and also project to the dLGN (Harting et al., 1991). However, to my knowledge, it is not known whether these neurons are also binocular in mice. In summary, binocularity could arise from different sources and this might also vary between species.

1.1.3.2 Retinotopic organization

One central feature of the visual system that is conserved across all mammalian species is its retinotopic organization. In the retina, cells selectively respond to a restricted region within the visual field and neighbouring cells can be activated or inhibited by visual stimulation in neighbouring regions of the visual field. This feature is largely maintained throughout the visual system due to the spatial organization of the feed-forward and feed-back inputs (Dräger, 1975; Hubel and Wiesel, 1959; Wiesel, 1968; Wiesenfeld and Kornel, 1975; Wang and Burkhalter, 2007).

In V1, for example, an image presented to a mouse is approximately maintained on the cortical surface, but upside down. Therefore, stimuli in the upper visual field are represented caudally, whereas stimuli in the lower visual field are represented more rostral. The lateral part of V1 respond to visual stimuli in the nasal visual field, while the medial part of V1 is activated by visual stimuli in the temporal visual field (Grinvald et al., 1986; Schuett et al., 2002).

Similarly, the mouse dLGN is also organized retinotopically. The ventronasal visual field is represented in the caudal region, while rostrolateral cells respond to stimuli in the temporal visual field (Wagner et al., 2000; Piscopo et al., 2013). The binocular visual field is represented in the dorsomedial tip (compare Fig. 1.1 B), occupying approximately a third of the dLGN. Within it, the ipsilateral termination zone represents 9 - 12 % of the entire dLGN (border of the binocular segment at the edge of the ipsilateral termination zone) and roughly 28 % of the binocular segment (Coleman et al., 2009).

Importantly, in the binocular dLGN the ratio of contralateral to ipsilateral cells changes from 6-8:1 on the level of RGCs projecting to the dLGN to 2:1 on the level of individual TRCs projecting to binocular V1 (Dräger and Olsen, 1980; Coleman et al., 2009). This has two reasons: First, several contralateral RGCs converge onto one single TRC. Second, though a minority, nearly all RGCs from the ipsilateral eye (3 - 5 %) project to the dLGN (Coleman et al., 2009). In contrast, from the 95 - 97 % of RGCs projecting contralaterally, only half terminate in the dLGN.

1.1.3.3 Orientation and direction tuning

In 1959, Hubel and Wiesel first described neurons in cat V1 that are best driven by bars of a particular orientation (Hubel and Wiesel, 1959). They also noted that neighbouring cells often prefer the same orientation (Hubel and Wiesel, 1962). It has been shown that neurons with a similar orientation preference cluster together and form orientation columns throughout all cortical layers. These are organized around singularities such as pinwheel centers where neurons of all orientation-preferences can be found (Swindale et al., 1987; Bonhoeffer and Grinvald, 1991). The mouse visual cortex does not show this organization (Ohki et al., 2005; Mrsic-Flogel et al., 2005), although individual neurons show orientation selectivity (Dräger, 1975) and the tuning curves closely resemble those observed in other species (Métin et al., 1988; Niell and Stryker, 2008). A substantial fraction of neurons in the visual cortex is also selective for a specific direction (Mangini and Pearlman, 1980; Métin et al., 1988).

Classically, orientation selectivity is considered to be a feature computed in the cortex at the first stage of thalamocortical interaction. Hubel and Wiesel hypothesized that orientation tuning is computed from untuned thalamocortical inputs with aligned receptive fields (Hubel and Wiesel, 1962). The receptive fields of thalamocortical cells resemble those of RGCs with an excitatory ON-center and inhibitory OFF-periphery or the other way around (Hubel and Wiesel, 1961). However, several recent studies have found a subpopulation with more selective properties including direction and orientation selectivity in the shell region of the dLGN (Marshel et al., 2012; Piscopo et al., 2013), which is supported by direction- and orientation-selective thalamocortical axons in layer I of the visual cortex (Cruz-Martín et al., 2014; Roth et al., 2016). The degree of orientation and direction selectivity in thalamocortical axons projection to layer IV of the visual cortex is still under debate (Kondo and Ohki, 2016; Sun et al., 2016a; Roth et al., 2016).

1.1.3.4 RF properties

So far, only few studies have performed a dedicated characterization of RF properties of dLGN neurons. In 2003, Grubb and Thompson applied a white-noise mapping procedure and found no evidence for different functional cells classes. All cells show classical center-surround RF structure with an average diameter of 11 deg. Most cells prefer a spatial frequency of 0.03 cycles/degree and a temporal frequency of 4 Hz (Grubb and Thompson, 2003).

In contrast, a more comprehensive study using multi-site extracellular recordings and a broad set of visual stimuli shows that a substantial fraction of dLGN cells also encodes other properties like orientation selectivity and a suppression by contrast (Piscopo et al., 2013). Furthermore, there is activity related to perceptual decisions in monkey dLGN (Jiang et al., 2015) and projections from mouse dLGN convey information about running speed and saccades (Roth et al., 2016). Taken together, it slowly becomes clear that the concept of the dLGN being merely a relay station is too simplified as it is functionally more sophisticated than previously suspected. However, so far, it is unclear whether this reflects local visual processing or is a result of the complex relationship between thalamus and cortex (see also 1.1.2.5).

1.2 Experience-dependent plasticity

Experience-dependent plasticity is the continuous reorganization and adaptation of neural networks in responses to changes in the environment. One of the most frequently employed chronic modifications of sensory experience is the temporary closure of one eye, known as monocular deprivation (MD).

1.2.1 Monocular deprivation

In 1963, Hubel and Wiesel demonstrated for the first time that binocular responses in the primary visual cortex are susceptible to changes in the visual input. In the classic view, the inputs from the two eyes first converge onto single neurons in the binocular visual cortex. Each neuron can be classified based on the relative responsiveness to contra- and ipsilateral stimuli. Based on that, an ocular dominance index (ODI) can be calculated. Normally, the distribution of the ODI shows a bias for the contralateral eye. However, in kittens, MD of the dominant contralateral eye lead to a shift in this distributions towards the open, ipsilateral eye (Wiesel and Hubel, 1963b). This shift in ocular dominance (OD) was later also found in other mammalian systems such as primates (Hubel et al., 1977, LeVay et al., 1980) and in mice (Dräger, 1978).

1.2.2 Critical-period OD plasticity

Strong OD shifts are most prominent during a critical period in the development. In mice, the critical periods peaks around 3-5 weeks after birth (Gordon and Stryker, 1996). Further characterization of the deprivation-induced shift in OD revealed a maximal functional effect on the eye-specific responsiveness of MD already after four days of eye closure, both in mice (Gordon and Stryker, 1996) and cats (Hubel and Wiesel, 1970). In carnivorans and primates, OD plasticity is limited to the critical period (Hubel and Wiesel, 1970), but in mice OD shifts also occur in adult animals. However, the effect is less strong (Sato and Stryker, 2008) and the mechanisms differ to some extent from critical-period OD plasticity (Ranson et al., 2012, see also 1.2.5). In cats, normal visual experience in adulthood is not able to correct the OD shift induced by prolonged MD during the critical period, leading to non-correctable amblyopia (Hubel and Wiesel, 1970).

The opening of the critical period is dependent on the maturation of GABAergic inhibitory circuits (Hensch et al., 1998) and can be influenced externally. For example, enhancing inhibitory transmission pharmacologically accelerates the onset of the critical period (Fagiolini and Hensch, 2000). Similarly, transgenic overexpression of brain-derived neu-

rotrophic factor (BDNF) promotes the maturation of GABAergic neurons (Huang et al., 1999). In contrast, dark rearing of animals from birth on delays the beginning of the critical period (Mower, 1991) by delaying GABAergic maturation in a BDNF-dependent manner (Gianfranceschi et al., 2003). Specifically, fast-spiking neurons expressing parvalbumin (PV) are important for this process (Fagiolini et al., 2004) and a recent study suggests that specific clock genes are underlying PV circuit maturation (Kobayashi et al., 2015). Several molecules, especially Nogo Receptor 1, Neuregulin-1 and EphB4 seem to be important for PV cell disinhibition (see 1.2.4) and the opening and closing of the critical period (Baohan et al., 2016; Gu et al., 2016; Sun et al., 2016b; Stephany et al., 2016).

1.2.3 Mechanism of OD plasticity

One of the first theories for the shift in responsiveness suggest binocular competition for resources, such as neurotrophic factors (Wiesel and Hubel, 1965; Domenici et al., 1991; Bonhoeffer, 1996). This theory is based on the observation that after binocular deprivation most of the cells are still responsive in the visual cortex. Thus the change in OD is not just a reflection of disuse, but depends on the interactions between the contralateral and the ipsilateral pathway (Wiesel and Hubel, 1965). However, contralateral responses are also reduced in monocular V1, in which no competition occurs (Heynen et al., 2003). Additionally, the shift in OD is composed of two components, the weakening of the closed contralateral eye responses and the strengthening of open eye responses with different contribution of the two mechanism in juvenile and adult OD plasticity (Frenkel and Bear, 2004). A decrease in the deprived eye occurs already 6 h after temporary closure of the contralateral eye with an eye patch (Mioche and Singer, 1989).

The weakening of the deprived eye is not a consequence of a complete loss of retinal responses (Rittenhouse et al., 1999). It is rather thought to be caused by residual retinal activity in response to low contrast and low amplitude images through the closed eyelid. The dampened retinal activity leads to uncorrelated and therefore non-summating weak input to cortical neurons (Bear et al., 1986), which is thought to induce NMDA receptor-dependent LTD in the visual cortex (Heynen et al., 2003; Sawtell et al., 2003).

It is however less clear, whether open-eye strengthening is also due to Hebbian mechanism (in this case LTP) or rather homeostatic plasticity. The Bienenstock-Cooper-Munro (BCM) model proposes a flexible threshold (Bienenstock et al., 1982), that determines the strength and the direction of plasticity at synapses on the basis of the overall strength. As the overall activity level goes down due to contralateral depression, the threshold

for potentiation is also lowered. As a consequence, LTP is promoted in weaker inputs from the open-eye. In contrast to this specific potentiation, homeostatic plasticity leads to global increase of all inputs (ipsilateral and contralateral) to compensate for the decrease in activity in the visual cortex (Smith et al., 2009; Espinosa and Stryker, 2012). There is growing evidence for homeostatic plasticity as deprived-eye responses increase in cells with little or no ipsilateral input (Mrsic-Flogel et al., 2007) and knock-out of a molecule involved in homeostatic plasticity prevented open-eye strengthening (Kaneko et al., 2008; Ranson et al., 2012). However, it seemes that LTP is also important for open-eye strengthening (Cho et al., 2009).

Importantly, the mechanisms differ between juvenile and adult OD plasticity (see 1.2.5).

1.2.4 Role of inhibition in OD plasticity

The role of inhibition in OD plasticity and whether changes in inhibition have instructive or permissive effects during OD plasticity remain unclear. Specifically, during MD, enhancd intracortical inhibition of deprived-eye inputs could lead to a decrease in excitatory visual responses evoked by the deprived-eye.

On the one hand, several studies support a permissive rather than an instructive role of inhibition. Kuhlman et al., 2013 show that after only one day of MD, the excitatory drive from layer IV and upper layer V onto PV cells is generally reduced, leading to decreased firing rates of PV cells in response to both open-eye and deprived eye stimulation. Consequently, firing rates of excitatory layer II/III cells increase for both eyes to roughly the same levels of binocular stimulation in normal mice. This increased activity is thought to be permissive for Hebbian changes (see 1.2.3). Two further days of MD then lead to normal PV responses to open-eye stimulation, while deprived-eye responses continue to be decreased. A similar early disinhibition has been observed in freely behaving rats: Hengen et al., 2013 show generally decreased firing rates in putative PV fast-spiking basket cells after one day of MD. Additionally, Saiepour et al., 2015 have found an effect of disinhibition on the absolute change in ODI in individual neurons after 7 days of MD. Briefly, they specifically express Arch-GFP in PV cells and observe that there is an increase in absolute ODI change after MD. The mean ODI, however, does not change, indicating that inhibition rather causes an increase in noise due to disruption of excitation-inhibition matching after MD than being instructive for OD plasticity.

On the other hand, a study using *in vivo* intracellular recordings in mouse binocular cortex shows fast-spiking interneurons shifting towards the closed, contralateral eye after three

days of MD followed by a shift towards the open eye after two weeks of MD (Yazaki-Sugiyama et al., 2009). The authors suggest an instructive effect of these counter-shifters on excitatory OD changes.

1.2.5 Adult OD plasticity

Contrary to carnivorans and primates, OD plasticity can be induced in adult mice (Sawtell et al., 2003; Tagawa et al., 2005), although only after longer deprivation periods of about a week (Sato and Stryker, 2008; Hofer et al., 2006). Importantly, in contrast to juvenile OD plasticity, open-eye strengthening is the major mechanism of OD plasticity in adults (Sawtell et al., 2003; Sato and Stryker, 2008), which might be accompanied by closed-eye depression (Tagawa et al., 2005; Frenkel et al., 2006). In addition, open-eye strengthening seems to depend on α-calcium/calmodulin-dependent protein kinase II (αCaMKII), indicating LTP as an underlying mechanism (Ranson et al., 2012).

The effect of adult OD plasticity decreases with age (Lehmann and Löwel, 2008), but environmental enrichment with bigger social groups (Greifzu et al., 2014) and prolonged visual stimulation during MD (Matthies et al., 2013) extends this phase in aged mice. It has been suggested that the effect of the environmental enrichment is due to a decrease in intracortical inhibition (Greifzu et al., 2014; Fu et al., 2015). Interestingly, one day of reduced PV firing is sufficient to restore juvenile-like OD plasticity (Kuhlman et al., 2013). Other interventions such as brief dark exposure (He, 2006; Stodieck et al., 2014), repeated MD (Hofer et al., 2006), activation of Rho GTPases (Cerri et al., 2011) or transplantation of inhibitory neurons (Southwell et al., 2010; Davis et al., 2015) also lead to prolonged OD plasticity or the opening of a new critical period.

1.2.6 Subcellular changes in the visual cortex

Functional OD plasticity during the critical period is accompanied by structural changes in V1. After two days of MD, the motility of spines in layer II/III is increased (Oray et al., 2004) and after four days of MD a significant spine loss on apical dendrites of layer II/III neurons is observable, which is specific to the binocular part of V1 (Mataga et al., 2004). In adult mice, four days of MD does not induce spine loss (Mataga et al., 2004), but eight days of MD lead to an increase in spine gain of layer V (but not layer II/III) neurons in binocular cortex (Hofer et al., 2009). Interestingly, a second MD induced the growth of spines gained during the first MD instead of adding new spines. It has been speculated that initially formed new synapses serve as a structural memory trace, thus rendering

it easier to adapt to a second period of MD (Hofer et al., 2006; Hofer and Bonhoeffer, 2010).

1.2.7 Retina and retinogeniculate axons

After MD, RGCs show no physiological changes and size and density are also normal (Wiesel and Hubel, 1963a; Sherman and Stone, 1973; Kratz et al., 1979). Retinogeniculate axons on the other hand, show cell-type-specific changes: In cats, that are deprived from the first postnatal week until at least 8 month of age, Y-cell axons from the deprived eyes have reduced or absent axonal arbors in lamina A. In contrast, X-cell axons have unusually broad dendritic trees in both lamina A and A1 (Sur et al., 1982).

Recently, Etxeberria et al., 2016 measured how monocular deprivation modulates the myelination of the optic nerve. They observe that long-term juvenile MD increases oligodendrogenesis and reduced the internode length in deprived optical nerves. This results in a reduced conduction velocity of the contralateral retinogeniculate axons, perhaps serving as possible mechanism for deprived-eye depression.

Even though there is some evidence for retinogeniculate plasticity, its effect on OD plasticity is mostly overlooked.

1.2.8 dLGN and thalamocortical axons

1.2.8.1 Anatomical changes in cats

Parallel to their study in the primary visual cortex, Hubel and Wiesel also examine the effect of prolonged MD on neurons in the dLGN. When the contralateral eye of the kitten is closed right before eye-opening and at the age of three months, they observe strong atrophy in all deprived layers (Wiesel and Hubel, 1963a).

Many studies have confirmed that overall the cell area is approximately 40 % smaller in deprived layers (Guillery and Stelzner, 1970; Chow and Stewart, 1972; Hickey et al., 1977). Specifically, it seems that mostly large Y cells are effected (LeVay and Ferster, 1977; Garey and Blakemore, 1977) and that the effect is strongest in the part of the dLGN that projects to the binocular primary visual cortex (Guillery and Stelzner, 1970, Sherman et al., 1972). It increases with prolonged MD duration (Hickey et al., 1977; Kalil, 1980). Significant differences in the size of cells is observed after only four weeks of MD (Kalil, 1980). Reverse suture only seems to reverse the effect if it is applied still during the critical period (Garey and Dürsteler, 1975; Hoffman and Holländer, 1978).

1.2.8.2 Physiological changes in cats

Regardless of cellular atrophy, Hubel and Wiesel show that the response properties of most dLGN neurons were normal. Although they also found four cells in the dorsal A layer with highly increased RF size and an overall activity that is lower in visually deprived layers then in normal ones, they conclude that "...the geniculate physiology was relatively normal" (Wiesel and Hubel, 1963a).

Further studies also revealed only minor cell-type specific changes in comparison to the fast and strong changes in V1. In one study, half of the units that are recorded from in the deprived eye layers have significantly lower firing rates after at least six months of MD (Hamasaki et al., 1972) and another study shows longer latencies after at least eight weeks of MD (Mangel et al., 1983). Further studies applying long-term MD show reduced peak responses (Derrington and Hawken, 1981) and abnormal cells with weak, inconsistent or no responses and non-linear spatial summation (Friedlander et al., 1982). Spatial and temporal resolution is normal for all Y-cells, but the spatial resolution is reduced in X-cells in the deprived layers due to a specific reduction in responsiveness to higher spatial frequencies (Maffei and Fiorentini, 1976; Lehmkuhle et al., 1980; Mangel et al., 1983). There seem to be no effect on W-cells and cells projecting to layer C (Spear et al., 1989). Two studies measuring evoked potentials show depression in the deprived layers (Mitzdorf and Neumann, 1980; Jones and Berkley, 1983). A comparative study with different duration of MD in different mice observed a decrease in the percentage of recordable Y-cells only after 12 weeks of MD and a decrease in the spatial resolution of X-cells after 24 weeks (Mangel et al., 1983).

1.2.8.3 Structural and functional effect of MD on mouse dLGN

To date, only few studies have looked at the effect of MD on the mouse dLGN. But also here the onset of apoptosis can be observed after two days of MD (Nucci et al., 2000). Extracellular recordings from the dLGN 30 min into monocular deprivation surprisingly reveal no change in the overall firing rate, but rather a decorrelation of simultaneously recorded neurons, showing that the TRCs are not the direct reflection of retinal input (Linden et al., 2009). An *in vitro* study shows an increase in the frequency and amplitude of miniature EPSCs in the deprived part of the dLGN, indicating homeostatic plasticity. This seems to be due to enhanced corticothalamic feedback (Krahe et al., 2011).

1.2.8.4 Structural and functional plasticity at the thalamocortical synapse

In the cat, OD plasticity is accompanied by presynaptic structural changes in thalamocortical axons as becomes evident from a substantial loss of thalamocortical synapses from the deprived eye with a reduction of the total axonal arbor length and the number of branch points after one week of MD (Shatz and Stryker, 1978; Tieman, 1984; Antonini and Stryker, 1993). A prolonged MD for several weeks also induced an expansion of thalamocortical axons from non-deprived eye (Antonini and Stryker, 1996). Similar effects were observed for mice following several weeks of MD (Antonini et al., 1999).

Yet, these macroscopic structural changes as well as cellular atrophy in dLGN occur long after the physiological change in neuronal response properties has already been established. However, a quantitative immuno-electron microscopy study suggest that after 3 days of MD thalamocortical synapse density and size are reduced (Coleman et al., 2010). Additionally, it has been demonstrated that even though large-scale structural rearrangements appear late, the early-onset physiological change after short MD is still largely dependent on a quick modification of the strength of thalamocortical synapses (Khibnik et al., 2010).

1.3 Technical advances and impact of study

1.3.1 Benefits of two-photon calcium imaging

1.3.1.1 Two-photon microscopy

In the last two decades, two-photon imaging has become one of the leading techniques in neuroscience. It enables to examine the function of individual neurons with high precision. It is based on the idea of two-photon absorption: Two photons with approximately half the energy necessary for one-photon excitation collide with a fluorescent molecule, which brings this molecule to a higher energy level. Once the molecule returns to its lower energy state, the additional energy is released in the form of a photon.

Normally, the probability of two-photon excitation is extremely low. Two-photon imaging (Denk et al., 1990) utilizes pulsed infrared lasers to generate the high photon density required for two-photon absorption. The focused laser beam excites only a very small volume at a time, which drastically reduces the out-of focus excitation providing optical sectioning capabilities.

This has several benefits: Practically all emitted photons are derived from the focal point and could ideally be detected as signal, phototoxicity and bleaching outside of the focal point is strongly decreased and the infrared lights enables high tissue penetration allowing deep-brain imaging (Helmchen and Denk, 2005).

1.3.1.2 Calcium imaging

Two-photon imaging is especially powerful when combined with calcium indicators to measure neuronal activity (Yuste and Denk, 1995; Svoboda et al., 1997; Stosiek et al., 2003). Most calcium indicators are based on a single fluorescent molecule that can bind or trap at least one calcium ion, which is connected to a change of likelihood of fluorescence excitation or changes in the emission spectrum. As neuronal firing is tightly coupled to calcium influx and therefore to an increase in the intracellular calcium concentration, the fluorescence intensity is changed according to the firing of this neuron. Typically, two kinds of calcium indicators are distinguished: The first category are synthetic indicators, which show fast calcium-binding kinetics and rather linear fluorescence changes in response to neuronal activity. However, they label tissue indiscriminately. Additional, practical limitation of the indicator loading are its short half-life (Stosiek et al., 2003) and invasiveness shortly before imaging. The second category are genetically encoded calcium indicators (GeCIs, see Rose et al., 2014 for review). Their binding kinetics

are generally slower and less sensitive than those of synthetic indicators and the fluorescence changes are often non-linear, but the indicator can be expressed over long periods of time. This allows identification and re-finding of individual neurons over the course of many days, weeks or months to observe longitudinally changes in neuronal activity (Mank et al., 2008; Tian et al., 2009; Andermann et al., 2010). Additionally, GeCIs allow for exclusive labelling of specific cell types.

1.3.1.3 Methodological advantages

Techniques like intrinsic optical imaging enable studying functional changes on the population level. However, such population recording techniques often lack single-cell resolution. On contrast, while electrophysiology directly records action potential activity from single units with high temporal resolution, two-photon calcium imaging offers several advantages. Generally, it reveals information about the morphology of neurons and their anatomical organization and allows for an unbiased sampling of large neuronal populations with single-cell or even subcellular spatial resolution. In contrast, extracellular recordings are biased toward very active neurons that also stay active throughout the experiment. Hence silent neurons that become responsive can be missed and neurons losing responsiveness could be attributed to technical difficulties. Specifically in this study, two-photon calcium imaging enabled me to chronically follow the activity of subcellular structures over a period of up to four weeks.

1.3.2 Aims of the study

Most theories of OD plasticity assume a cortical locus of plasticity and early recordings from cells in dLGN have supported this notion (Wiesel and Hubel, 1963a; Sherman et al., 1972; Mangel et al., 1983). Yet, none of the measurements have been performed chronically with single-cell resolution. Several changes, for example the recruitment of initially inactive and silencing of active neurons or eye preference changes in single cells could have been easily missed. Additionally, recent studies provide evidence that computations in the mouse dLGN are far more complex than previously suggested (Marshel et al., 2012; Piscopo et al., 2013; Cruz-Martín et al., 2014) and that a significant fraction of cells is responding robustly to visual stimulation of both eyes in rodents and primates (Howarth et al., 2014; Zeater et al., 2015). This raises the possibility of competitive plasticity (see 1.2.3) between the input from the two eyes. Furthermore, there is only very limited data on mouse TRCs after MD even though mice have long replaced other species as most widely used model organism for the study of OD plasticity.

Therefore, the main aim of this thesis was to re-examine the question of experience-dependence plasticity in the mouse dLGN by following the functional plasticity of thalamocortical axons in adult mice. I performed chronic two-photon calcium imaging of individual thalamocortical boutons in layer I of the binocular V1 over nearly a month and analysed the functional characterisitics of thalamocortical axons and their changes after MD and after recovery from MD.

2 Materials and Methods

2.1 Materials

2.1.1 Viruses

All viruses were obtained from University of Pennsylvania Vector Core Services (Philadelphia, Pennsylvania, USA).

Virus	Titer (GC/ml)	Reference
AAV2/1-CAG-flex-tdTomato	9.55 x 10^{13}	
AAV2/1-CAG-flex-eGFP	1.59 x 10^{13}	
AAV2/1-hSyn-GCaMP5G	2.35 x 10^{13}	Akerboom et al., 2012
AAV2/1-hSyn-GCaMP6s	3.58 x 10^{13}	Chen et al., 2013
AAV2/1-hSyn-GCaMP6f	3.04 x 10^{13}	Chen et al., 2013
AAV2/1-hSyn-flex-GCaMP6m	1.89 x 10^{13}	Chen et al., 2013
AAV2/1-hSyn-GCaMP6m	2.23 x 10^{13}	Chen et al., 2013
AAV2/9-hSyn-GCaMP6m	1.21 x 10^{13}	Chen et al., 2013
AAV2/1-CAG-flex-mRuby2-P2A-GCaMP6s	1.18 x 10^{13}	
AAV2/1-hSyn-flex-mRuby2-P2A-GCaMP6s	3.74 x 10^{13}	
AAV2/1-hSyn-mRuby2-P2A-GCaMP6m	2.47 x 10^{13}	
AAV2/9-CAG-flex-mTurquoise2-P2A-GCaMP6s	3.95 x 10^{13}	
AAV2/1-CAG-flex-iGluSnFr	5.40 x 10^{12}	Marvin et al., 2013
AAV2/1-hSyn-flex-Twitch3A	3.37 x 10^{13}	Thestrup et al., 2014
AAV2/1-CAG-flex-Twitch2B	1.05 x 10^{13}	Thestrup et al., 2014

2.1.2 Antibodies and staining solutions

Antibody/staining solution	Supplier	dilution
chicken anti-GFP	Merck Millipore (Billerica, USA)	1:1,000
mouse anti-GAD67	Merck Millipore (Billerica, USA)	1:2,000
anti-chicken Alexa488	Thermo Fisher Scientific (Waltham, USA)	1:200
anti-mouse Alexa633	Thermo Fisher Scientific (Waltham, USA)	1:200
DAPI	Molecular Probes, Inc. (Eugene, USA)	1:1,000
NeuroTrace™ 433/455 blue fluorescent Nissl stain	Molecular Probes, Inc. (Eugene, USA)	1:100
NeuroTrace™ 530/615 red fluorescent Nissl stain	Molecular Probes, Inc. (Eugene, USA)	1:100

2.1.3 Solutions

Composition	Concentration
Artifical cerebral spinal fluid (ACSF)	
NaCl	125 mM
KCl	5 mM
Glucose * H_2O	10 mM
HEPES	10 mM
$CaCl_2$ * 2 H_2O	2 mM
$MgSO_4$ * 7 H_2O	2 mM

The pH of the buffer was adjusted to 7.4 with 1N NaOH and filtered sterile.

Sodium citrate buffer	
Tri-sodium citrate	10 mM
Tween-20	0.05 %

The pH of the buffer was adjusted to 6.0 with 1N HCl.

Paraformaldehyde (PFA)	
Paraformaldehyde	4 %
PBS	0.1 M

2.1.4 Drugs and chemicals

Drug/Chemical	Supplier
Flumazenil-HEXAL	HEXAL AG (Holzkirchen, Germany)
Antisedan®(Atipamezole)	Orion Pharma (Espoo, Finland)
Braunol®7.5 (Iodine solution)	B. Braun Melsungen AG (Melsungen, Germany)
Midazolam-ratiopharm (Midazolam)	ratiopharm (Ulm, Germany)
Dormitor®(Medetomidine)	Orion Pharma (Espoo, Finland)
Fentanyl	HEXAL AG (Holzkirchen, Germany)
Isopto-Max eye lubricant	Alcon Pharma GmbH (Freiburg, Germany)
Isotone Kochsalzlösung	B. Braun Melsungen AG (Melsungen,Germany)
Naloxon-ratiopharm (Naloxone)	ratiopharm (Ulm, Germany)
Oculotect®fluid sine 50 mg/ml PVD Augentropfen	Novartis Pharma GmbH (Melsungen, Germany)
Rimadyl®(Carprofen)	zoetis (Florham Park, New Jersey, USA)
Xylocain®Pumpspray	AstraZeneca GmbH (Wedel, Germany)

2.1.5 Equipment

Material	Supplier
Surgical instruments and material	
Cotton tips, 15 cm	medical care & serve®(Wurmlingen, Germany)
Cover slips, round, 4 mm	Menzel GmbH (Braunschweig, Germany)
Dumont #5/45 Cover Slip Forceps	Fine Science Tools GmbH (Heidelberg, Germany)
Dumont #5/45 Forceps - Dumoxel Standard Tip	Fine Science Tools GmbH (Heidelberg, Germany)
Dumont #3 Forceps, standard	Fine Science Tools GmbH (Heidelberg, Germany)
Dumont #5 Forceps - Assorted Styles, straight	Fine Science Tools GmbH (Heidelberg, Germany)
Dumont #7 Forceps, standard	Fine Science Tools GmbH (Heidelberg, Germany)

Drill bits HP-1004	Hager & Meisinger GmbH (Neuss, Germany)
Headplate (chamber type, 46 x 14 mm, metal)	Max Planck Institute machine shop (Martinsried, Germany)
Infra-red lamp	Glamox Luxo GmbH (Bremen, Germany)
Injekt®	B. Braun Melsungen AG (Melsungen, Germany)
K.1070 High Speed Rotary Micromotor Kit, 2.35mm	Foredom Electric Co. (Connecticut, USA)
K802H PERMA-HAND Suture 6-0	Ethicon (Sommerville, USA)
NanoFil needles, 36g blunt	World Precision Instruments, Inc. (Berlin, Germany)
NanoFil 10 µl syringe	World Precision Instruments, Inc. (Berlin, Germany)
OMNICAN®	B. Braun Melsungen AG (Melsungen, Germany)
Scalpel blades #11	Fine Science Tools GmbH (Heidelberg, Germany)
Scalpel handle #7	Fine Science Tools GmbH (Heidelberg, Germany)
Student Iris Scissor, 11.5 cm, straight	Fine Science Tools GmbH (Heidelberg, Germany)
Sterican®	B. Braun Melsungen AG (Melsungen, Germany)
Sugi®	Kettenbach Medical (Eschenburg, Germany)
Vannas-Tübingen Spring Scissors - 5 mm Blades, Angled up	Fine Science Tools GmbH (Heidelberg, Germany)

Dental cement and glues

Histoacryl®	Aesculap AG (Tuttlingen, Germany)
Paladur®	Heraeus Kulzer GmbH (Hanau, Germany)
Pattex®Ultra Gel	Henkel AG & Co. KGaA (Düsseldorf, Germany)

Instrumentations and further equipment

Homeothermic blanket with rectal probe	Harvard Apparatus (Holliston, Massachusetts, USA)
Injection Robot	Neurostar (Tübingen, Germany)
LCD monitor	DELL (Round Rock, Texas, USA)
Mouse House	Tecniplast (Buguggiate, Italy)
Operationsmikroskop SOM-62	Karl Kaps GmbH (Asslar, Germany)

Running wheel 60821	Trixie Heimtierbedarf (Tarp, Germany)
StereoDrive Motorized Stereotaxic	Neurostar (Tübingen, Germany)

Intrinsic optical imaging components

Basler scA1400-17gm CCD camera	Basler AG (Ahrensburg, Germany)
Fiber-Coupled LED, 530 nm	Thorlabs (Dachau, Germany)
Fiber-Coupled LED, 735 nm	Thorlabs (Dachau, Germany)
Olympus 4x/0.28 NA Objective	Olympus (Tokyo, Japan)

Two-photon microscope components

B-scope	Thorlabs (USA)
CFI75 LWD 16x, 0.8 NA, water-immersion objective	Nikon (Tokyo, Japan)
Controller for Pockels cell, model 302RM	conoptics (Danbury, USA)
Pockels cell, model 350-80	Conoptics (Danbury, Connecticut, USA)
Dichroic beam splitter, 560 nm	Semrock (Rochester, USA)
Emission filter 525/50-25 nm bandpass filter	Semrock (Rochester, USA)
Emission filter 607/70-25 nm bandpass filter	Semrock (Rochester, USA)
Emission filter 720/25 nm short pass filter	Semrock (Rochester, USA)
GaAsP photomultiplier tubes, H7422P	Hamatsu (Toyooka, Japan)
MaiTai HP DeepSee	Spectra-Physics/ Newport (Santa Clara, California, USA)
Nanosecond Delay, 425A	Ortec (Oak Ridge, USA)
PCI Digitizers, 125 MS/s	Alazartech (Pointe-Claire, Canada)
P-726 PIFOC®High-Load Objective Scanner	Physik Instrumente (Karlsruhe, Germany)

Software	
ImageJ	Wayne Rasband, National Institutes of Health (Bethesda, Maryland, USA, http://rsbweb.nih.gov/ij)
MATLAB	The MathWorks (Natick, Massachusetts, USA)
Psychophysics Toolbox	David H. Brainard, Department of Psychology, University of California (Santa Barbara, California, USA, http://psychtoolbox.org)
ScanImage 4.2	Vidrio Technologies, LLC (Janelia Farm, Virginia, USA)
StereoDrive	Neurostar (Tübingen, Germany)

2.2 Methods

All experimental procedures were carried out in compliance with institutional guidelines of the Max Planck Society and the local government (Regierung von Oberbayern).

2.2.1 Virus injection and chronic window implantation

Surgeries were performed on female C57Bl/6 or *Scnn1a-Tg3-Cre mice* (postnatal day 35-45), following a protocol modified from Holtmaat and Svoboda, 2009. Mice were anaesthetized by an intraperitoneal injection of a mixture of the opioid receptor agonist Fentanyl (0.075 mg/kg), the benzodiazepine Midazolam (7.5 mg/kg) and the α 2-adrenergic receptor agonist Medetomidine (0.75 mg/kg). Additional analgesia was achieved by local application of 10 % Lidocaine and subcutaneous injection of Carprofen (5 mg/kg) before surgery and on the first day of post-surgical recovery. Eye dehydration was prevented by applying a thin layer of cream on both eyes.

The mouse was then mounted in a motorized stereotactic apparatus. Part of the skin over the skull was removed with scissors. The skull was cleared of hairs, roughened with a scalpel and the edges of the skin were fixed with Histoacryl. Using a drill, a circular craniotomy (4 mm diameter) located over the somatosensory and primary visual cortex of the right hemisphere was made. After removal of the bone lid, the brain was kept moist with ACSF and blood from meningeal vessels was removed with Sugis until bleeding stopped.

For precise injection, the head of the mouse was aligned to a mouse brain atlas by sending the actual positions of lambda and bregma to StereoDrive, the software of the motorized stereotaxic. A Hamilton Glass Syringe (gauge 36) was targeted to the lateral geniculate nucleus using the following stereotactic coordinates relative to bregma: anterior 2.06 mm, lateral 2.05 mm. A total volume of about 0.5 to 1 µl of a virus solution was injected at a depth of 2.85 mm at a rate of 3-5 nl/s using an automated microinjector.

A cover slip (4 mm) was placed over the craniotomy and sealed with cyanoacrylate glue. A custom-made aluminium head-plate (oval with an 8 mm opening and two screw notches) was fixed to the skull with dental cement.

Anaesthesia was counteracted by subcutaneous injection of the opioid receptor antagonist Nalaxone (1.2 mg/kg), the $GABA_A$ receptor antagonist Flumazenil (0.5 mg/kg) and the α2-adrenergic receptor antagonist Atipamezole (2.5 mg/kg). During recovery from anaesthesia, mice were kept under an infra-red lamp.

2.2.2 Monocular deprivation

Mice underwent monocular deprivation at the age of P70-90 following a protocol from Hofer et al., 2009. Anaesthesia was induced by intraperitoneal injection of Fentanyl (0.05 mg/kg), Midazolam (5 mg/kg) and Medetomidine (0.5 mg/kg). To prevent eye dehydration, a thin layer of cream was applied on the right eye and left eye was kept moist with drops of saline.

Eye lids were sutured with three mattress stitches using 6-0 silk. Anesthesia was counteracted with a mixture of Nalaxone (1.2 mg/kg), Flumazenil (0.5 mg/kg) and Atipamezole (2.5 mg/kg). After 6-8 days, mice were re-anaesthetized and sutures were removed directly before imaging.

Before and during MD, Animals were housed together with at least three littermates in an enriched environment (mouse house, nesting material, running wheels) in large cages (1500 cm^2 floor area, Greifzu et al., 2014). High contrast moving grating stimulation (8 direction) was employed for 6 h/d during the light period (14 h/d, during MD only, Matthies et al., 2013; Rose et al., 2016).

Mice with corneal injuries were omitted from experiments.

2.2.3 Chronic *in vivo* imaging

2.2.3.1 Anaesthesia

Mice were initially anaesthetized with an intraperitoneal injection of Fentanyl (0.035 mg/kg), Midazolam (3.5 mg/kg) and Medetomidine (0.35 mg/kg) and additional anaesthetics (25 % of induction level) were injected subcutaneously every 60 min to maintain anaesthesia level. Mice were placed on a heated blanket under the microscope to ensure a stable thermal homeostasis. Fixation of the mice was achieved by screwing the metal head-plate to two posts to allow a reproducible positioning between imaging sessions. Eye and pupil positions were monitored with two cameras.

2.2.3.2 Intrinsic optical imaging

Intrinsic optical imaging was applied to monitor the population response strength to stimulation of either eye in the binocular region of the visual cortex as a readout for ocular dominance. The imaging optical axis was adjusted to be orthogonal to the window for each animal. The surface of the brain was side-illuminated with light of 530 nm to vi-

sualize the blood vessel pattern and with 735 nm from two sides for mapping ocular dominance. Images were collected with a CCD camera (12 bit, 260 x 348 pixel at 40 Hz), which was focused to 400-450 μm below the pial surface, through a 4x air objective (Olympus, NA 0.28). Acquisition and analysis software were custom written in Matlab.

2.2.3.3 Two-photon imaging

For *in vivo* imaging, a two-photon laser scanning microscope as described earlier (Rose et al., 2016) was used. Briefly, a beam from a pulsed femtosecond Ti:Sapphire laser (tuned to 940 nm and blanked with a Pockels cell during turnarounds) was used to excite GCaMP6m/s. Signal detection through a 16 x 0.8 NA objective was achieved after emitted photons were directed through a 720/25 nm filter, a primary beam splitter and a secondary bandpass filter (525/50-25 or 707/70-25 nm, respectively) using GaAsP photomultiplier tubes.

For functional imaging, a 57 μm x 57 μm field of view was scanned at 30 Hz with an 8 kHz resonant scanner and 512 x 512 pixel resolution. The objective was moved in the z-axis by a high-load piezo to acquire four subsequent planes in rapid succession, each separated by 3 μm in depth (effective frame rate of 7.6 Hz). Structural images were acquired by averaging 30-50 images per slice and slices were separated in the z-axis by 1 μm. The average power for imaging was less than 50 mW (below the objective). For each recording, the imaging position in x,y and z was realigned with the initial image from the first recording session. ScanImage 4.2 (Pologruto et al., 2003) and custom written hardware drivers were used for data acquisition.

2.2.4 Visual stimulation

All visual stimuli were generated with Matlab using the Psychophysics Toolbox extension (Brainard, 1997; Pelli, 1997) and presented on a gamma-corrected LCD monitor that was located 13 cm in front of the mouse. The screen was positioned in portrait (24.9 cm x 44.3 cm) and had a refresh rate of 60 Hz. Its position was adjusted for each mouse so that it was centered to the binocular visual field of the mouse. The same position was kept throughout all imaging sessions. A spherical-to-Cartesian transformation was applied using an OpenGL shader to correct for the increasing eccentricity on a flat screen relative to spherical mouse visual space. Motorized eye shutters were used to ensure monocular vision.

2.2.4.1 Visual stimulation for intrinsic optical imaging

Eight directions with a spatial frequency of 0.04 cycles/degree and a temporal frequency of 2 cycles/s were presented in a defined part of the visual field. This patch had a size of 20° x 40° of visual angle and was presented randomly at two different positions (next to each other in the central visual field) to either the left or the right eye. In each trial, a blank grey screen (50 % contrast) was presented for 5 s followed by 7 s of visual stimuli (angle of the direction was changed every 0.6 s). Trials were separated by 8s and the whole stimulus sequence was repeated at least 10 times per eye and patch position.

2.2.4.2 Visual stimulation for orientation and direction tuning

Visual stimuli were presented in -15° to 35° elevation and -25° to 25° azimuth relative to midline to achieve stimulation in the binocular visual space. Eight direction with a spatial frequency of 0.04 cycles/degree and a temporal frequency of 3 cycles/s were presented in a random order to either the left or the right eye. Moving gratings were shown for 5 s, followed by 6 s of a full-field grey screen. Trials were repeated 4-6 times per eye and direction. To minimize the light leak from the LCD screen during stimulation, the backlight of the monitor was synchronized to the line clock of the resonant scanner (mean luminance with 16 kHz pulsed backlight: white, 4.1 cd/m^2; black: 0.01 cd/m^2). That way, the screen backlight was switched on only during the bidirectional turnaround time that was not used for image generation (Leinweber et al., 2014).

2.2.4.3 Receptive field mapping

Stimuli consisted of black or white patches (8° x 8°) displayed on a grey background. These patches appeared randomly for 0.5 s with an interstimulus interval of 0.1 s at 30 different positions covering a total of 40° x 48° . For each eye, this stimulus block was repeated at least ten times.

2.2.5 Immunohistochemistry

Mice were anaesthetized by an intraperitoneal injection of Fentanyl (0.07 mg/kg), Midazolam (7 mg/kg) and Medetomidine (0.7 mg/kg) and decapitated. The brain was removed from the skull and fixed with 4 % (w/v) PFA for a week at 4 °C. Afterwards, the brain was transferred to 30 % (w/v) sucrose in phosphate buffered saline (PBS) and kept at 4 °C for at least three days. Brains were cut in 50 µm coronal slices using a freezing sliding microtome. For stainings against GAD-67, slices were pre-processed by incubation for 10 min in sodium citrate buffer at 95 °C under continouse shaking at 300 rpm and then cooled down for an 1h at room temperature. Slices were incubated over-night

with 1 % (v/v) Triton X-100 and 10 % (v/v) normal goat serum at 4 °C. Subsequently primary antibodies were applied over-night in 1 % Triton X-100, 5 % (v/v) goat serum in PBS. Slices were washed three times with PBS for 10 min. Secondary antibodies were diluted in PBS containing 4 % goat serum and incubated with the slices for 3h at room temperature followed by extensive washing with PBS. For Nissl stainings, slices were incubated for 20 min in fluorescent Nissl stain in PBS. Washing was repeated as before and DAPI solution was applied. After a last washing with PBS, the sections were mounted on microscope slides.

2.2.6 Data analysis

2.2.6.1 Intrinsic optical imaging

Acquisition and analysis software were custom written in Matlab. Images were clipped (1.5 %) and high-pass-filtered to calculate blank-corrected image averages for each condition. These maps were thresholded (image background mean + 4 * standard deviation) and the largest object was defined as the responsive region. Contralateral regions were based on region derived from the ipsilateral region of the same stimulus. The mean background value of the non-responsive area was subtracted from each pixel and all pixel values within the defined region were summed to yield an integrated measure of response strength.
The ocular dominance index (ODI) was calculated as a measure for ocular dominance: $ODI = \frac{R_{contra} - R_{ipsi}}{R_{contra} + R_{ipsi}}$, where R_{contra} and R_{ipsi} are the integrated response strength to contralateral or ipsilateral eye stimulation, respectively.

2.2.6.2 Image analysis

Custom-written software in MATLAB and ImageJ (http://rsbweb.nih.gov/ij/) were used for image and data analysis. The average of 160 images acquired without laser excitation was subtracted from all frames to correct for non-uniform background signals. Motion artefacts were removed by translation registration of all frames against the average of the initial 100 signal frames of the recording.

2.2.6.3 Detection of boutons

Region of interests (ROIs) corresponding to putative boutons were automatically selected using ImageJ. A global threshold was applied to an average activity map, edge artefacts were removed and particle-ROIs were selected based on a set of morphological filters for size and shape. The resulting ROIs were visually inspected and, if necessary, artefacts

were removed. If applicable, ROIs were manually matched from one time point to another, selecting the z-plane with optimal optical sectioning of a respective bouton for each recording.

2.2.6.4 Determining responsiveness

All pixel values within a ROI were averaged to determine the fluorescence time course (F) of this ROI. A sample-wise F_0 trace was generated for each ROI by linear extrapolation over the low-pass filtered (0.004 Hz cutoff) local minima of the raw fluorescence signal in the absence of drifting grating stimulation (pre-stimulus periods). This F_0 trace was used to generate the $\Delta F/F_0$ trace which was aligned to stimulus-onsets and was further corrected for residual offset by subtracting the individual average pre-stimulus $\Delta F/F_0$ signal. Boutons were defined as responsive for a specific eye, if a significant change in peak fluorescence (peak $\Delta F/F_{0\_Stimulus} > 8 * \sigma \Delta F/F_{0\_Baseline}$) was observed in at least 50 % of the trials of a single stimulus condition of a specific eye.

2.2.6.5 Analysis of ocular dominance

Ocular dominance was determined by calculating the ODI for each individual bouton:

$$ODI = \frac{\frac{\Delta F}{F_0} contra_{pref\_dir} - \frac{\Delta F}{F_0} ipsi_{pref\_dir}}{\frac{\Delta F}{F_0} contra_{pref\_dir} + \frac{\Delta F}{F_0} ipsi_{pref\_dir}}$$

Contralateral and ipsilateral dominance are indicated by an ODI of 1 or -1, respectively. Pixel-based ODI maps were similarly generated by using the maximum fluorescence change of individual pixels. Hue is set by the ODI (red: ipsilateral dominance, blue: contralateral dominance) and lightness codes the mean of the summed ipsilateral and contralateral response amplitude. Contra/ipsi ratio was calculated as the ratio of the mean fluorescence response to ipsilateral or contralateral eye stimulation, respectively, over all responsive boutons or layer II/III cell bodies of one animal.

2.2.6.6 Analysis of orientation and direction tuning

The orientation selectivity index (OSI) was calculated as the ratio between the difference of the response to the preferred and opposite orientation, and the sum of both responses: $OSI = \frac{R_{pref\_ori} - R_{opp\_ori}}{R_{pref\_ori} + R_{opp\_ori}}$. Similarly, the direction selectivity index (DSI) was determined as the ratio between the difference of the response to the preferred and opposite direction, and the sum of both responses: $DSI = \frac{R_{pref\_dir} - R_{opp\_dir}}{R_{pref\_dir} + R_{opp\_dir}}$. Additionally, global orientation

selectivity index (gOSI) was calculated as 1 - circular Variance, circ. Var.:

$$gOSI = 1 - circ.var. = \left| \frac{\sum R(\theta_k) e^{2i\theta_k}}{\sum R(\theta_k)} \right|,$$

with $R(\theta_k)$ as the mean response to the direction angle θ_k. Perfect orientation selectivity is indicated as gOSI = 1. Similarly, direction tuning was additionally assessed by calculating the global direction selectivity index (gDSI)

$$gDSI = 1 - dir.circ.var. = \left| \frac{\sum R(\theta_k) e^{i\theta_k}}{\sum R(\theta_k)} \right|,$$

2.2.6.7 Analysis of receptive fields

Traces were sorted according to stimulus position and type (black or white, representing ON and OFF subfields). Response latency was defined as the first imaging frame during a set time window, in which there was a a significant increase (ANOVA, $p < 0.05$) in fluorescence. If the ROI was determined responsive for both the black (OFF) and white (ON) patches with different latencies, only the RF with the shorter latency was considered for further analysis. A thresholded RF subfield was derived by interpolating the raw RF at 1° resolution and only taking the region with the strongest average response. This subfield was used to compute further parameters such as RF area size and length of the major and minor axis length.

2.2.6.8 Grouped data analysis

Mice were imaged at least three times before MD and up to three times afterwards over a time period of one month. Imaging session were spaced 4 days apart. To determine similarity of tuning across imaging sessions, Pearson's correlation coefficient and pair-wise difference between tuning indices of the same boutons were calculated. For chronic single-bouton changes, only boutons that were responsive throughout baseline, after MD and, if applicable, during recovery were considered. For the quantification of changes in eye-specific response amplitude relative to the mean baseline ODI the 3 baseline sessions had to be responsive. For further analysis, criteria are indicated in individual figures.

2.2.6.9 Statistics

Results are reported as median ± interquartile range or as mean ± standard error of the mean (SEM) or mean ± standard deviation (STD) as indicated in individual figures. Paired parametric (t-test) or paired and unpaired non-parametric (Wilcoxon signed-rank test, Mann-Whitney U test, Kruskal-Wallis test on ranks with Bonferroni's post hoc test for

multiple comparisons, Friedman's test with Bonferroni's post hoc test for multiple comparisons) statistics were used for comparison. For cumulative distributions, the Kolmogorov-Smirnov test was applied, while distributions were compared using the χ^2 test. Asterisks indicate significance values as follows: * $p < 0.05$, ** $p < 0.01$ and *** $p < 0.001$.

3 Results

3.1 Establishing functional imaging of thalamocortical axons

3.1.1 Labelling of thalamocortical axons

The goal of this thesis was to assess physiological changes in thalamocortical axons after monocular deprivation. In order to address this question, it was essential to establish functional imaging of thalamocortical axons. After installing a new surgical setup for virus injection and verifying stereotactic coordinates, I tested injections with a construct for a structural marker (AAV2/1-CAG-flex-tdTomato). The labelled thalamocortical axons showed the following projection pattern in V1 (Fig. 3.1): dense innervation in layer IV, only very few axons in layer II/III (most going up to layer I) and scattered projection to layer I. This was consistent with what has been previously reported (Ji et al., 2016; Cruz-Martín et al., 2014; Hubel and Wiesel, 1972).

After establishing an effective and reliable injection, I tested several viruses encoding genetically encoded calcium indicators (GCaMP and Twitch variants) or a glutamate-sensing fluorescent reporter (iGluSnFr) to visualize responses to visual stimuli (see table 3.1). Surprisingly, only viruses expressing GCaMP6m showed both good labelling and fluorescent changes in response to visual stimuli. Many other viruses, expressing for example GCaMP6s or viruses with more than one fluorescent protein, were either not expressed or only at a very low level. Other viruses showed no or only minor changes in fluorescence level in response to visual stimuli. Ideally, the structure of the thalamocortical axons would be visualized with a second fluorophore with a constant fluorescence. However, co-expression of two viruses was not possible: Axons were never labelled with both fluorophores.

Virus	Labelling	Responses	Comment
AAV2/1-hSyn-GCaMP5g	--	n. a.	
AAV2/1-hSyn-GCaMP6s	+	++	only very few axons labelled, (1)
AAV2/1-hSyn-GCaMP6m	++	++	(1)
AAV2/1-hSyn-GCaMP6f	--	n. a.	(1)
AAV2/1-CAG-flex-mRuby2-P2A-GCaMP6s	--	n. a.	
AAV2/1-hSyn-flex-mRuby2-P2A-GCaMP6s	--	n. a.	
AAV2/1-hSyn-mRuby2-P2A-GCaMP6m	-	n. a.	
AAV2/9-CAG-flex-mTurquoise2-P2A-GCaMP6s	-	n. a.	
AAV2/1-CAG-flex-tdTomato and AAV2/1-hSyn-GCaMP6m	++	++	no co-labelling
AAV2/1-CAG-flex-iGluSnFr	++	--	(2)
AAV2/1-hSyn-flex-Twitch3A	+	--	(3)
AAV2/1-CAG-flex-Twitch2B	--	n. a.	(3)

Table 3.1: **Viruses for functional imaging of thalamocortical axons.** Various viruses were tested to functionally image thalamocortical axons in layer I of V1 to achieve both good labelling and changes in fluorescence intensity upon visual stimulation (n. a. = not applicable, original material by (1) GENIE, (2) Looger, (3) Griesbeck).

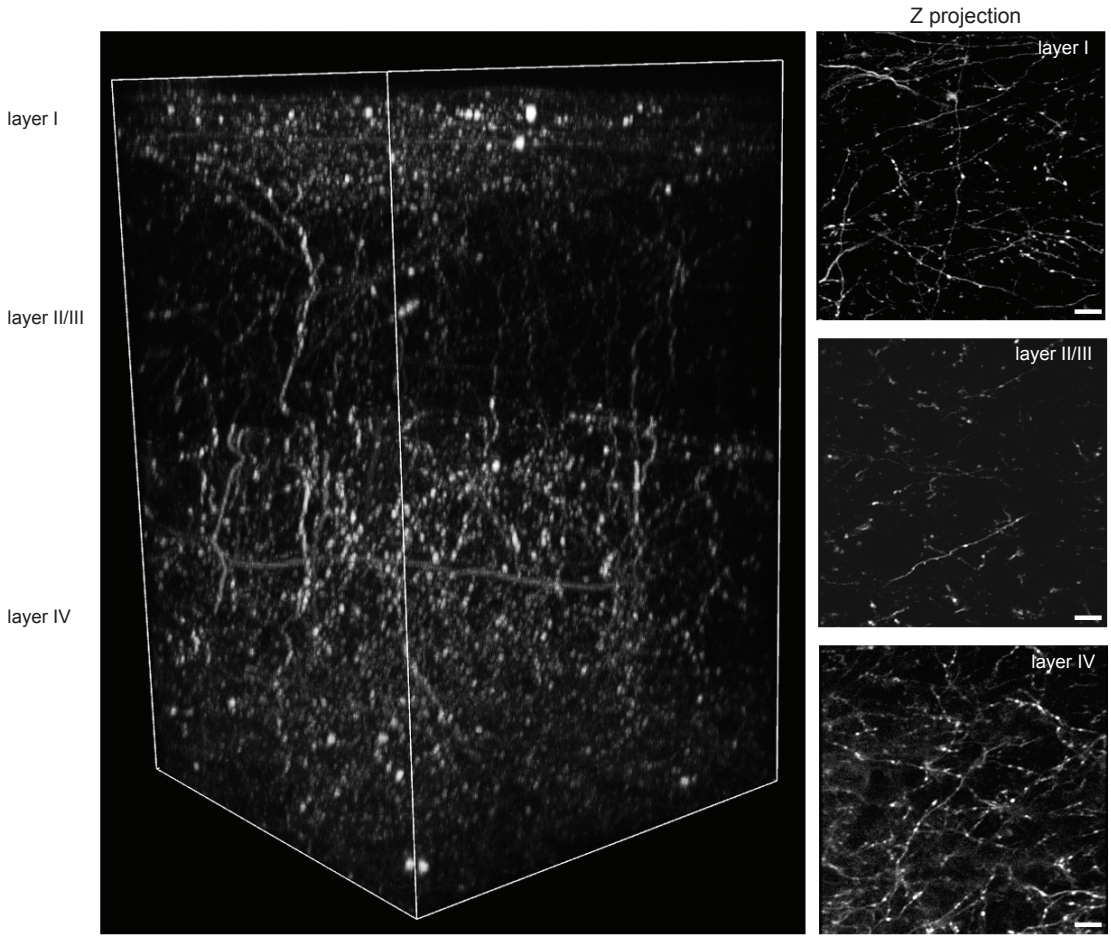

Figure 3.1: **Projection pattern of thalamocortical axons in V1.** After stereotactic injection of AAV2/1-CAG-flex-tdTomato in dLGN, thalamocortical axons showed the expected projection pattern in layers I to IV of V1 (scale bar: 10 μm).

3.1.2 *Scnn1a-TG3-Cre* mice

I verified injection sites post hoc and many brains also showed virus expression in the cortex and the hippocampus above the dLGN due to virus leakage during the virus injection (data not shown). Though the injection area directly above the dLGN is part of the somatosensory cortex, it is flanked by higher visual areas such as A (anterior area), RL (rostrolateral area) and AL (anterolateral area). Anterograde labelling from, for example, RL, shows connections with V1 (Wang et al., 2012). Hence, virus leakage during the injection could lead to labelling of axons from RL projecting to V1.

Cre lines offer the opportunity to restrict the expression to defined areas by combining them with floxed viruses: The sequence of the desired protein is flanked by specific sequences, the loxP sites. The enzyme Cre recombinase is necessary to recognize those

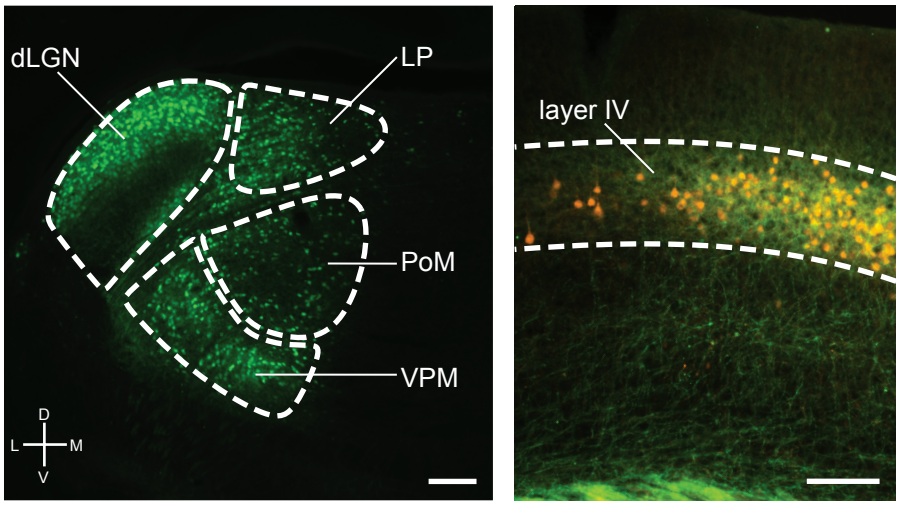

Figure 3.2: **Expression pattern of *Scnn1a-TG3-Cre* mice after stereotactic injection.** A *Scnn1a-TG3-Cre* mouse was injected with AAV2/1-CAG-flex-eGFP in dLGN and AAV2/1-CAG-flex-tdTomato in V1. Left panel: Coronal section (Bregma -2.06) showing expression in dLGN, LP (lateral posterior thalamic nucleus), PoM (posteromedial thalamic nucleus) and VPM (ventral posteriomedial thalamic nucleus), scale bar: 200 µm. Right panel: Coronal slice (Bregma -3.08) with cells in layer IV of V1 labelled in red and thalamocortical axons in green, scale bar: 100 µm.

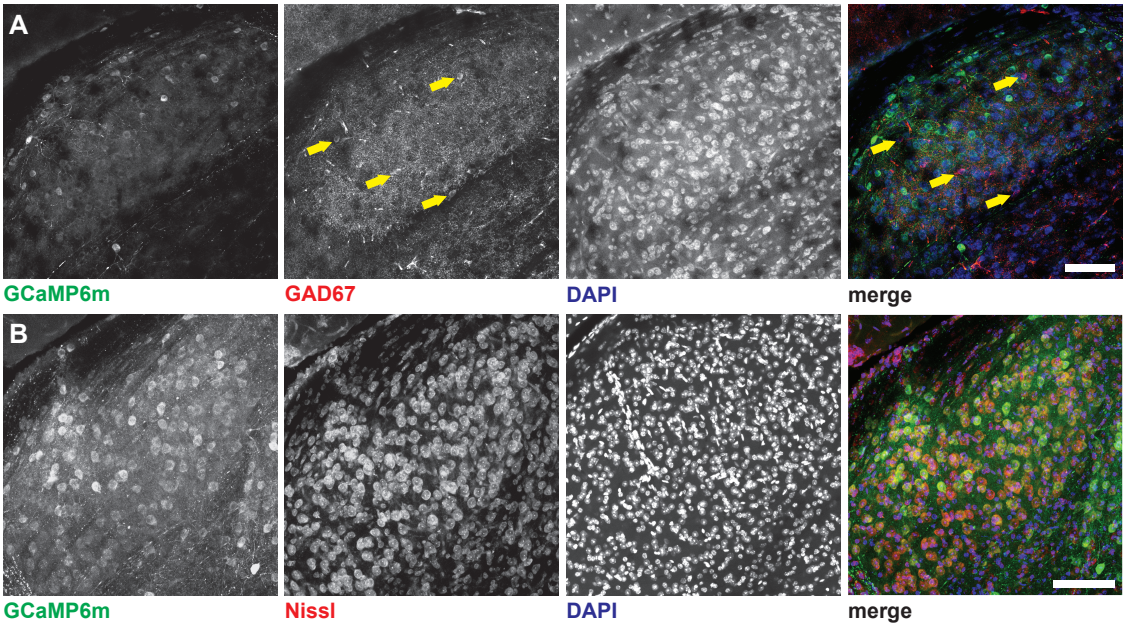

Figure 3.3: **Immunohistochemical characterization of GCaMP6m-expressing cells in the dLGN of *Scnn1a-TG3-Cre* mice after stereotactic injection.** *Scnn1a-TG3-Cre* mice were injected with AAV2/1-hSyn-flex-GCaMP6m (green) in dLGN. **A** Immunohistochemical staining for the inhibitory marker GAD67 (red) and nuclear marker DAPI (blue) of coronal slices of the dLGN. Arrows indicate exemplary GAD67-positive neurons. **B** Example confocal images showing coronal section of dLGN stained with neuronal marker (Nissl staining, red) and nuclear marker DAPI (blue). Scale bar: 100 µm

sequences and enables gene transcription. Cre lines express this enzyme in specific cells. For example, *Scnn1a-TG3-Cre* mice (Madisen et al., 2010) show Cre expression in cortical layer IV and in restricted populations within cortex, in the cerebellum and in thalamus, including the dLGN. The expression pattern was confirmed by injecting a virus encoding floxed eGFP (an eGFP flanked by two loxP sites) into the thalamus with the simultaneous injection of a virus expressing the floxed red fluorescent protein tdTomato into layer IV of V1 (Fig. 3.2). I found eGFP expression in dLGN, lateral posterior thalamic nucleus (LP), posteromedial thalamic nucelus (PoM) and ventral posteromedial thalamic nucleus (VPM) with thalamocortical axons projecting to V1, preferably to layer IV, but also layer I, similar to Fig. 3.1. Cells in layer IV of V1 were positive for tdTomato. This confirms the previously reported expression pattern.

Further immunohistochemical characterizations showed excitatory neuron specificity of *Scnn1a-TG3-Cre* mice (Fig. 3.3). Nissl and DAPI staining demonstrated that on average 67.7 % ± 4.6 % SEM (n = 3 animals, 1045/1518 cells) of cells in the dLGN were neurons and of those 26.7 % ± 2.7 % SEM (266/1045 cells) expressed GCaMP6m after stereotactic injections. Of those, none were positive for GAD67 (n = 3 animals, 0/381 GCaMP6m-positive cells), confirming that none of the cells were inhibitory. However, the overall percentage of GAD67+ neurons in the dLGN was surprinsingly low: only 2.7 % ± 0.3 % SEM (118/4438 neurons). Other studies report 20 % inhibitory neurons (Arcelli et al., 1997; Golding et al., 2014).

3.2 Functional characterization of thalamic relay cell (TRC) boutons in layer I

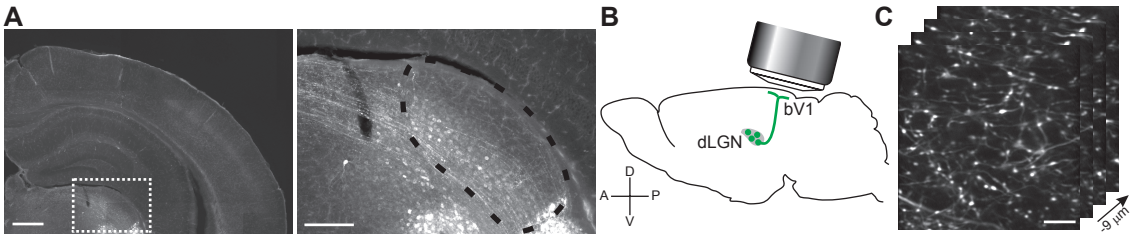

Figure 3.4: **Experimental setup.** **A** Stereotactic injection of AAV2/1-hSyn-flex-GCaMP6m in a *Scnn1a-TG3-Cre* mouse (dLGN outlined, scale bar: left, 500 µm, right, 200 µm). **B** Schematic of imaging strategy: AAV2/1-Syn-flex-GCaMP6m was injected in dLGN of *Scnn1a-TG3-Cre* mice and a glass window was placed over V1. **C** Data was acquired in a small volume of the binocular visual cortex in adult mice using sequential acquisition of four imaging planes (distance between slices: 3 µm, frame rate 7.5 Hz, scale bar: 10 µm)

Currently, there is considerable disagreement concerning some of the visual response properties of thalamic neurons (e.g. binocularity, orientation and direction selectivity, Sun et al., 2016a; Roth et al., 2016; Kondo and Ohki, 2016; Cruz-Martín et al., 2014). Therefore, as a first step, I assessed the visual tuning properties of thalamocortical axons by *in vivo* calcium imaging of TRC boutons in layer I of binocular V1 (Fig. 3.4).

3.2.1 Binocularity

To determine the eye-specificity of visual responses in TRC boutons, mice were exposed to sinusoidal moving gratings of eight different directions while stimulation of one eye was always blocked by a mechanical shutter.

Consistent with expectations, I observed that the majority of visually responsive TRC boutons were driven exclusively by the contralateral eye (Fig. 3.5 B, ROI 2, C). Ipsilaterally tuned boutons were also found (Fig. 3.5 B, ROI 3) as well as binocular boutons that showed a change in fluorescence in response to visual stimulation of either eye (Fig. 3.5 B, ROI 1). The distribution of these types varied between animals (probably due to differences in injection and imaging sites), but in total 66.3 % were purely contralaterally, 19.3 % purely ipsilaterally and 14.3 % binocularly driven (n = 725 boutons in 9 animals).

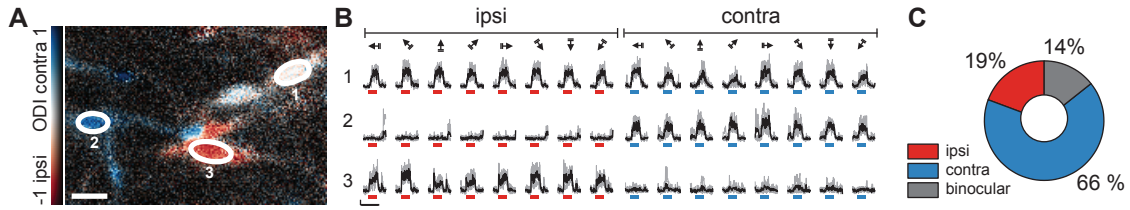

Figure 3.5: **Eye-specific responses of thalamocortical axons. A** ODI pixelmap of thalamocortical axons in layer I of the visual cortex with the hue coding for the ODI (red: ipsilateral and blue: contralateral dominance) and the brightness for the response amplitude (scale bar: 3 µm). **B** Calcium traces of the region of interests (ROIs) marked in A in response to moving gratings (8 direction, 4 trials) presented to either the ipsilateral or the contralateral eye (scale bars: $\Delta F/F_0 =$ 200 %, 10 s). **C** Quantification of the fractions of boutons showing purely ipsilateral, contralateral or binocular visual responses (n = 725 boutons in 9 animals).

3.2.2 Orientation and direction tuning

Next, I addressed orientation and direction tuning. In primates, binocular responses are restricted to cells in the koniocellular layers of the dLGN (Zeater et al., 2015), leading to the speculation that binocular cells represent a specific channel of visual processing. Therefore, to assess differences between monocular and binocular boutons, I quantified orientation and direction tuning separately for contralateral, ipsilateral and binocular boutons.

Examples of orientation-selective boutons are displayed in Fig. 3.6 D/E: The contralaterally tuned bouton in the lower panel was selective for horizontal orientations and the ipsilaterally tuned bouton (middle panel) for diagonal orientations going from upper left to lower right. The binocular bouton (upper panel) showed similar orientation selectivity for both eyes, preferring the vertical orientation and orientations going from upper left to lower right. None of these examples were also direction selective.

To quantify orientation selectivity, the orientation selectivity index (OSI) and the global orientation selectivity index (gOSI, equivalent to 1 - circular variance) were calculated. The OSI is widely used in the literature and ranges from 0 (no selectivity) to 1 (perfect selectivity), but it has been implicated that gOSI might be better suited for quantification of orientation selectivity as it is more robust to noise (Mazurek et al., 2014). Similarly, gOSI varies between 0 (no selectivity) and 1 (perfect selectivity). The distribution of both indices is displayed in Fig. 3.7 A and B for the three different response types (ipsilateral, contralateral and binocular boutons).

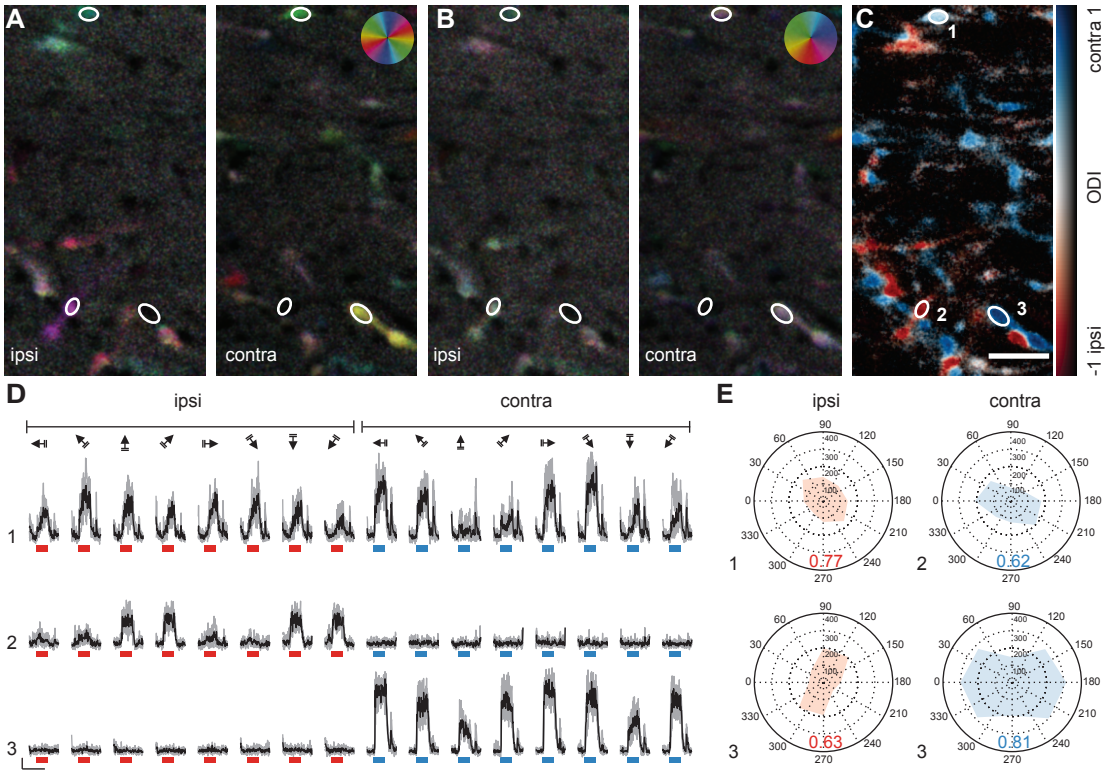

Figure 3.6: **Orientation and direction selectivity of thalamocortical axons. A** Orientation pixelmaps coding for preferred orientation (hue) and response amplitude (brightness) after ipsilateral (left panel) or contralateral (right panel) stimulation, respectively, of thalamocortical axons in layer I of the visual cortex. **B** Corresponding direction pixelmaps, in which the hue is representing the preferred direction and the brightness the response amplitude. **C** Corresponding ODI pixelmap (scale bar: 5 µm). **D** Calcium traces of the region of interests (ROIs) marked in C in response to moving grating presented to either the ipsilateral or the contralateral eye. Scale bar: 200 % $\Delta F/F_0$, 10 s. **E** Polar plots of orientation and direction tuning of the ROIs marked in C and the values of the corresponding gOSI.

The majority of boutons responded to all orientations. But some boutons were also highly orientation-selective. The OSI was low with a population median of 0.35 ± 0.43 (IQR). The gOSI showed a more distinct distribution, with a very high fraction of orientation selective boutons with a very low gOSI (population gOSI: 0.14 ± 0.19). The orientation selective fraction of boutons was 19.9 % ± 22.8 (OSI $>$ 0.5, median ± IQR of all categories per animal) or 15.7 % ± 18.7 (gOSI $>$ 0.33, n = 9 mice, compare also Fig. 3.7 C).

There was no significant difference between ipsilateral, contralateral and binocular boutons, both in the distribution of the OSI (P = 0.39) and the gOSI (P = 0.65, ipsi: n = 140 boutons, contra: n = 481, binocular: n = 104) as well as in the percentage of orientation-selective boutons based on the gOSI (P = 0.62, Kruskal-Wallis test, n = 9 mice).

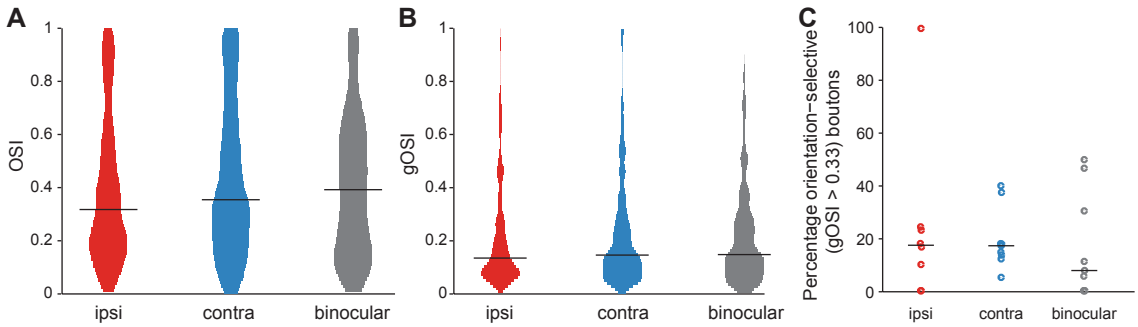

Figure 3.7: **Quantification of orientation selectivity of TRC boutons. A, B** Distribution of OSI (A) and gOSI (B) for ipsilateral (left panel, n = 140), contralateral (middle panel, n = 481) and binocular boutons (right panel, n = 104). Horizontal lines indicate medians. Pooled data from 9 mice (OSI, P = , 0.39, gOSI, P = 0.65, Kruskal-Wallis test). **C** Percentage of orientation-selective (gOSI > 0.33) boutons (n = 9 mice, P = 0.62, Kruskal-Wallis test).

Likewise, the direction selectivity index (DSI) and the global direction selectivity index (gDSI) were calculated, and the distributions are shown in Fig. 3.8. Both indices showed comparable results. Based on the DSI, only a small fraction of boutons were direction selective (DSI > 0.5, 19.9 % ± 22.8) with a population median of 0.29 ± 0.41 (3.8 A). The fraction of direction-selective boutons is even smaller based on the gDSI (gDSI > 0.33): 12.9 % ± 16.3, and the population median was also lower (0.14 ± 0.19). Similar to the indices for orientation selectivity, the shape of the distribution was much more defined for the gDSI.

In contrast to orientation selectivity, the classes of boutons differed in their direction selectivity (DSI: P = 0.0048, gDSI: P = 0.0162, Kruskal-Wallis test). Contralateral boutons were significantly more tuned than ipsilateral boutons (DSI: P = 0.004, gDSI: 0.015, Kruskal-Wallis test, Bonferroni corrected) with a lower median DSI (0.30 ± 0.44 vs. 0.24 ± 0.32) and a lower median gDSI (0.11 ± 0.19 vs. 0.09 ± 0.10). Interestingly, binocular boutons did not show any significant differences from ipsilateral (DSI: P = 0.053, gDSI: 0.11) or contralateral (DSI: P = 1, gDSI: P = 1, Kruskal-Wallis test, Bonferroni corrected) boutons (median DSI: 0.29 ± 0.36; median gDSI: 0.13 ± 0.17, Fig. 3.8).

To my knowledge, there is no other study comparing stimulus selectivity of monocular and binocular cells or ipsilaterally and contralaterally-tuned cells in the dLGN. These results, however, hint that at least for orientation and direction selectivity, binocular boutons do not compromise a separate channel of visual processing as there was no significant difference to monocular boutons.

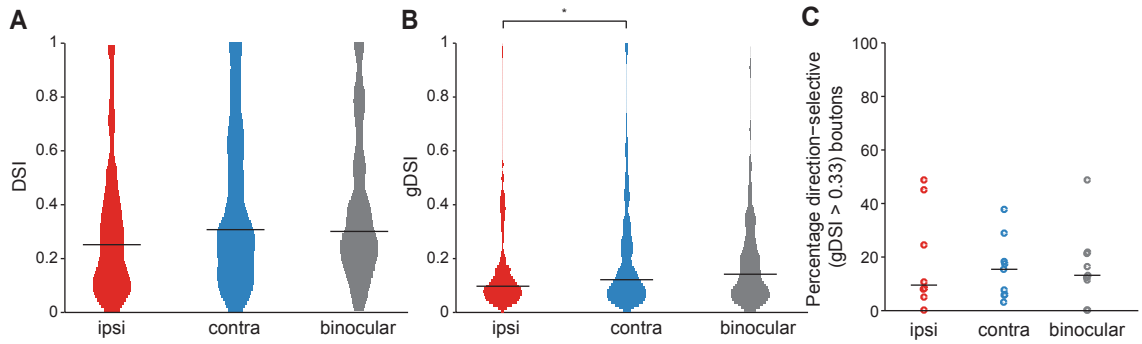

Figure 3.8: **Quantification of direction selectivity of TRC boutons. A, B** Distribution of DSI (A) and gDSI (B) for ipsilateral (left panel, n = 140), contralateral (middle panel, n = 481) and binocular boutons (right panel, n = 104). Horizontal lines indicate medians. Pooled data from 9 mice (DSI, P = 0.004, gDSI, P = 0.015, Kruskal-Wallis test, Bonferroni corrected). **C** Percentage of direction-selective (gDSI > 0.33) boutons (n = 9 mice, P = 0.99, Kruskal-Wallis test).

3.2.3 Spatial receptive field properties

The visual response properties were further characterized by mapping the spatial receptive field structure. In *Scnn1a-TG3-Cre* mice, Cre is expressed both in the dLGN as well as in the LP, which also projects to V1. The spatial receptive field size greatly differs between dLGN and LP neurons (Roth et al., 2016, Durand et al., 2016). Hence, contamination of the data by projections from LP can be determinded by analysing the spatial receptive fields of boutons in layer I of binocular V1. Therefore, black and white squares were presented on defined positions in the visual field of mice to compute ON and OFF receptive field subdomains. This was performed both for the ipsilateral and the contralateral eye (Fig. 3.9 A).

Pixelmaps were computed to easily visualize the response properties (Fig. 3.9 B).These maps show a highly focused spatial selectivity that is inconsistent with inputs from LP. For example ROI 1 seemed to prefer a position in the upper left part of the visual field, while the contralateral bouton in ROI 2 preferred a position that was a bit lower in the visual field. The calcium traces in response to stimulation in the different positions (Fig. 3.9 C/E) and the receptive fields that were computed from those traces (Fig. 3.9 D/F) confirmed this. Both boutons showed an ON and an OFF subfield in the same position, but the ON field of the ipsilateral bouton was bigger than its OFF field.

For all receptive fields, the area size, both axis lengths and aspect ratio (major/minor

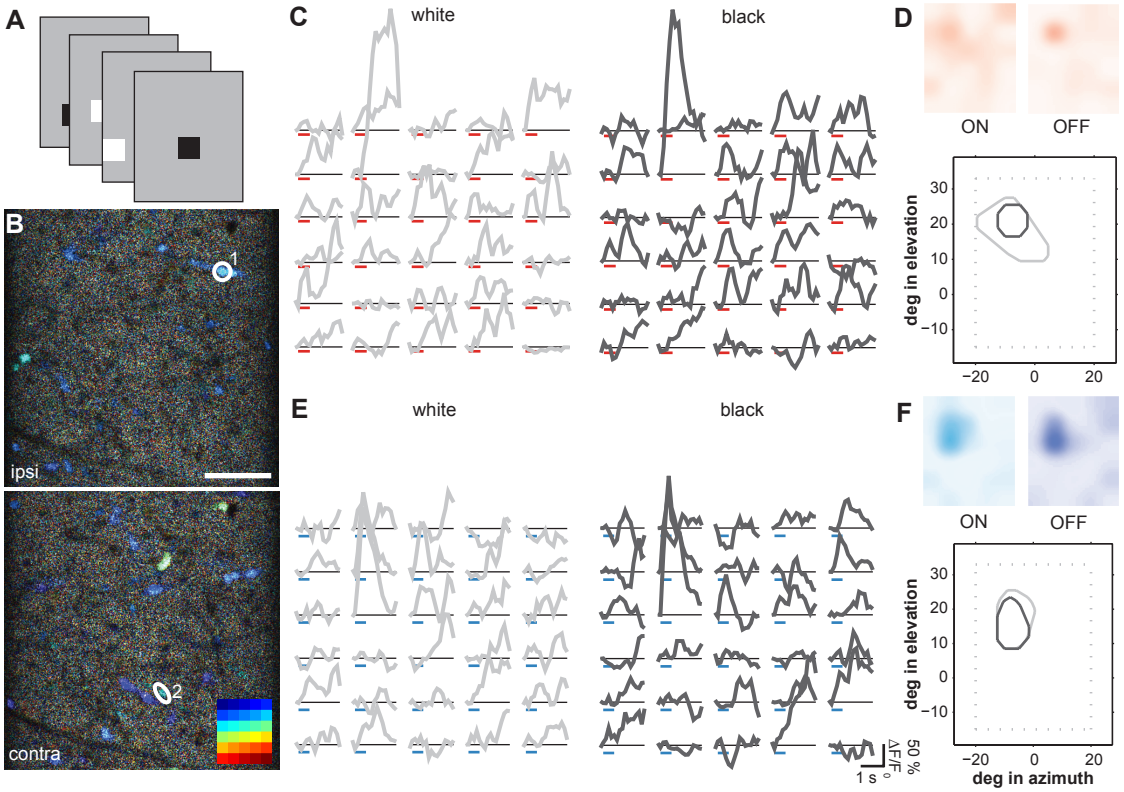

Figure 3.9: **Example of spatial receptive field properties of TRC boutons. A** Schematic of receptive field mapping stimuli: black and white patches on a gray background. **B** Pixel-based map of receptive field position for the ipsilateral (upper panel) and contralateral (lower panel) eye mapped with a 5x6 visual stimulation grid. Position of each stimulus is colour-coded and shown in the lower right corner. Scale bar: 10 µm. **C, E** Responses of an ipsilaterally (C) and a contralaterally (E) tuned bouton to white (left panel) and black squares (right panel) at different locations. Calcium traces were derived from the boutons marked in B (C from ROI 1, E from ROI 2) **D, F** Receptive fields of the corresponding boutons in C/E. Lower panels indicate outlines of the ON and OFF receptive fields (grey: ON field, black: OFF field).

axis) were calculated. In general, the majority of receptive fields were relatively small, both for ipsilateral and contralateral eye stimulation, with an area size between 100 and 400 deg^2 for most boutons and a median of 195 ± 88 deg^2 (IQR), respectively (Fig. 3.10 A). The shape of the fields was not very elongated as indicated by the low aspect ratio (major axis length divided by minor axis length, Fig. 3.10 D) and the small difference between major and minor axis lengths (Fig. 3.10 B/C).

This was quite comparable to Roth et al., 2016, who measure receptive field properties of LP and TRC boutons. In this study, TRC boutons have much smaller (median 183 deg^2) receptive fields than LP boutons (median 415 deg^2). Aspect ratio (median 1.26) and

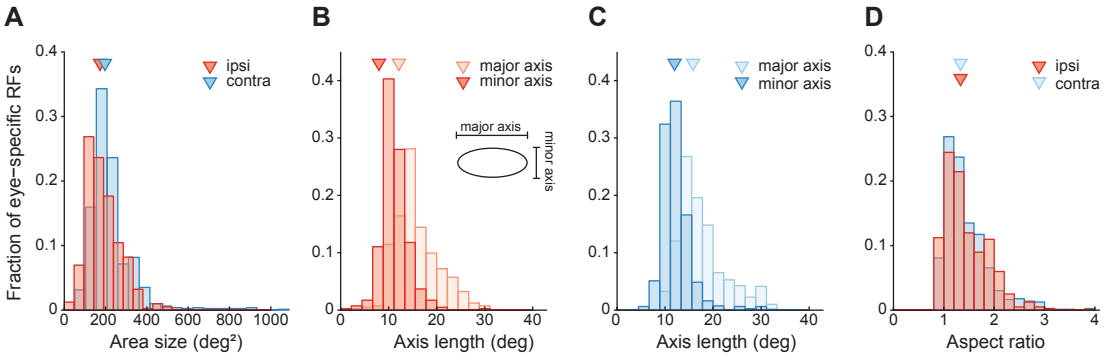

Figure 3.10: **Spatial receptive field properties of TRC boutons.** Distribution of spatial receptive field size (A), of minor and major axis length (B, C) and the ratio of major to minor axis length (D) of ipsilateral (A, B, D) and contralateral (A, C, D) receptive fields of TRC boutons in layer I. Triangles indicate medians (n = 1198 receptive fields, 9 mice).

length of major and minor axis are similar between those two nuclei. Similarly, a recent electrophysiological study (Durand et al., 2016) comparing visual response properties in dLGN and V1 of awake and anaesthetized mice observes small receptive fields that are six times smaller than the receptive fields of LP cells. Therefore, it seemed unlikely that there was a substantial contamination of my data with projection from LP.

Receptive fields evoked by the ipsilateral eye were slightly but significantly smaller than those evoked by the contralateral eye (ipsi: 173.5 ± 11 deg^2, n = 402 receptive fields; contra: 197 ± 84.5 deg^2, n = 796, $P < 10^{-12}$, Mann-Whitney test). Similarly, both major (ipsi: 15 ± 6 deg, contra: 16 ± 6 deg, $P < 10^{-9}$) and minor (ipsi: 11 ± 4 deg, contra: 12 ± 3 deg, $P < 10^{-10}$, Mann-Whitney U test) axis of the ipsilateral receptive fields were smaller. However, the aspect ratio was comparable between ipsilateral and contralateral receptive fields (ipsi: 1.33 ± 0.60, contra: 1.33 ± 0.49, P = 0.06, Mann-Whitney U test).

Fig. 3.11 shows the RF centers of all measured RFs. The highest density was found between -20 and -5 deg in azimuth and -10 and 10 deg in elevation.

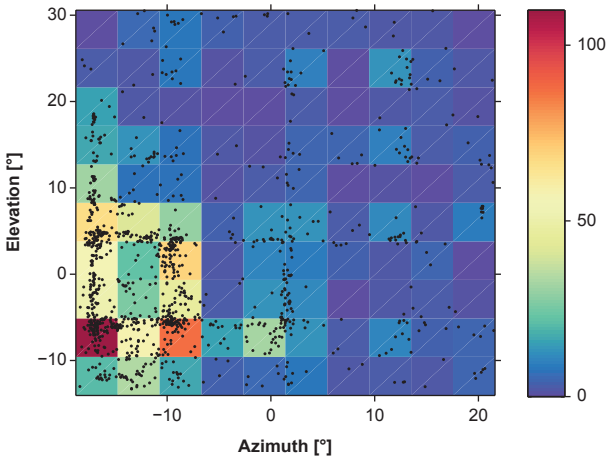

Figure 3.11: **Receptive field centers of all TRC boutons.** Distribution of TRC bouton receptive field centers from all mice across the visual field, colour coded by the number of boutons per sector (n = 1198 receptive fields, 9 mice).

3.3 Comparison with layer II/III cells in V1

Visual properties of TRC boutons in layer I of V1 were compared with layer II/III cells. For this purpose, our previously reported dataset (Rose et al., 2016) was re-analysed to match the eye-specific responsiveness criterion (see 2.2.6), as described here for TRC boutons.

3.3.1 Binocularity

Compared to TRC boutons, the fraction of binocular cells (significantly responsive to both eyes) in layer II/III (42 %) is significantly higher (Fig. 3.12 A, dLGN, n = 725 boutons, 9 mice; V1, n = 2095 cells, 14 mice, $P < 10^{-3}$, χ^2 test). The fraction of ipsilateral boutons is comparable between layer II/III cells and TRC boutons (17-19 %).

The normalized peri-stimulus population response to contralateral (blue traces) and ipsilateral moving grating stimulation (red traces, Fig. 3.12 B) is similar between TRC boutons and layer II/III cells apart from a clear response to pseudo-random eye-shutter switches in TRC boutons. Both TRC boutons and excitatory layer II/III cells showed a sustained response throughout the visual stimulus. As expected, the response to contralateral eye stimulation was stronger, both for TRC boutons and V1 cells. This suggests that under anaesthetised conditions the OD of layer II/III cells was largely determined by the integration of eye-segregated input from the dLGN.

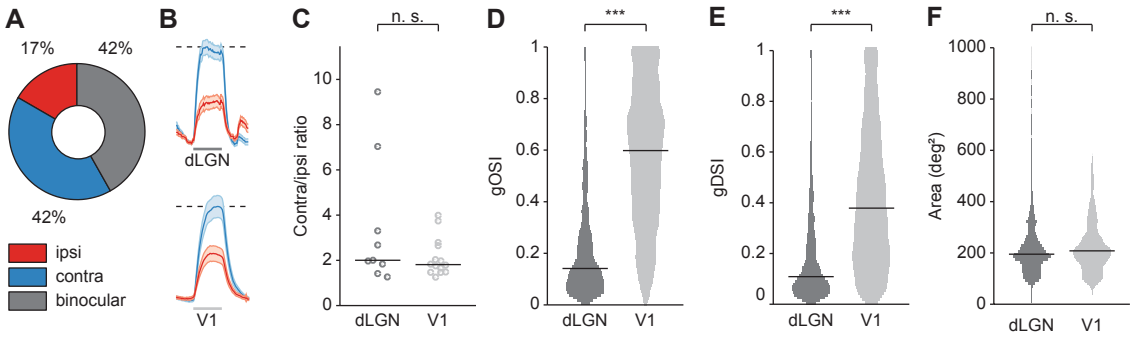

Figure 3.12: **Comparison of tuning properties of layer II/III cells and TRC boutons in layer I of V1. A** Fraction of responsive excitatory layer II/III cells showing purely ipsilateral, purely contralateral or binocular significant responses (n = 2095 cells, 14 mice) **B** Population response amplitude to visual stimulation of the contra- (blue) or ipsilateral (red) eye in TRC boutons (n = 725) and excitatory layer II/III cells (n = 2095), normalized to the peak contralateral response amplitude (dashed lines). **C** Population contra/ipsi ratios in TRC boutons and V1 cells (dLGN, n = 9 mice, V1, n = 14 mice, P = 0.36, Mann-Whitney U test). **D, E** Violin plots of gOSI (D) and gDSI (E) of TRC boutons and layer II/III cells. Horizontal lines indicate median and shaded areas the mirrored probability density estimates.(dLGN, n = 725 boutons, 9 mice; V1, n = 2095 cells, 14 mice, gOSI: $P < 10^{-193}$, gDSI: $P < 10^{-120}$, Mann-Whitney U-test). **F** Violin plots of spatial receptive field size of TRC boutons and layer II/III cells (dLGN, n = 1198 receptive fields, 9 mice; V1, n = 123 receptive fields, 14 mice, P = 0.18, Mann-Whitney U test).

Additionally, the ratio of contralateral- to ipsilateral-eye population response was calculated for each animal. For this purpose, the mean peak response to the preferred drifting grating over all boutons in response to stimulation of the contralateral or ipsilateral eye, respectively, and the resulting ratio was determined for each animal. For both V1 and dLGN, the ratio varied between 1.5 and 4 with two exceptions (Fig. 3.12 C). In these two exceptions, the ratio was very high for TRC boutons (7.03 and 9.45), resulting in a slightly higher (not significant, P = 0.36, Mann-Whitney U-test) median contra/ipsi-ratio for TRC boutons (dLGN: 2.02 ± 2.5, n = 9 mice; V1: 1.81 ± 1.17, n = 14 mice).

3.3.2 Orientation and direction tuning

Orientation and direction tuning of cells in V1 was determined by drifting grating stimulation and subsequent calculation of gOSI and gDSI. As expected (Dräger, 1975; Niell and Stryker, 2008), V1 cells were strongly orientation-tuned (median gOSI: 0.60 ± 0.41) with a high fraction of orientation-selective cells (gOSI > 0.33, median 78.3 ± 17.1 %). Thus, they were far more orientation-selective than TRC boutons (Fig. 3.12 D; median gOSI: 0.14 ± 0.19, $P < 10^{-193}$, median percentage of orientation-selective boutons: 15.69

± 18.77, $P < 10^{-10}$, Mann-Whitney U-test).

Similarly, layer II/III cells also exhibited strong direction tuning with a median gDSI of 0.38 ± 0.42, although it was less pronounced than their orientation tuning and hence the fraction of direction-selective cells is lower (gDSI > 0.33, 57.7 % ± 16.6). In comparison, TRC boutons were far less direction-selective (Fig. 3.12 E; median gDSI: 0.11 ± 0.18, $P < 10^{-120}$, median percentage of direction-selective boutons: ± 16.3, $P < 10^{-10}$. Mann-Whitney U-test).

Comparable results have been previously published (Roth et al., 2016; Sun et al., 2016a; Kondo and Ohki, 2016; Durand et al., 2016): all four studies show stronger orientation and direction tuning of layer II/III cells than layer I TRC boutons. Whereas Sun et al., 2016a observe a very similar median gOSI for layer II/III cells, the mean gOSI was considerably lower in Kondo and Ohki, 2016 (0.30 ± 0.01 SEM vs. 0.58 ± 0.01 in the present data) and consequently, also the percentage of orientation-selective cells is lower (62.9 %).

3.3.3 Spatial receptive field properties

Additionally, cortical RF size was measured using the same sparse noise stimulus as for TRC boutons. Layer II/III cells had slightly (but not significantly) bigger RFs than TRC boutons (V1, median: 208 ± 99, n = 123 RFs, 4 mice; dLGN, median 195 ± 88, n = 1198 RFs, n = 9 mice, P = 0.18, Mann-Whitney U-test).

In comparison, Roth et al., 2016 observe slightly smaller RFs for TRC boutons (184 deg^2 ± 88) and bigger RFs for layer II/III cells (246 deg^2 ± 157), resulting in a significant difference between layer II/III cells and TRC boutons. Similarly, Durand et al., 2016 also find that dLGN cells had smaller RFs than cells in V1, though the difference is not as pronounced as in Roth et al., 2016. However, data is obtained from recordings in cells throughout layer II/III to VI and the cell number is much lower than in Roth et al., 2016, especially for V1.

3.4 Experience-dependent functional plasticity of TRC boutons

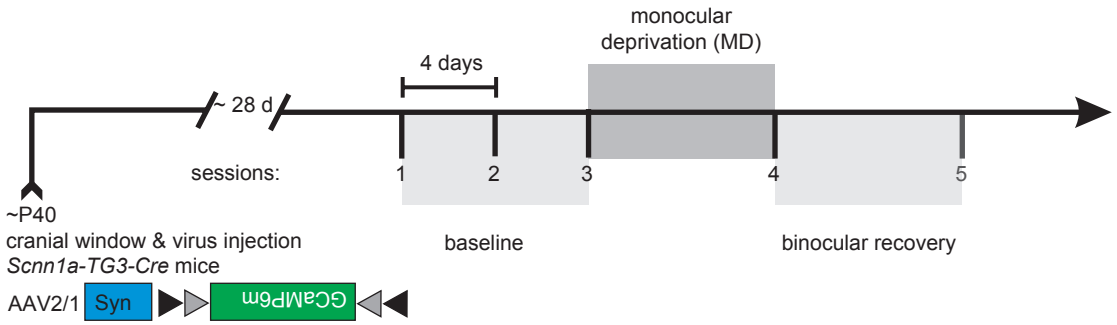

Figure 3.13: **Experimental timeline.** Around P40, virus encoding GCaMP6m was injected into the dLGN of *Scnn1a-TG3-Cre* mice, and a cranial window was implanted. Approximately four weeks later, GCaMP6m expression was sufficient and stable for imaging, and mice underwent three baseline two-photon imaging sessions that were spaced four days apart. After the third baseline imaging session, the contralateral eye was closed for 6-8 days. Subsequently, animals were imaged again for up to two imaging sessions.

For this study, nine *Scnn1a-TG3-Cre* mice expressing GCaMP6m in dLGN underwent chronic *in vivo* two-photon calcium imaging and monocular deprivation of the contralateral eye. The visually evoked activity of the same thalamocortical axons was followed in layer I of the binocular visual cortex over a period of up to four weeks (Fig 3.13). In addition, intrinsic optical imaging was performed to map the representation of the ipsilateral and contralateral eye in the binocular region of V1 and to verify the cortical OD shift in all imaged animals. All dLGN injections were post hoc verified histologically.

3.4.1 Intrinsic optical imaging of OD plasticity in adult mice

For intrinsic optical imaging, elongated visual stimuli were presented at two neighbouring positions in front of the animal, resulting in evoked activity in retinotopically corresponding regions in V1 (Fig 3.14 A, B). As expected, the neighbouring stimuli elicited responses in neighboring regions of the visual cortex as indicated in colour-coded retinotopic maps, in which each pixel was assigned the colour of the stimulus position that evoked the strongest response. OD shifts were determined by calculating the ocular dominance index (ODI) at each time point.

As expected (Hofer et al., 2009), contralateral MD resulted in a shift of the OD of the binocular visual cortex towards the open ipsilateral eye (Fig 3.14 C, $P = 0.0006$, Kruskal-

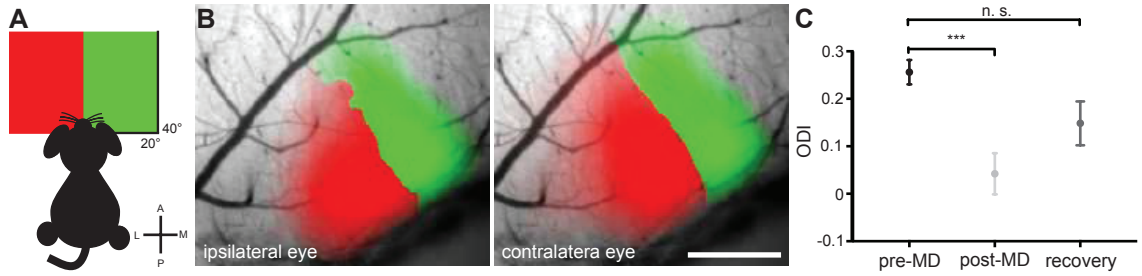

Figure 3.14: **OD plasticity was verified with intrinsic optical imaging. A** Schematic of stimulus presentation: Visual stimuli were presented at two different spatial locations on a screen in front of the mouse. **B** Colour-coded maps of the responses to stimulation of the ipsilateral (left panel) or contralateral (right panel) eye during baseline conditions. Scale bar: 0.5 mm. **C** ODI values for normal adult mice (mean 0.26 ± 0.03 SEM, n = 9), after 6-8 days of MD (0.04 ± 0.04, n = 9), and after 1-2 weeks of recovery (0.15 ± 0.05, n = 6, all: $P < 10^{-4}$, Kruskal-Wallis, Bonferroni corrected, baseline vs. MD P = 0.0006, baseline vs. recovery P = 0.45, MD vs. recovery P = 0.41).

Wallis, Bonferroni corrected for multiple comparisons). After at least one week of normal vision by both eyes, the binocular responses and thereby the ODI slowly recovered (Fig 3.14 C, P = 0.41). I therefore confirmed that the animals which I used for imaging of TRC boutons expressed cortical OD shifts.

3.4.2 TRC boutons show robust OD plasticity

Using *in vivo* two-photon imaging, individual TRC boutons were repeatedly imaged during at least three baseline sessions and directly after contralateral eye MD. I recorded four image planes separated by 3 μm in rapid succession. Due to small changes in tissue morphology and positioning inaccuracies, individual boutons might be optimally sectioned by different imaging planes at different time points. Thus, automatically detected boutons were manually matched across all time points (Fig. 3.15). At each time point, visual stimuli consisting of drifting gratings presented to one eye at the time were used to assess functional properties, such as eye-specific response amplitudes and ODI, of the TRC boutons.

A representative experiment for one mouse is shown in Fig. 3.16 A: Pixel-wise ODI maps of all matched boutons that were responsive throughout all baseline sessions and after MD, of this animal are displayed. The boutons are sorted by their pre-MD (third baseline session) ODI. As previously observed, most of the boutons are contralaterally dominated during the baseline, resulting in mostly blue-appearing boutons in the pixel-maps. When

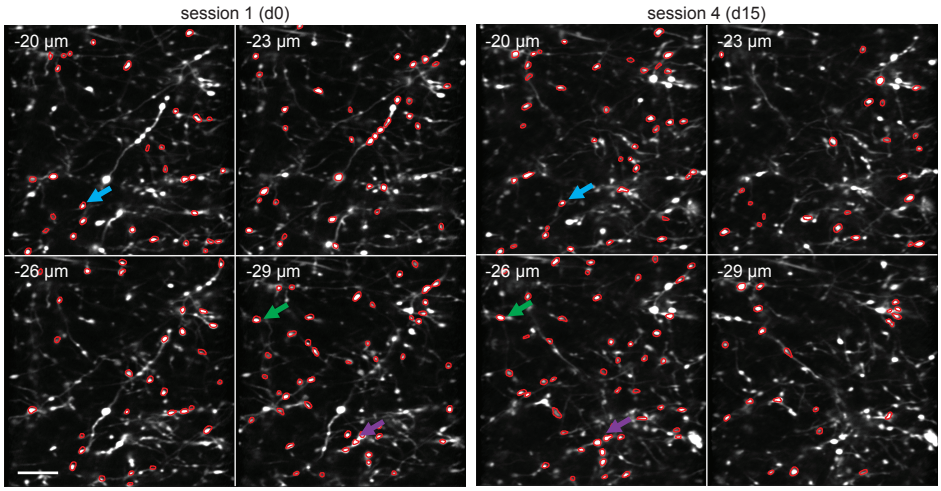

Figure 3.15: **Matching of regions of interest (ROIs) across sessions.** Two example volumes from the same imaging region spaced 15 days apart with their corresponding ROIs illustrating the matching of boutons across sessions. Arrows of the same colour indicate ROIs of the same group, image plane depth increment: 3 µm, first plane of volume 20 µm below pial surface; scale bar: 10 µm.

comparing individual boutons throughout all session, the structure remains similar - illustrating that those boutons are very well matched in all time points. The functional property, the ODI, is quite stable from one baseline session to the next. Only few boutons, such as bouton number 49, display a change in colour (e. g. from light blue to dark blue) due to a change in their ODI (more contralaterally dominated). Strikingly, after MD, many previously blue boutons switch to a light-blue or even red colour (more ipsilateral dominated), indicating a prominent change in their ODI.

An additional qualitative example is show in Fig. 3.16 B. For a single bouton, the calcium traces in response to drifting grating stimulus presentation to either the ipsi- or the contralateral eye throughout selected sessions are displayed, showing a decrease in visual responsiveness evoked by the contralateral eye and an increase in responsivness towards ipsilateral eye stimulation transiently after MD.

The effects of contralateral MD are analysed in Fig. 3.17. Generally, there seemed to be a reversible shift towards the open, ipsilateral eye. This is illustrated for one animal and all of its boutons that were responsive throughout all imaging sessions in panel A. During baseline, there were only small changes in the ODI of individual boutons (with one exception). After MD, many boutons showed a decrease in their ODI leading to an overall lower mean ODI (black line). Binocular visual experience for one week reversed this effect, both on the level of individual boutons and the mean ODI, demonstrating that

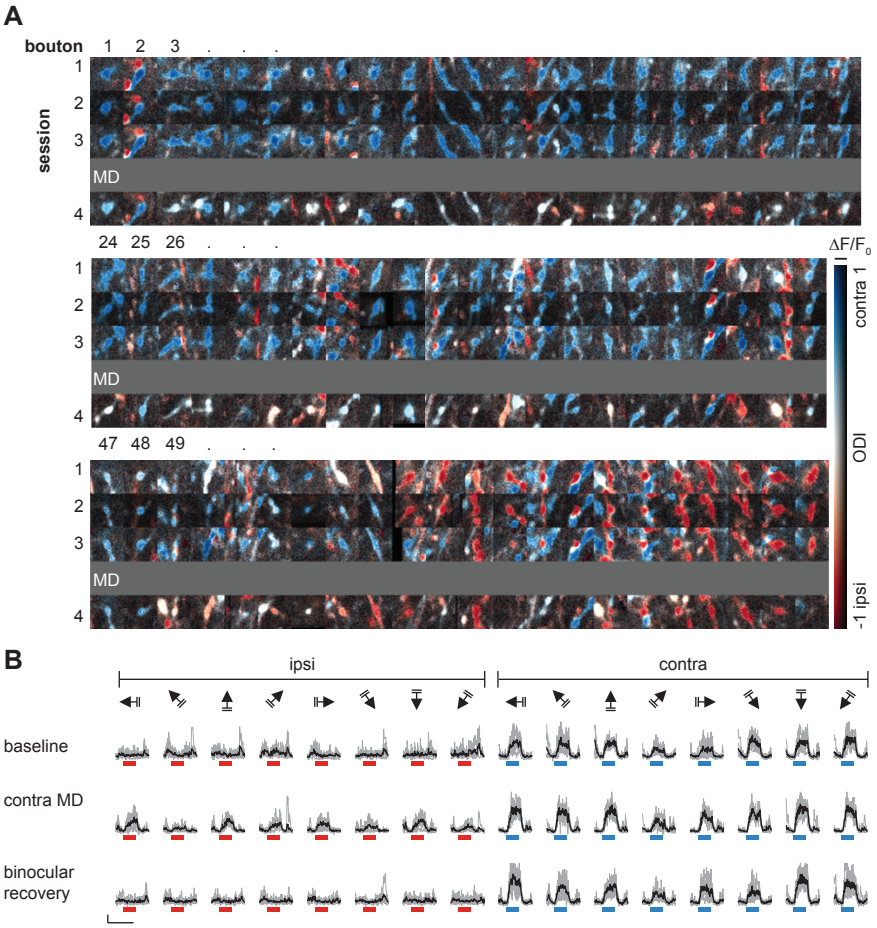

Figure 3.16: **Example of changes in response properties after MD. A** Functional map examples of TRC boutons of a single animal (sorted by pre-MD ODI) imaged over four sessions before and after contralateral-eye MD. **B** Calcium signals in an example bouton in response to ipsi- and contralateral eye drifting grating stimulation over selected sessions covering OD plasticity (scale bars: $\Delta F/F_0 = 200$ %, 10 s).

the shift in ODI is reversible on the single-bouton level.

The data of all animals is summarized in Fig. 3.17 B. Based on their ODI, boutons that were responsive throughout all baseline sessions and after MD were divided into seven classes. Class 1 consisted of strongly contralateral boutons, whereas strongly ipsilateral boutons were in class 7. During baseline (left histogram), most TRC boutons were classified as strongly monocular (class 1 and 7), but the contralateral boutons acquired binocularity after MD leading to an increased fraction of boutons in the middle classes (right histogram). The mean monocularity index (MI) reflects this: It is calculated as the absolute value of the ODI and varies between 1 and 0 with 0 indicating that the same response was elicited in each eye. It significantly changes from 0.71 ± 0.23 (SD) during baseline to 0.63 ± 0.30 after MD (n = 258 boutons, 9 mice, P = 0.0016, Wilcoxon signed-rank test).

Equally prominent was the general shift towards the open, ipsilateral eye, resulting in a highly significant decrease in the mean ODI from 0.40 ± 0.63 SD to 0.19 ± 0.67 ($P < 10^{-8}$, Wilcoxon signed-rank test). This was due to a large fraction of plastic boutons (Fig. 3.17 C), meaning boutons with a change in their ODI that was greater than at least one standard deviation over pre-MD baseline fluctuation. Roughly a quarter of the plastic boutons (37 out of 142) were "counter-shifters", i. e. boutons that shifted towards the closed, contralateral eye. In addition to shifting boutons, there was a loss of responsive boutons (Fig. 3.17 D, P = 0.021, χ^2 test), leading to a drop from 52 to 46 % responsive boutons.

3.4.3 MD evokes deprived-eye depression and open-eye strengthening

Did this OD shift result from a decrease in contralateral or an increase in ipsilateral eye responsiveness? In cortical neurons, deprived-eye depression is the dominant driving force of the OD shift during critical period (Frenkel and Bear, 2004), while open-eye strengthening is the primary mechanism of adult OD plasticity (Espinosa and Stryker, 2012). Adult mice housed in an enriched environment or stimulated with high-contrast stimuli during MD show a juvenile-like MD effect: The shift towards the open eye is mainly driven by a decrease in contralateral responsiveness, even in old animals (Greifzu et al., 2014)

On the population level, the OD shift in TRC boutons resulted both from a decrease in

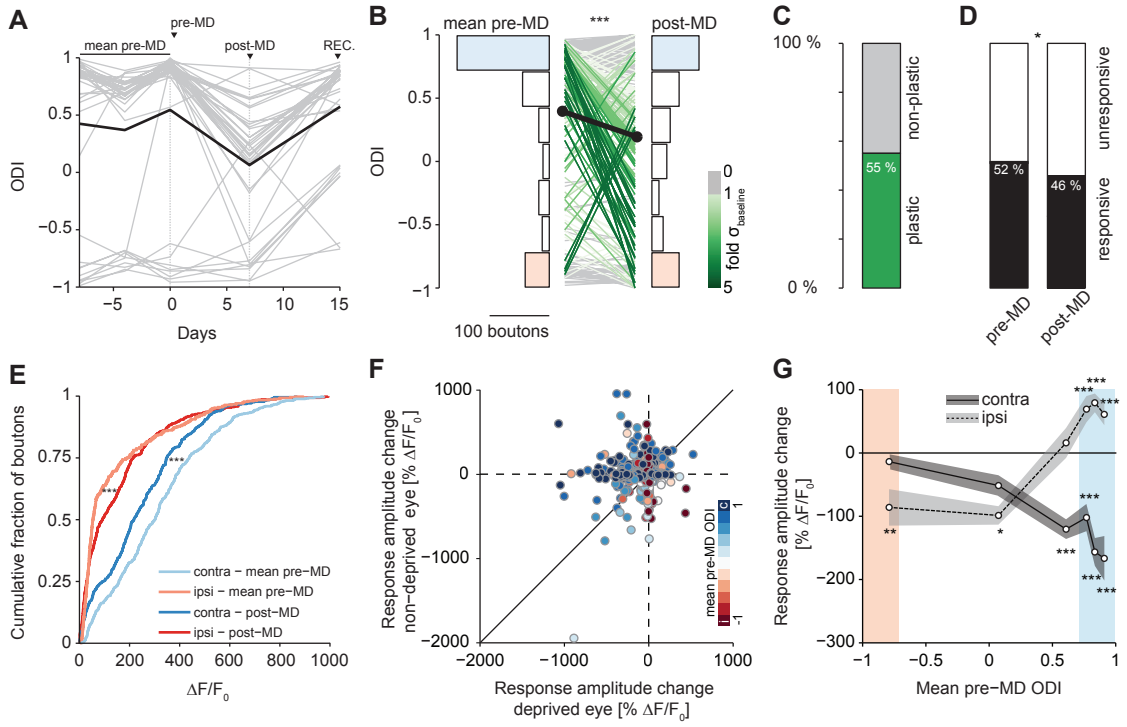

Figure 3.17: **TRC boutons show robust and specific OD shifts after MD. A** Example time course of TRC single-bouton ODI (gray lines) from one animal over baseline, contralateral eye MD and recovery (black line: mean ODI). **B** Single-bouton ODI distribution during baseline (mean of three pre-MD sessions, ODI = 0.40 ± 0.63, standard deviation, SD) and after 6-8 days of MD (post-MD: ODI = 0.19 ± 0.67, SD, n = 258 boutons, 9 animals, $P < 10^{-8}$, Wilcoxon signed-rank test). Lines connect individual, continuously responsive boutons; line colour indicates shift significance in units of SDs over pre-MD baseline fluctuations. Coloured ODI histogram bins indicate class definitions for contralateral (blue), binocular (white) and ipsilateral (red) boutons. **C** Fraction of boutons showing a significant (>1 SD) MD-evoked ODI change (n = 142 out of 258 boutons). **D** Fraction of responsive and unresponsive boutons before and after MD (n = 896 boutons, P = 0.021, χ^2 test). **E** Cumulative eye-specific response amplitude before and after MD (n = 456 TRC boutons, responsive during baseline and post-MD, ipsilateral eye responses baseline vs. post-MD $P < 10^{-5}$, contralateral eye responses baseline vs. post-MD $P < 10^{-6}$, two-sample Kolmogorov-Smirnov tests). **F** Bouton-wise change in eye-specific response amplitude after MD (n = 352 boutons responsive in all pre-MD sessions, colour-coded for mean pre-MD ODI). **G** Quantification of E, grouped into pre-MD ODI sextiles comprising similar numbers of boutons (58-59 boutons per class, paired t-tests; monocular ODI classes indicated by red and blue shading as defined in D).

contralateral eye and an increase in ipsilateral eye responsiveness (Fig. 3.17 E). More precisely, the cumulative distribution of the contralateral responses shifted nearly uniformly to the left (blue curves, n = 456 boutons, responsive during baseline and after MD, 9 animals, $P < 10^{-6}$, two-sample Kolmogorov-Smirnov test), while there was a more specific increase in the ipsilateral responsiveness resulting in a different shape of the distribution (red curves, same boutons, $P < 10^{-5}$, two-sample Kolmogorov-Smirnov-test).

Fig. 3.17 F shows the bouton-wise change in eye-specific responses (for boutons that were responsive throughout all baseline sessions). The eye-specific change in response amplitude is indicated on the axes, while the colour code indicates the pre-MD ODI. There was a high density of previously contralaterally dominated boutons in the upper left quadrant, which showed deprived eye-depression and open-eye strengthening. This is quantified in Fig. 3.17 G: Boutons that were exclusively responsive to the contralateral eye during baseline showed the most prominent decrease in contralateral-eye responsiveness and the most prominent increase in ipsilateral-eye evoked activity. Additionally, there was open-eye depression in initially ipsilaterally-driven boutons. These are the counter-shifters that shift towards the closed eye.

3.4.4 Full recovery of eye-specific tuning

After 1-2 weeks of normal binocular vision after MD, eye-specific response properties were measured again in some of the animals (Fig. 3.18). Overall, the population shift in OD was not only fully reversed after recovery, but the ODI was actually slightly increased in comparison to baseline (mean pre-MD: 0.40 ± 0.66 SD, post-MD: 0.13 ± 0.66, recovery: 0.46 ± 0.63, n = 166 boutons, 5 mice, $P < 10^{-15}$, baseline vs. MD $P < 10^{-5}$, baseline vs. recovery $P = 0.002$, MD vs. recovery $P < 10^{-16}$, Friedman's test, Bonferroni corrected). Individual boutons shift back towards their pre-MD ODI (Fig. 3.18 A). Similiarly, the MI was increased after recovery in comparison to after MD (mean pre-MD: 0.75 ± 0.20 SD, post-MD: 0.60 ± 0.30, recovery: 0.73 ± 0.28, $P < 10^{-5}$, baseline vs. MD $P < 10^{-4}$, baseline vs. recovery $P = 1$, MD vs. recovery $P < 10^{-5}$, Friedman's test, Bonferroni corrected).

Likewise, after recovery, the eye-specific response amplitudes resembled those of the baseline session. After an overall increase in ipsilateral response strength, they decreased after recovery, even below baseline levels (mean pre-MD: 157.5 $\Delta F/F_0$ ± 16.4 % SD, post-MD: 215.8 $\Delta F/F_0$ ± 16.5 %, recovery: 119.39 $\Delta F/F_0$ ± 14.6 %, $P < 10^{-13}$, baseline vs. MD $P = 0.01$, baseline vs. recovery $P < 10^{-6}$, MD vs. recovery $P < 10^{-13}$, Friedman's test, Bonferroni corrected). This is likely the reason why the mean ODI was lower after recovery

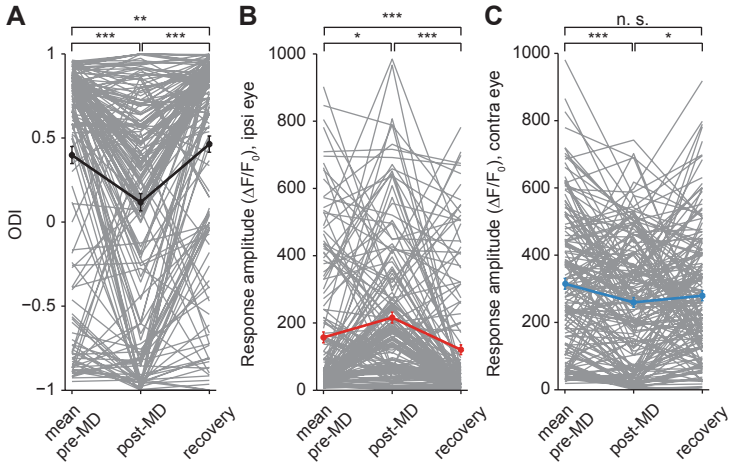

Figure 3.18: **Recovery of individual TRC boutons after binocular vision. A** ODI of boutons (n = 166 boutons from 5 mice, responsive during baseline, MD and recovery) after MD and at least one week of binocular vision ($P < 10^{-15}$, baseline vs. MD $P < 10^{-5}$, baseline vs. recovery $P = 0.002$, MD vs. recovery $P < 10^{-16}$, Friedman's test, Bonferroni corrected). **B** Response amplitude to ipsilateral eye stimulation after MD and at least one week of binocular vision ($P < 10^{-13}$, baseline vs. MD: $P = 0.01$, baseline vs. recovery $P < 10^{-6}$, MD vs. recovery $P < 10^{-13}$, Friedman's test, Bonferroni corrected). **C** Response amplitude to contralateral eye stimulation after MD and at least one week of binocular vision ($P < 10^{-5}$, baseline vs. MD $P < 10^{-6}$, baseline vs. recovery $P = 0.06$, MD vs. recovery $P = 0.04$, Friedman's test, Bonferroni corrected).

in comparison to baseline.

The opposite is true for the response amplitude after contralateral eye stimulation: It decreases after MD and increases after recovery, but does not fully recover (mean pre-MD: 314.3 % $\Delta F/F_0$ ± 16.4 SD, post-MD: 262.3 % $\Delta F/F_0$ ± 14.7, recovery: 279.39 % $\Delta F/F_0$ ± 15.2, $P < 10^{-5}$, baseline vs. MD $P < 10^{-6}$, baseline vs. recovery $P = 0.06$, MD vs. recovery $P = 0.04$, Friedman's test, Bonferroni corrected).

3.4.5 Verification of stereotactic injections

At the end of these chronic experiments, all injections were post-hoc verified. For that purpose, brains were sliced and GCaMP6m labelling was reinforced with immunohistochemical staining against GFP and cellular nuclei were visualized using DAPI staining (Fig. 3.19).

All mice that underwent chronic two-photon calcium imaging showed GCaMP6m-expression in neurons of the dLGN. Although there was some virus spread towards PoM and VPM,

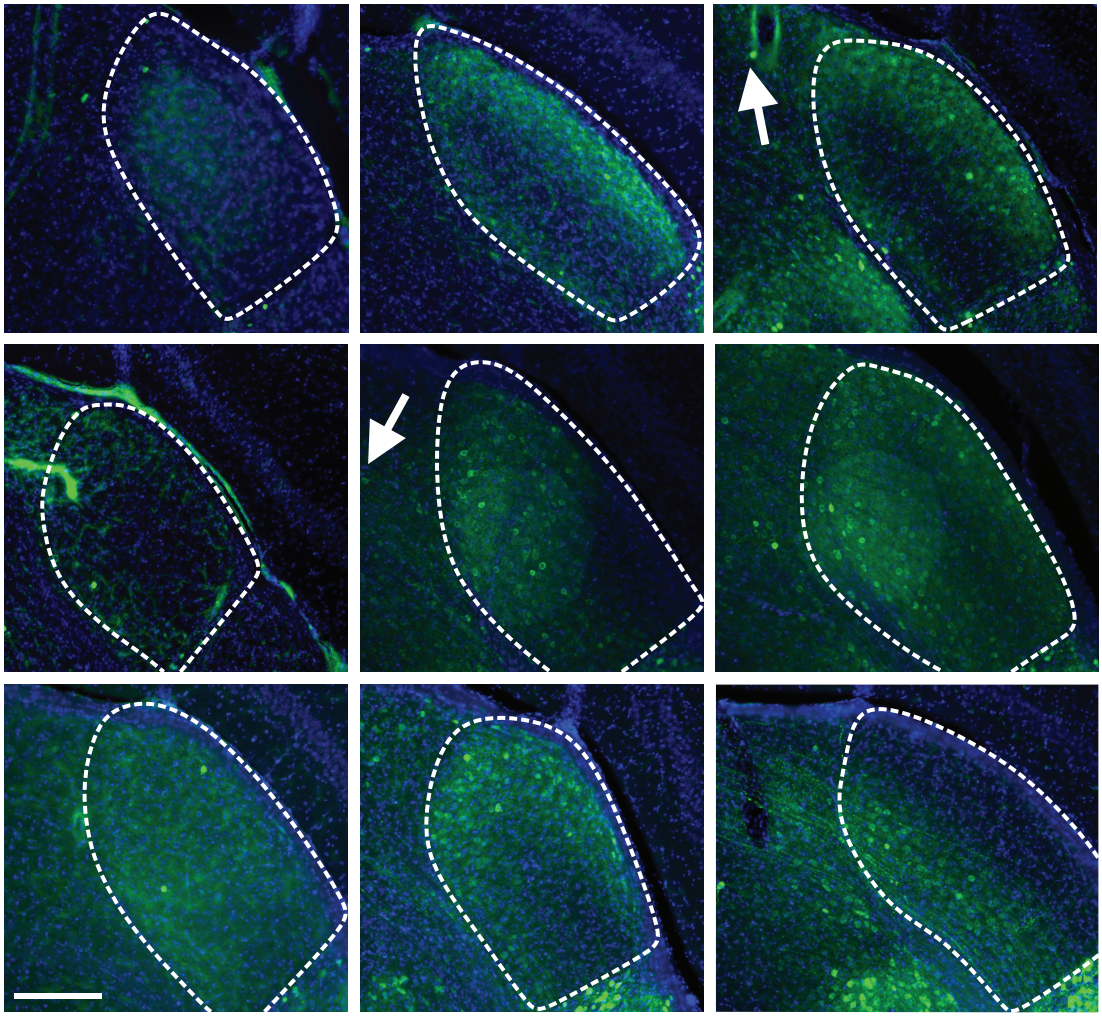

Figure 3.19: **Verification of stereotactic injections.** Coronal sections showing GCaMP6m-labeled neurons (green) and nuclear marker DAPI (blue) in the dLGN of all nine mice that underwent MD and chronic two-photon imaging. Arrows point toward putative GCaMP6m expression in LP. Scale bar: 200 μm.

nearly no neurons were labelled in the medially neighbouring region LP (see arrows).

4 Discussion

Traditionally, the thalamus, especially the dLGN, has been thought of as a relay transmitting sensory information from the periphery to the (visual) cortex without major changes to the transmitted signal. However, in recent years, this view slowly started to change with the discovery of functionally more sophisticated properties such as binocularity (Howarth et al., 2014), orientation and direction selectivity (Marshel et al., 2012; Piscopo et al., 2013; Cruz-Martín et al., 2014) or modulation by running (Erisken et al., 2014; Roth et al., 2016). Additionally, anatomical connections between the retina and the dLGN are far more complex than previously assumed (Hammer et al., 2015; Morgan et al., 2016; Rompani et al., 2017)). These new features provide the possibility of a more complex role of TRCs in experience-dependent plasticity. Similar to thalamocortical axon retraction following long-term MD in juvenile mice (Antonini et al., 1999), there is evidence for structural long-term changes (De Paola et al., 2006; Wimmer et al., 2010; Yu et al., 2012; Oberlaender et al., 2012) following nerve damage and sensory deprivation in adulthood. However, so far, activity-dependent changes after segregation of eye-specific inputs to the dLGN and robust OD changes in the dLGN have not been reported at all. Moreover, a functional thalamic component to experience-dependent cortical plasticity seemed unlikely (Fox et al., 2002).

In this thesis, I re-evaluated the functional properties of TRCs and their role in experience-dependent plasticity. To this end, I specifically labelled thalamocortical axons in layer I of the binoculuar visual cortex with the functional indicator GCaMP6m. Using chronic two-photon *in vivo* imaging, I was able to follow and characterize the same TRC boutons over several weeks.

The main findings of these thesis are: 1. Binocular TRCs were present, but more rarely than previously reported using *in vivo* electrophysiology. 2. TRCs robustly and reversibly shifted their OD tuning following MD. This was due to a decrease in contralateral responsiveness and a gain of binocularity by an increase in responsiveness evoked by visual stimulation of the ipsilateral eye.

4.1 Specific labelling of thalamocortical axons in layer I of binocular visual cortex

Difficulties with virus expression in the dLGN initially hindered functional characterization of TRCs projecting to layer I. For unknown reasons, only labelling with GCaMP6m was successful, whereas other indicators resulted in none or only very few labelled axons. The difference between the related indicators GCaMP6m and GCaMP6s or GCaMP6f are only a few amino acids, resulting in minor changes in kinetics and sensitivity (Chen et al., 2013). Surprisingly, several other studies achieved the expression of GCaMP6s (Sun et al., 2016a; Kondo and Ohki, 2016) or GCaMP6f (Roth et al., 2016) in dLGN for imaging of TRC boutons in layer I. It can only be speculated that the difference lies in the applied injection method (Hamilton syringe in this dataset in comparison to thin glass pipettes in all other studies), possibly resulting in a different level of infection of individual cells. Perhaps lowering the viral titer might have enabled the expression of other calcium indicators - however, potentially at the cost of a lower expression level.

Similarly, it was not possible to express two different fluorophores simultaneousy, probably due to two reasons: On the one hand, TRCs might be more sensitive to changes in intracellular calcium levels than, for example, cortical cells, leading perhaps to cell death. On the other hand, expression of two fluorophores generally leads to an overall lower expression level.

After testing numerous constructs, I accomplished specific labelling of thalamocortical axons by a combination of an AAV coding for a floxed GCaMP6m in combination with the Cre driver line *Scnn1a-TG3-Cre*. Specificity was validated as followed:

1. Post-hoc stainings for GCaMP6m verified that injections were restricted to the thalamus without virus expression in cortical cells above the injection site. This simultaneously confirmed the specificity of the Cre driver line, which should not express in the cortex. Importantly, only very few cells in LP expressed GCaMP6m.

2. Injections resulted in the expected projection pattern in visual cortex with highest density of axons in layer IV, additional axons in layer I and only very few axons in layer II/III (see also Ji et al., 2016).

3. The average receptive field size of TRC boutons was similar to previous reports: 195 ± 88 deg^2. Importantly, receptive fields of LP neurons are at least more than two-fold

bigger (Roth et al., 2016; Durand et al., 2016), thereby confirming specificity of TRC bouton labelling and exclusion of contamination from LP neurons.

4.2 Functional characterization of TRC boutons

4.2.1 Binocularity

The presence of binocular neurons in the dLGN of the mouse has been debated. A single-cell initiated transsynaptic study provides evidence for the existence of binocular TRCs (Rompani et al., 2017). Electrophysiological studies support both their absence (Grubb et al., 2003; Ziburkus and Guido, 2006) and presence (Howarth et al., 2014). However, multielectrode recordings, as used in these studies, face the difficulty of single unit isolation. Two-photon calcium imaging, which I applied in this study, circumvents this problem because axon boutons can be spatially distinguished.

I observed binocular TRCs, albeit to a lower percentage than reported recently in an electrophysiological study (Howarth et al., 2014). More specifically, in the electrophysiological study, there are two striking differences to the data presented here: First, in contrast to my data, no cells exhibited purely ipsilateral visual responses. Second, in the part of the dLGN that projects to binocular visual cortex (and hence should represent the same population of cells I recorded from), the majority of cells exhibited binocular responses. Additionally, Howarth et al., 2014 observed cells that show a facilitation of contralateral-driven responses to bright stimuli to the ipsilateral eye, or antagonistic responses (for example ipsilateral ON and contralateral OFF responses). These differences might be due to difficulties in single unit isolation in multielectrode recordings or other subtle methodological differences.

Binocular cells are also present in rats (Grieve, 2005, 27 % of all cells, no purely ipsilaterally driven cells) and the monkey (Zeater et al., 2015, 29 % , restricted to K cells). Moreover, binocular cells in the monkey are specifically identified as neurons in the koniocellular layer, this argues for a separate channel of visual processing possibly important for form and motion analysis (Zeater et al., 2015). Subcortical projections from the superior colliculus specifically targets these cells, which is similar to W-like cells in the shell region of the mouse dLGN, leading to the hypothesis that mouse W-like cells might be equivalent to the primate K cells (Krahe et al., 2011; Wallace et al., 2016). It is rather unlikely however, that all W-like cells are binocular, as not all of the W-like cells are located in the binocular part of mouse dLGN. I investigated whether binocular TRCs are different from monocular TRCs by comparing their orientation and direction selectivity. There was no significant difference. However, binocular TRCs could still represent a separate processing channel. They receive input from more RGCs as well as more RGC types

than monocular TRCs (Rompani et al., 2017). Additional experiments are necessary to look for differences in, for example, spatial and temporal frequency preferences, contrast-sensitivity and modulation by running.

Compared with binocular cells in layer II/III of binocular V1, the percentage of binocular TRC boutons is significantly lower. This support the notion that cells in V1 integrate the eye-segregated dLGN input leading to a higher percentage of binocular cells. However, the C/I ratio was comparable between dLGN and V1. Therefore at the population level, the dLGN contra/ipsi input appears to be enough to explain cortical binocularity in the anesthetized state. This argues against the theory that much of the ipsilateral input is provided by callosal projections (Dräger, 1975; Dräger, 1978), although callosal axons might still contribute ipsilateral input.

4.2.2 Orientation and direction selectivity

In addition to binocularity, TRCs exhibit clear orientation and direction selective responses (see Fig. 3.6 D for examples).

Three other studies quantify orientation and direction selectivity in thalamocortical axons in layer I of the visual cortex (Sun et al., 2016a; Roth et al., 2016; Kondo et al., 2016; see also table 4.1). In all studies, the median OSI is higher, between 0.44 and 0.56 (OSI). Additionally, the fraction of orientation-selective (OSI $>$ 0.5 or gOSI $>$ 0.33) boutons is at least 30 % in the other studies. However, in one electrophysiological study recording from cells in the dLGN (Durand et al., 2016), the mean gOSI is similar with a mean of around 0.2.

However, two of those studies also investigate orientation tuning in TRC boutons in layer IV of V1 and reach different conclusions: While Kondo and Ohki, 2016 calculate a mean gOSI of 0.20 (and therefore less orientation-selectivity compared to layer I with a mean of 0.32), Sun et al., 2016a find a similar level of orientation-selectivity in both layers (median of 0.27 in both layers). Thus it appears that slight methodological differences can lead to different conclusions.

Importantly, there are also several methodological differences in the three imaging studies in comparison to my data: 1. In other studies, data is derived from TRC boutons in both monocular and binocular V1. In contrast, I selectively recorded activity from TRC boutons projecting to binocular V1. As seen in Fig. 3.11, I specifically targeted TRC boutons with a RF of -15 to 30 deg in elevation and -20 to 20 deg in azimuth. Piscopo et al.,

	This dataset	Sun et al. (2016a)	Roth et al. (2016)	Kondo and Ohki (2016)	Durand et al. (2016)
TRC boutons in layer I of V1					
OSI	*median: 0.35*	median: 0.56	median: 0.44	mean: 0.47	n. a.
gOSI	*median: 0.14*	median: 0.25 for OS, 0.12-0.13 for non-OS	n. a.	mean: 0.32	mean: 0.22
OSI > 0.5	*19.9 %*	≈ 50* %	≈ 30 %	n. a.	n. a.
gOSI > 0.33	*15.7 %*	n. a.	n. a.	41.3 %	n. a.
DSI	*median: 0.29*	median: 0.46 for OS	median: 0.25	mean: 0.22	mean: 0.37
DSI > 0.5	*19.9 %*	≈ 25 %	≈ 10 %	27.6 %**	n. a.
Receptive field size	*median: 195 deg^2*	n. a.	median: 183 deg^2	n. a.	mean: 101.6 deg^2
layer II/III cells in V1					
OSI	*median: 0.71*	median: 0.78	median: 0.74	mean: 0.62	n. a.
gOSI	*median: 0.6*	median: 0.58	n. a.	mean: 0.46	mean: 0.42
OSI > 0.5	*62.9 %*	≈ 83* %	≈ 90 %	n. a.	n. a.
gOSI > 0.33	*78.3 %*	n. a.	n. a.	62.9 %	n. a.
DSI	*median: 0.55*	median: 0.37	median: 0.51	mean: 0.27	mean: 0.48
DSI > 0.5	*55.3 %*	≈ 52 %	≈ 50 %	45.1 %**	n. a.
Receptive field size	*median: 208 deg^2*	n. a.	median: 246 deg^2	n. a.	mean: 122.3 deg^2
Technical details					
Indicator	*GCaMP6m for TRC boutons, GCaMP6s for V1 neurons*	GCaMP6s	GCaMP5g, GCaMP6m, GCaMP6f	GCaMP6s for TRC boutons, OGB-1 for V1 neurons	extracellular multisite recordings
Field of view	*binocular V1*	V1	V1	V1	dLGN or monocular V1
Objective	*Nikon 16x*	Nikon 16x, Olympus 25x	Olympus 40x	Nikon 25x, lens adjustment	
Adaptive optics	*no*	yes	no	no	

Table 4.1: **Functional properties of TRC boutons in layer I and layer II/III cells in V1 as previously compared.** n.a. = not available, OS = orientation selective, *boutons whose tuning curves were well-fitted by a bimodal Gaussian function (Sun et al., 2016a), ** DSI > 0.3 Note that values for Durand et al., 2016 are based on data acquired in cells in layer II/III to VI in V1.

2013 provide evidence that orientation- and direction-selective TRCs are more likely to occur at the dorsolateral surface and the posterior pole of the dLGN. The RF of cells at the dorsolateral surface is located at 15 to 25 deg in elevation and 0 to 20 deg in azimuth, whereas the posterior pole correspond retinotopically to an azimuth higher than 30 deg. Therefore, it can be expected that in binocular V1 the fraction of orientation- and direction-selective is lower. 2. Data from Sun et al., 2016a is derived from awake animals, whereas Kondo and Ohki, 2016 and Roth et al., 2016 use isofluorane anesthesia. In this dataset, I applied a mix of Fentanyl, Midazolam and Medetomidine. However, according to Durand et al., 2016, there is no difference in orientation and direction-selectivity in dLGN neurons in awake and anaesthetized mice, at least with urethane anesthesia. 3. Only Kondo and Ohki, 2016 correct spherical aberrations by adjusting the axial position of a lens in the objective. 4. In contrast to my data and the two other studies, Sun et al., 2016a adjust for spherical aberrations using adaptive optics. The authors comment that tuning curves of boutons are highly sensitive to optical aberrations due to differences in the refractive indices of the immersion medium, the cranial window and the brain. Depending on the thickness of the window and whether adaptive optics were applied or not, between 7 and 48 % of boutons were classified as orientation-selective. 5. Sun et al., 2016a fitted the normalized response tuning curves with a bimodal Gaussian function, possibly leading to an overestimation of orientation-tuning as it already assumes that boutons are orientation-selective. In contrast, I calculate orientation and direction tuning indices based on the peak response amplitudes in response to stimulation with all orientations and directions. 6. Sun et al., 2016a and Kondo and Ohki, 2016 studies used animals expressing GCaMP6s, which has a higher affinitiy for calcium than GCaMP6m. This could lead to sharper tuning in TRC boutons. Data from Roth et al., 2016 is acquired from animals with a variety of different GCaMPs 7. In contrast to all three studies, I imaged TRC boutons in *Scnn1a-TG3-Cre*. It is possible, that in these mice, a specific subpopulation of TRCs is labelled. However, given that I observed a variety of different response properties, this seems rather unlikely.

My results for direction selectivity are quite comparable to two of the other studies: Roth et al., 2016 calculate a similar DSI distribution with a median of 0.25 and around 10 % direction-selective boutons and Kondo and Ohki, 2016 measure a mean DSI of 0.22 and a fraction of 27.6 % direction-selective boutons (DSI $>$ 0.3). The mean DSI for the dataset presented here is 0.24 with 28.9 % of all boutons showing a DSI $>$ 0.3. In the third study (Sun et al., 2016a), however, the direction selectivity is more pronounced with a higher median DSI. This might partly be due to similar reasons as for orientation selectivity (especially 1, 4 and 5).

A study targeting specifically the shell of the dLGN, shows that 60 % of the labelled TRC boutons in layer I of V1 are direction-selective (DSI $\geq$ 0.4) and $\approx$ 85 % are orientation-selective (OSI $\geq$ 0.5) (Cruz-Martín et al., 2014), which is much higher than in my dataset. However, the number of boutons is relatively small (n = 58). Furthermore, the neurons in this area might have different characteristics for three reasons: 1. These neurons are linked to a specific circuit linking direction-selective RGCs with V1 and 2. Input from the superior colliculus is specifically targeted to this area. 3. Visual stimuli are presented around 35 deg in azimuth and 23.5 deg in elevation, which corresponds to cells located at the dorsolateral surface of the dLGN, where the fraction of orientation- and direction-selective cells is high (Piscopo et al., 2013).

For quantification of orientation and direction selectivity, I calculated both OSI/DSI and gOSI/gDSI (selectivity measure based on circular variance). Overall, OSI and gOSI as well as DSI and gDSI showed similar results as, for example, the fraction of orientation- or direction-selective TRC bouton was comparable between these indices. As gOSI/gDSI is less sensitive to noise and overall response amplitude (Mazurek et al., 2014), properties of dLGN and V1 were compared with those indices as response amplitude of layer II/III was considerably lower than in TRC boutons.

Consistent with predictions from other studies (Roth et al., 2016; Durand et al., 2016), I found that TRC boutons were significantly less orientation- and direction-selective than excitatory layer II/III cells. Importantly, the fraction of selective neurons was pronouncedly smaller in TRC boutons than in layer II/III cells. This points towards at least a partial *de novo* generation of orientation and direction selectivity in V1 as classically suggested (Hubel and Wiesel, 1962). It remains possible, although highly unlikely, that orientation- and direction-selective TRC massively diverge onto V1 neurons. Moreover, it remains unclear to which extent the observed orientation and direction selectivity in TRC boutons influences some neurons in V1. It has been suggested that selectivity in dLGN developmentally might shape and refine orientation and direction selectivity in V1 (Rochefort et al., 2011; Piscopo et al., 2013).

Recent studies suggest a direct link between direction selective RGCs (Huberman et al., 2009; Cruz-Martín et al., 2014) and orientation and direction selective TRCs in the shell of the dLGN, although a direct functional characterization of TRCs receiving input from direction-selective RGCs is still missing. Additionally, it is likely that additional mechanisms play a role in the emergence of orientation and direction selectivity: How does

orientation and direction selectivity arise in ipsilateral or binocular neurons? Based on the ipsilateral termination zone, one would assume that at least ipsilateral (if not also binocular) TRCs localize solely to the core of the dLGN, whereas those direction-selective RGCS project exclusively to the shell region.

To answer these kinds of questions, further experiments, which are slowly becoming feasible, must be carried out. For example, direct calcium imaging and characterization of dLGN neurons (as previously done in Marshel et al., 2012) in transgenic mice expressing a fluorophore in individual RGC subtypes could be combined with post-hoc input mapping. Alternatively, inputs from specific RGCs cell types or the superior colliculus could be silenced, while repeatedly characterizing binocularity and orientation and direction selectivity in individual TRC boutons in layer I.

4.3 Lateral geniculate neurons projecting to mouse V1 show robust ocular dominance plasticity

While it is known that long-term MD can lead to structural changes in thalamocortical axons (Antonini et al., 1999), so far robust changes in eye-specific responsiveness or the population OD of the dLGN have not been reported (Wiesel and Hubel, 1963a; reviewed in Sherman and Spear, 1982), leading to the assumption that experience-dependent plasticity is purely cortical.

The dLGN plays a greater computational role in visual processing than previously thought (Marshel et al., 2012; Piscopo et al., 2013; Howarth et al., 2014), and there is at least some evidence that it is more plastic than originally assumed. Particularly for juvenile MD, it has been implicated that in the monocular segment of the mouse dLGN contralateral to the deprived eye, cells compensate for MD through a homeostatic plasticity mechanism of increasing the frequency and amplitude of miniature EPSCs (Krahe and Guido, 2011), potentially reflecting an increase in corticothalamic feedback. In addition, in adult cats, blockade of visual responses in On-center RGCs with 2-amino-4-phosphonobutyric acid leads to rapid development of Off-center responses in previous On-center responsive dLGN neurons (Moore et al., 2011). This is accompanied by a decrease in response latency in these cells, leading the authors to speculate that it is not the result of polysynaptic inputs.

However, direct and *in vivo* evidence of experience-dependent functional plasticity in the thalamus has not been previously reported.

4.3.1 MD evokes changes in eye-specific responses

In this dataset, TRC boutons showed a clear OD shift after MD due to an overall net decrease in closed-eye and an increase in open-eye responsiveness. At the level of individual boutons, more than half of the boutons shifted their ODI significantly and the fraction of responsive boutons decreased. More specifically, this resulted from an overall contralateral depression combined with specific ipsilateral strengthening of boutons that were previously strongly dominated by the contralateral eye. Strikingly, this ipsilateral strenghtening was driven by cells acquiring binocularity during MD.

Why have population ODI changes in the dLGN not been reported before (e.g. Wiesel and Hubel, 1963a; reviewed in Sherman and Spear, 1982)? There are several important

differences to previous studies of OD plasticity in the dLGN:

1. The methodology: So far, none of the recordings have been performed chronically with single-cell resolution, leaving the possibility that subtle changes might have been overlooked. Most other studies are limited to comparisons between animals or at best between different cells of the same animal in the case of repeated insertion of electrodes in the same animal. Chronic electrophysiological recordings are difficult as they require strong mechanical stability and the percentage of cells dropping out within the first two weeks is very high. Additionally, extracellular recordings are biased towards very active neurons. Unfortunately, two classes of cells can be missed in such a comparison between two timepoints: 1. Silent cells, that become active and 2. Cells, that lose responsiveness. In the second case, it is not known whether the stop in responsiveness is actually due to a change in responsiveness or due to electrode issues such as slight movements of the electrode. In contrast, chronic two-photon imaging allowed me to overcome these issues and detect changes in boutons from individual cells that might have been missed before.

2. The species: Most earlier experiments were done in cats or monkeys. As briefly described, the rodent dLGN is very different from cats and primates as it is missing the strict architecture of specific, eye-segregated layers, albeit the segregation in ipsi- and contralateral RGC projection zones and separation in a core and shell region has been suggested to represent a "hidden lamination" (Reese, 1988). Furthermore, the visual cortex is remarkably different as there are no orientation- and ocular dominance columns in mice. Particularly for MD, adult OD plasticity is absent in other species, even rats (Sawtell et al., 2003), although adult OD plasticity in rats can be evoked by reduction of cortical inhibition (Vetencourt et al., 2008).

3. The age at the onset of the MD: With one exception (see below), studies focused on OD plasticity in dLGN of juvenile animals. However, it is known from cortical OD plasticity that there are qualitative differences between juvenile and adult OD plasticity (Frenkel et al., 2006; Ranson et al., 2012). It would be very interesting to investigate whether there is also a difference in thalamic OD plasticity between juvenile and adult mice. In her PhD thesis, Linden, 2008 looked at dLGN firing rate before and after MD for 30 min, both in juvenile and adult awake mice. She observed a reduction in simultaneous firing rates of neighbouring neurons. Additionally, in adult, but not juvenile mice, MD lead to a decrease in burst activity, already implying some contribution of dLGN to cortical plasticity. As structural changes in thalamocortical axons have been previously described after several weeks of juvenile MD (Antonini et al., 1999), these structural changes could be

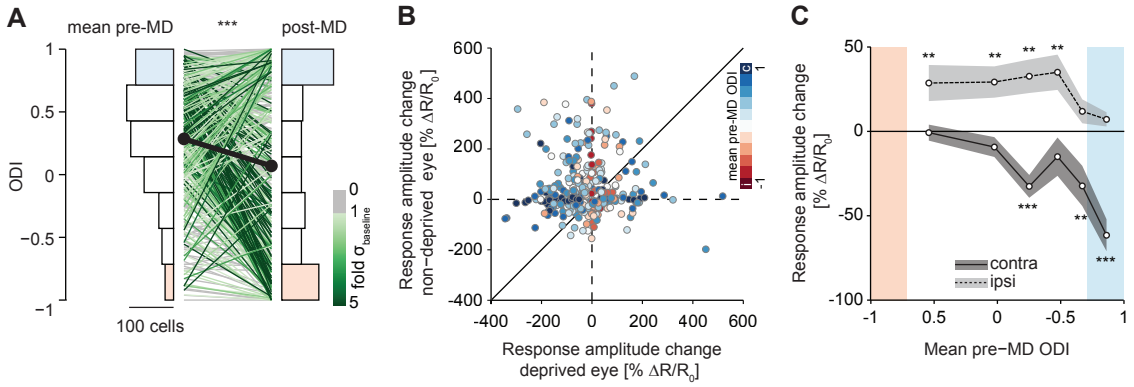

Figure 4.1: **Cell-specificity of OD plasticity in excitatory layer II/III cells in V1. A** ODI distribution of the same excitatory layer II/III cells in V1 during baseline (mean of three pre-MD sessions, 0.28 ± 0.47, SD) and after 5-8 days of MD (0.07 ± 0.67, SD, n = 430 cells in 10 mice, $P < 10^{-10}$, Wilcoxon signed-rank test). Lines connect individual, continuously responsive cells; line colour indicates shift significance in units of standard deviations over pre-MD baseline fluctuations. Coloured ODI histogram bins indicate class definitions for contralateral (blue), binocular (white) and ipsilateral (red) boutons (data re-analysed from Rose et al., 2016). **B.** Change in eye-specific response amplitude after MD for individual cells (n = 565 cells responsive in all pre-MD sessions, 10 animals). Cells are colour-coded by their mean pre-MD ODI. **C** Quantification of B, grouped into pre-MD ODI sextiles comprising similar numbers of cells (94-95 cells per group, paired t-tests; monocular ODI classes indicated by red and blue shading as defined in A). Note that for the purpose of better comparison between the two datasets, the cortical data was re-analysed with a different threshold for determining responsiveness.

correlated to functional changes.

4.3.2 Thalamic OD plasticity differs from cortical OD plasticity

Recently, we collected a similar dataset looking at OD plasticity of layer II/III cells in the binocular zone of V1 (Rose et al., 2016), allowing a direct comparison of thalamic and cortical OD plasticity. Briefly, in the cortex, we showed that after MD most cells responded more strongly to the open, ipsilateral eye, while a small fraction of cells shifted towards the deprived eye (Fig. 4.1A). Deprived-eye depression was the major driving force of this shift, which was strongest for cells that were mostly contralaterally dominated before MD. Additionally, all cells except originally contralaterally dominated cells exhibited ipsilateral strengthening (Fig. 4.1C).

There were several similarities, but also one profound difference between thalamic and cortical OD plasticity. Both areas showed an overall shift towards the open-eye as well as a deprived-eye depression. More precisely, in both cases the decrease in contralateral

eye responsiveness was most pronounced in initially contralaterally dominated boutons or cells, respectively. Moreover, both the fraction of plastic cells as well as the percentage of boutons or cells that lost responsiveness to visual stimulation after MD was comparable. However, in the dLGN the increase in open-eye responsiveness was preferentially targeted to previously contralaterally dominated boutons. These TRC boutons thereby gained binocularity, whereas the ipsilateral input was simply strengthened in layer II/III cells that were already ipsilaterally dominated or binocular before MD. This indicates that in V1 and dLGN different mechanisms led to the increase in ipsilateral responsiveness: In V1, existing functional synapses were strengthened, whereas in dLGN new connections were gained or unmasked.

Consequently, while layer II/III cells are mostly concentrated in the upper two quadrants of Fig. 4.1B, most of the TRC boutons are restricted to the upper left quadrant representing both a decrease in deprived-eye and an increase in non-deprived eye responsiveness.

4.4 Possible mechanisms for thalamic OD plasticity

Surprisingly, TRC boutons prominently changed their OD after MD, which raises the question: What are possible mechanisms for thalamic OD plasticity? The two most plausible possibilities are: 1. Modulation by feedback, especially corticothalamic feedback or 2. changes at the retinogeniculate synapse.

4.4.1 Corticothalamic feedback

As previously discussed, the dLGN receives modulatory feedback from V1 (both direct excitatory and indirect inhibitory via the thalamic reticular nucleus; Alitto and Usrey, 2003; Bickford, 2016) and the superior colliculus (Harting et al., 1991; Grubb and Thompson, 2003; Bickford et al., 2015). A decrease in the direct excitatory corticothalamic feedback could result in a decrease in TRC bouton responsiveness. Indeed, it has been shown that long-term MD (several months from birth on) in cats reduces corticothalamic feedback (Tsumoto and Suda, 1981). The authors speculate that normal myelination of corticothalamic cells is affected by visual deprivation. Additionally, there is some evidence of adult myelination that is dependent on cortical neuron activation (reviewed in O'Rourke et al., 2014).

For mice, less is known about the role of corticothalamic feedback in MD. Only Krahe and Guido, 2011 provide some evidence that synapse strength of corticothalamic terminals is enhanced in the deprived eye monocular pathway after juvenile MD in mice. Layer VI of V1 provides most of the corticothalamic feedback to dLGN. While changes in layer II to IV are well-established, it is less clear whether layer VI pyramidal cells similarly undergo changes. Although the number of animals reported is very low (n = 6), layer IV pyramidal cell seemed to not show a change in ODI after MD in rats (Medini, 2011).

In summary, a decrease in cortical deprived eye responsiveness could lead to a decrease in excitatory corticothalamic feedback followed by a decrease in TRC boutons responsiveness to the contralateral eye. However, it is rather unlikely to cause the observed open-eye strengthening. In order to explain the ipsilateral strengthening of contralateral boutons in the dLGN by corticothalamic feedback, the feedback would have to be highly target specific: contralateraly tuned TRCs in the binocular part of the dLGN would have to connect to cells in V1 showing cortical ipsilateral strengthening. So far there is no evidence for such specific corticothalamic connectivity.

The effect of corticothalamic feedback could be tested *in vivo* using similar approaches

to the one used in this thesis. Both, neurons in the dLGN and V1 could be transduced with genetically encoded calcium indicators of different colours to visualize their activity in binocular V1. After MD, the effect of the corticothalamic feedback can be shown, for example with local application of muscimol, a selective agonist for $GABA_A$receptors. This should result in silencing of cells in V1 as visualized by calcium imaging with one of the genetically encoded calcium indicators and possibly in an effect on TRC boutons. Alternatively, silencing of layer VI neurons could be achieved with designer receptors exclusively activated by designer drugs (DREADD). Clozapine-N-oxide can activate those receptors and this offers the possibility of both long-term systemic application or local intracranial injections. In combination with Ntsr1-Cre mice (Gong et al., 2007), DREADDs can be specifically targeted to layer VI. This allows a direct analysis of the influence of corticothalamic feedback on thalamic OD plasticity (see also Thompson et al., 2016; Erisken et al., 2015).

4.4.2 The retinogeniculate synapse

The second mechanism is based on upstream changes in the visual system. During development, the retinogeniculate synapse is very plastic, and connections depend both on spontaneous and visually driven activity. To this end, it has been shown that dark rearing alters the number of retinal inputs converging onto single dLGN cells (Hooks and Chen, 2006, 2008).

Further evidence for plasticity at the retinogeniculate synapse comes from a recent study showing that long-term MD in juvenile mice leads to a change in myelination of retinogeniculate axons, resulting in a reduced conduction velocity of the contralateral retinogeniculate axons (Etxeberria et al., 2016). However, this does not explain the strengthening of specific ipsilateral input to contralaterally dominant boutons.

It has been proposed that silent synapses may play a role in the plasticity of visual responses in the adult dLGN (Moore et al., 2011). Indeed, there is a dramatic mismatch between the structurally (Hammer et al., 2015; Morgan et al., 2016; Rompani et al., 2017) and functionally identified number (Ziburkus and Guido, 2006; Jaubert-Miazza et al., 2005) of RGCs converging onto TRCs. Rapid strengthening or unsilencing of preexisting but functionally dormant synapses may therefore be a mechanism for retinogeniculate plasticity. Adult retinogeniculate synapses express both NMDA and AMPA receptors (Esguerra et al., 1992). However, as functionally silent synapses only contain NMDA receptors, the insertion of AMPA receptors would lead to the activation of those synapses. Interestingly, it has been shown that both AMPA and NMDA receptors are involved in

short-term plasticity at the retinogeniculate synapse (Chen et al., 2002).

Another indication for the role of the dLGN and retinogeniculate refinement in cortical plasticity has been provided by studies using knock-out mice (Datwani et al., 2009): When two of the more than fifty major histocompatibility complex class I genes are knocked out, OD plasticity is enhanced. Interestingly, these genes seem to be important for retinogeniculate refinement. In the dLGN of mice lacking these genes, the segregation of RGC inputs is incomplete, leading to an ipsilateral termination zone that is almost double in size. One can speculate that this might lead to both an increase of the percentage of binocular neurons and more silent synapses providing ipsilateral input to contralaterally dominated TRCs. Potentially, this could explain the enhanced OD plasticity in those mice. However, studies of the electrophysiological properties of TRCs in such mice are necessary to better understand the underlying mechanism. It is also noteworthy that functional retinogeniculate refinement is regulated by corticothalamic feedback in juvenile animals (Thompson et al., 2016): Cortical changes in ODI may result in a change in corticothalamic feedback, which in turn may explain the structural changes in retinogeniculate axons (Sur et al., 1982).

Further electrophysiological experiments might provide insight into possible changes at the retinogeniculate synapse. In the last ten years, channelrhodopsin-assisted circuit mapping (Petreanu et al., 2007, 2009) has been developed to map the spatial distribution of synaptic inputs onto dendrites. It is based on the expression of the light-activated cation channel channelrhodopsin in the presynaptic cell, which upon light stimulation evokes postsynaptic potentials in the postsynaptic cell. Extensive research has yielded several different forms of channelrhodopsin that can be activated at different wavelengths, thus providing the opportunity to independently excite two distinct population of neurons (Klapoetke et al., 2014, Hooks et al., 2015). Intraocular injections with viruses coding for two different channelrhodopsins for labelling the two distinct inputs could be combined with laser scanning photo stimulation. This way, eye-specific input onto single TRCs can be mapped after MD and in control animals to detect eye-specific changes at the retinogeniculate synapse.

4.5 Conclusions

In summary, using chronic *in vivo* two-photon imaging of TRC boutons in layer I of the binocular visual cortex, this thesis yielded the following two main findings about the dLGN:

1. The data presented here demonstrate the functional diversity of the dLGN. While most TRC are monocular, there is a subset of binocular cells in the dLGN. While the origin of this functional diversity remains to be elucidated, these findings add to the emerging view of the more central role of the thalamus in visual processing.

2. Contrary to current models, the functional properties of dLGN neurons are not rigid, but undergo substantial functional experience-dependent plasticity. Deprived-eye responsiveness is decreased, whereas open-eye responses are increased, often accompanied by monocular boutons gaining binocularity. Interestingly, thalamic OD plasticity seems to differ from cortical OD plasticity, but further experiments are needed to gain insight into the precise mechanism of thalamic OD plasticity.

OD plasticity is an important model for experience-dependent plasticity and mice are a widely-used model organism. Therefore, these data strongly suggest that thalamic plasticity should be included into future models of experience-dependence plasticity.

Bibliography

Ahmadlou, M. and Heimel, J. A. (2015). Preference for concentric orientations in the mouse superior colliculus. *Nature Communications*, 6:6773.

Akerboom, J., Chen, T.-W., Wardill, T. J., Tian, L., Marvin, J. S., Mutlu, S., Calderon, N. C., Esposti, F., Borghuis, B. G., Sun, X. R., Gordus, a., Orger, M. B., Portugues, R., Engert, F., Macklin, J. J., Filosa, a., Aggarwal, a., Kerr, R. a., Takagi, R., Kracun, S., Shigetomi, E., Khakh, B. S., Baier, H., Lagnado, L., Wang, S. S.-H., Bargmann, C. I., Kimmel, B. E., Jayaraman, V., Svoboda, K., Kim, D. S., Schreiter, E. R., and Looger, L. L. (2012). Optimization of a GCaMP Calcium Indicator for Neural Activity Imaging. *Journal of Neuroscience*, 32(40):13819–13840.

Alitto, H. J. and Usrey, W. M. (2003). Corticothalamic feedback and sensory processing. *Current Opinion in Neurobiology*, 13(4):440–445.

Andermann, M. L., Kerlin, A. M., Roumis, D. K., Glickfeld, L. L., and Reid, R. C. (2011). Functional Specialization of Mouse Higher Visual Cortical Areas. *Neuron*, 72(6):1025–1039.

Andermann, M. M. L., Kerlin, A. M., and Reid, R. C. (2010). Chronic cellular imaging of mouse visual cortex during operant behavior and passive viewing. *Frontiers in Cellular Neurosciences*, 4(3):6–8.

Antonini, A., Fagiolini, M., and Stryker, M. P. (1999). Anatomical correlates of functional plasticity in mouse visual cortex. *Journal of Neuroscience*, 19(11):4388–4406.

Antonini, A. and Stryker, M. (1996). Plasticity of geniculocortical afferents following brief or prolonged monocular occlusion in the cat. *Journal of Comparative Neurology*, 369(1):64–82.

Antonini, A. and Stryker, M. P. (1993). Development of individual geniculocortical arbors in cat striate cortex and effects of binocular impulse blockade. *Journal of Neuroscience*, 13(8):3549.

Arcelli, P., Frassoni, C., Regondi, M. C., Biaslt, S. D. E., Spreafico, R., Besta, I., Neurofisiologia, D., Biochimicagenerali, D. F., Istologiae, S., and Umana, A. (1997). GABAergic Neurons in Mammalian Thalamus: A Marker of Thalamic Complexity? *Brain Research Bulletin*, 42(1):27–37.

Baden, T., Berens, P., Franke, K., Román Rosón, M., Bethge, M., and Euler, T. (2016). The functional diversity of retinal ganglion cells in the mouse. *Nature*, 529(7586):345–50.

Baohan, A., Ikrar, T., Tring, E., Xu, X., and Trachtenberg, J. T. (2016). Pten and EphB4 regulate the establishment of perisomatic inhibition in mouse visual cortex. *Nature Communications*, 7:12829.

Barlow, H. B., Hill, R. M., and Levick, W. R. (1964). Retinal ganglion cells responding selectively to direction and speed of image motion in the rabbit. *Journal of Physiology*, 173:377–407.

Bear, M. F., Cooper, L. N., and Ebner, F. F. (1986). A physiological basis for a theory of synapse modification. *Science*, 237(4810):42–48.

Bickford, M. E. (2016). Thalamic Circuit Diversity: Modulation of the Driver/Modulator Framework. *Frontiers in Neural Circuits*, 9:86.

Bickford, M. E., Zhou, N., Krahe, T. E., Govindaiah, G., and Guido, W. (2015). Retinal and Tectal "Driver-Like" Inputs Converge in the Shell of the Mouse Dorsal Lateral Geniculate Nucleus. *Journal of Neuroscience*, 35(29):10523–10534.

Bienenstock, E. L., Cooper, L. N., and Munro, P. W. (1982). Theory for the development of neuron selectivity: orientation specificity and binocular interaction in visual cortex. *The Journal of Neuroscience*, 2(1):32–48.

Bliss, T. V. P. and Lomo, T. (1973). Long-lasting potentiation of synaptic transmission in the dentate area of the anaesthetized rabbit following stimulation of the perforant path. *Journal of Physiology*, 232(2):331–356.

Bonhoeffer, T. (1996). Neurotrophins and activity-dependent development of the neocortex. *Current Opinion in Neurobiology*, 6(1):119–126.

Bonhoeffer, T. and Grinvald, A. (1991). Iso-orientation domains in cat visual cortex are arranged in pinwheel-like patterns. *Nature*, 353(6343):429–431.

Brainard, D. H. (1997). The Psychophysics Toolbox. *Spatial Vision*, 10(4):433–436.

Brody, C. D. (1998). Slow Covariations in Neuronal Resting Potentials Can Lead to Artefactually Fast Cross-Correlations in Their Spike Trains. *Journal of Neurophysiology*, 80(6):3345–3351.

Campbell, F. W. and Green, D. G. (1965). Monocular versus Binocular Visual Acuity. *Nature*, 208(5006):191–192.

Carter-Dawson, L. and LaVail, M. M. (1979). Rods and Cones in the Mouse Retina. *Journal of Comparative Neurology*, 188(2):263–272.

Casagrande, V. A. (1994). A third parallel visual pathway to primate area V1. *Trends in Neurosciences*, 17(7):305–10.

Cerri, C., Fabbri, A., Vannini, E., Spolidoro, M., Costa, M., Maffei, L., Fiorentini, C., and Caleo, M. (2011). Activation of Rho GTPases triggers structural remodeling and functional plasticity in the adult rat visual cortex. *Journal of Neuroscience*, 31(42):15163–72.

Chen, C., Blitz, D. M., and Regehr, W. G. (2002). Contributions of receptor desensitization and saturation to plasticity at the retinogeniculate synapse. *Neuron*, 33(5):779–788.

Chen, C. and Regehr, W. G. (2000). Developmental remodeling of the Retinogeniculate Synapse. 28:955–966.

Chen, T.-W., Wardill, T. J., Sun, Y., Pulver, S. R., Renninger, S. L., Baohan, A., Schreiter, E. R., Kerr, R. a., Orger, M. B., Jayaraman, V., Looger, L. L., Svoboda, K., and Kim, D. S. (2013). Ultrasensitive fluorescent proteins for imaging neuronal activity. *Nature*, 499(7458):295–300.

Cho, K. K. A., Khibnik, L., Philpot, B. D., and Bear, M. F. (2009). The ratio of NR2A / B NMDA receptor subunits determines the qualities of ocular dominance plasticity in visual cortex. *Proceedings of the National Academy of Sciences*, 106(13):5377– 5382.

Chow, K. L. and Stewart, D. L. (1972). Reversal of Structural and Functional Effects of Long-Term Visual Deprivation in Cats. *Experimental Neurology*, 34(3):409–433.

Coleman, J. E., Law, K., and Bear, M. F. (2009). Anatomical origins of ocular dominance in mouse primary visual cortex. *Neuroscience*, 161(2):561–71.

Coleman, J. E., Nahmani, M., Gavornik, J. P., Haslinger, R., Heynen, A. J., Erisir, A., and Bear, M. F. (2010). Rapid structural remodeling of thalamocortical synapses parallels experience-dependent functional plasticity in mouse primary visual cortex. *Journal of Neuroscience*, 30(29):9670–9682.

Cruz-Martín, A., El-Danaf, R. N., Osakada, F., Sriram, B., Dhande, O. S., Nguyen, P. L., Callaway, E. M., Ghosh, A., and Huberman, A. D. (2014). A dedicated circuit links direction-selective retinal ganglion cells to the primary visual cortex. *Nature*, 507(7492):358–61.

Datwani, A., McConnell, M. J., Kanold, P. O., Micheva, K. D., Busse, B., Shamloo, M., Smith, S. J., and Shatz, C. J. (2009). Classical MHCI Molecules Regulate Retinogeniculate Refinement and Limit Ocular Dominance Plasticity. *Neuron*, 64(4):463–470.

Davis, M. F. F., Figueroa Velez, D. X. X., Guevarra, R. P. P., Yang, M. C. C., Habeeb, M., Carathedathu, M. C. C., and Gandhi, S. P. P. (2015). Inhibitory Neuron Transplantation into Adult Visual Cortex Creates a New Critical Period that Rescues Impaired Vision. *Neuron*, 86(4):1–12.

De Paola, V., Holtmaat, A., Knott, G., Song, S., Wilbrecht, L., Caroni, P., and Svoboda, K. (2006). Cell type-specific structural plasticity of axonal branches and boutons in the adult neocortex. *Neuron*, 49(6):861–875.

Denk, W., Strickler, J. H., and Webb, W. W. (1990). Two-photon laser scanning fluorescence microscopy. *Science*, 248(4951):73–6.

Derrington, A. M. and Hawken, M. J. (1981). Spatial and temporal properties of cat geniculate neurons after prolonged deprivation. *Journal of Physiology*, 314:107–120.

Dhande, O. S., Hua, E. W., Guh, E., Yeh, J., Bhatt, S., Zhang, Y., Ruthazer, E. S., Feller, M. B., and Crair, M. C. (2011). Development of single retinofugal axon arbors in normal and $\beta 2$ knock-out mice. *Journal of Neuroscience*, 31(9):3384–3399.

Dhande, O. S. and Huberman, A. D. (2014). Retinal ganglion cell maps in the brain: Implications for visual processing. *Current Opinion in Neurobiology*, 24(1):133–142.

Domenici, L., Berardi, N., Carmignotot, G., and Vantini, G. (1991). Nerve growth factor prevents the amblyopic effects of monocular deprivation. *Proceedings of the National Academy of Sciences*, 88(19):8811–8815.

Douglas, R. M., Alam, N. M., Silver, B. D., McGill, T. J., Tschetter, W. W., and Prusky, G. T. (2005). Independent visual threshold measurements in the two eyes of freely moving rats and mice using a virtual-reality optokinetic system. *Visual Neuroscience*, 22(5):677–684.

Dräger, U. C. (1975). Receptive fields of single cells and topography in mouse visual cortex. *Journal of Comparative Neurology*, 160(3):269–90.

Dräger, U. C. (1978). Observations on monocular deprivation in mice. *Journal of Neurophysiology*, 41(1):28–42.

Dräger, U. C. and Hubel, D. H. (1975). Responses to visual stimulation and relationship between visual, auditory, and somatosensory inputs in mouse superior colliculus. *Journal of Neurophysiology*, 38(3):690–713.

Dräger, U. C. and Olsen, J. F. (1980). Origins of crossed and uncrossed retinal projections in pigmented and albino mice. *Journal of Comparative Neurology*, 191(3):383–412.

Dudek, S. M. and Bear, M. F. (1992). Homosynaptic long-term depression in area CA1 of hippocampus and effects of N-methyl-D-aspartate receptor blockade. *Proceedings of the National Academy of Sciences*, 89(10):4363–7.

Durand, S., Iyer, R., Mizuseki, K., de Vries, S., Mihalas, S., and Reid, R. C. (2016). A Comparison of Visual Response Properties in the Lateral Geniculate Nucleus and Primary Visual Cortex of Awake and Anesthetized Mice. *Journal of Neuroscience*, 36(48):12144–12156.

Engert, F. and Bonhoeffer, T. (1999). Dendritic spine changes associated with hippocampal long-term synaptic plasticity. *Nature*, 399(6731):66–70.

Erisir, A., Van Horn, S. C., Bickford, M. E., and Sherman, S. M. (1997a). Immunocytochemistry and distribution of parabrachial terminals in the lateral geniculate nucleus of the cat: A comparison with corticogeniculate terminals. *Journal of Comparative Neurology*, 377(4):535–549.

Erisir, A., Van Horn, S. C., and Sherman, S. M. (1997b). Relative numbers of cortical and brainstem inputs to the lateral geniculate nucleus. *Proceedings of the National Academy of Sciences*, 94(4):1517–20.

Erisken, S., Vaiceliunaite, A., and Busse, L. (2015). Dissecting corticothalamic feedback during active behavior in the mouse visual system. In *Meeting of the Society for Neuroscience*.

Erisken, S., Vaiceliunaite, A., Jurjut, O., Fiorini, M., Katzner, S., and Busse, L. (2014). Effects of Locomotion Extend throughout the Mouse Early Visual System. *Current Biology*, 24(24):2899–907.

Esguerra, M., Kwon, Y. H., and Sur, M. (1992). Retinogeniculate EPSPs recorded intracellularly in the ferret lateral NMDA receptors. *Vision Neuroscience*, 8(6):545–555.

Espinosa, J. S. and Stryker, M. P. (2012). Development and Plasticity of the Primary Visual Cortex. *Neuron*, 75(2):230–249.

Etxeberria, A., Hokanson, K. C., Dao, D. Q., Mayoral, S. R., Mei, F., Redmond, S. A., Ullian, E. M., and Chan, J. R. (2016). Dynamic Modulation of Myelination in Response to Visual Stimuli Alters Optic Nerve Conduction Velocity. *Journal of Neuroscience*, 36(26):6937–48.

Fagiolini, M., Fritschy, J.-M., Löw, K., Möhler, H., Rudolph, U., and Hensch, T. K. (2004). Specific GABAA circuits for visual cortical plasticity. *Science*, 303(5664):1681–3.

Fagiolini, M. and Hensch, T. K. (2000). Inhibitory threshold for critical-period activation in primary visual cortex. *Nature*, 404(6774):183–6.

Feinberg, E. H. and Meister, M. (2014). Orientation columns in the mouse superior colliculus. *Nature*.

Fox, K., Wallace, H., and Glazewski, S. (2002). Is there a thalamic component to experience- dependent cortical plasticity ? *Philosophical Transactions of the Royal Society B: Biological Sciences*, 357(1428):1709–1715.

Frenkel, M. Y. and Bear, M. F. (2004). How monocular deprivation shifts ocular dominance in visual cortex of young mice. *Neuron*, 44(6):917–923.

Frenkel, M. Y., Sawtell, N. B., Diogo, A. C. M., Yoon, B., Neve, R. L., and Bear, M. F. (2006). Instructive effect of visual experience in mouse visual cortex. *Neuron*, 51(3):339–49.

Friedlander, M. J., Lin, C. S., Stanford, L. R., and Sherman, S. M. (1981). Morphology of functionally identified neurons in lateral geniculate nucleus of the cat. *Journal of Neurophysiology*, 46(1):80–129.

Friedlander, M. J., Stanford, L. R., and Sherman, S. M. (1982). Effects of monocular deprivation on the structure-function relationship of individual neurons in the cat's lateral geniculate nucleus. *The Journal of neuroscience : the official journal of the Society for Neuroscience*, 2(3):321–330.

Fu, Y., Kaneko, M., Tang, Y., Alvarez-Buylla, A., and Stryker, M. P. (2015). A cortical disinhibitory circuit for enhancing adult plasticity. *eLife*, 2015(4):1–12.

Garey, L. J. and Blakemore, C. (1977). Monocular Deprivation: Morphological Effects on Different Classes of Neurons in the Lateral Geniculate Nucleus. *Science*, 195(4276):414–416.

Garey, L. J. and Dürsteler, M. H. (1975). Reversal of deprivation effects in the lateral geniculate nucleus of the cat. *Neuroscience Letters*, 1(1):19–23.

Ghose, D., Maier, A., Nidiffer, A., and Wallace, M. T. (2014). Multisensory Response Modulation in the Superficial Layers of the Superior Colliculus. *Journal of Neuroscience*, 34(12):4332–4344.

Gianfranceschi, L., Fiorentini, A., and Maffei, L. (1999). Behavioural visual acuity of wild type and bcl 2 transgenic mouse. *Vision Research*, 39(3):569–574.

Gianfranceschi, L., Siciliano, R., Walls, J., Morales, B., Kirkwood, A., Huang, Z. J., Tonegawa, S., and Maffei, L. (2003). Visual cortex is rescued from the effects of dark rearing by overexpression of BDNF. *Proceedings of the National Academy of Sciences*, 100(21):12486 – 12491.

Gilbert, C. and Wiesel, T. (1979). Morphology and intracortical projections of functionally characterised neurones in the cat visual cortex. *Nature*, 280(5718):120–125.

Gilbert, C. D. and Kelly, J. P. (1975). The projections of cells in different layers of the cat's visual cortex. *Journal of Comparative Neurology*, 163(1):81–105.

Glickfeld, L. L., Andermann, M. L., Bonin, V., and Reid, R. C. (2013). Cortico-cortical projections in mouse visual cortex are functionally target specific. *Nature neuroscience*, 16(2):219–26.

Godement, P., Salaün, J., and Imbert, M. (1984). Prenatal and postnatal development of retinogeniculate and retinocollicular projections in the mouse. *Journal of Comparative Neurology*, 230(4):552–575.

Golding, B., Pouchelon, G., Bellone, C., Murthy, S., Di Nardo, A. a., Govindan, S., Ogawa, M., Shimogori, T., Lüscher, C., Dayer, A., and Jabaudon, D. (2014). Retinal input directs the recruitment of inhibitory interneurons into thalamic visual circuits. *Neuron*, 81(5):1057–69.

Gong, S., Doughty, M., Harbaugh, C. R., Cummins, A., Hatten, M. E., Heintz, N., and Gerfen, C. R. (2007). Targeting Cre recombinase to specific neuron populations with bacterial artificial chromosome constructs. *Journal of Neuroscience*, 27(37):9817–9823.

Gordon, J. and Stryker, M. (1996). Experience-dependent plasticity of binocular responses in the primary visual cortex of the mouse. *Journal of Neuroscience*, 16(10):3274–3286.

Greifzu, F., Pielecka-Fortuna, J., Kalogeraki, E., Krempler, K., Favaro, P. D., Schlüter, O. M., and Löwel, S. (2014). Environmental enrichment extends ocular dominance plasticity into adulthood and protects from stroke-induced impairments of plasticity. *Proceedings of the National Academy of Sciences*, pages 1–6.

Grieve, K. L. (2005). Binocular visual responses in cells of the rat dLGN. *Journal of Physiology*, 566(Pt 1):119–24.

Grinvald, A., Lieke, E., Frostig, R., Gilbert, C. D., and Wiesel, T. N. (1986). Functional architecture of cortex revealed by optical imaging of intrinsic signals. *Nature*, 324(6095):361–364.

Grubb, M. S., Rossi, F. M., Changeux, J. P., and Thompson, I. D. (2003). Abnormal functional organization in the dorsal lateral geniculate nucleus of mice lacking the beta 2 subunit of the nicotinic acetylcholine receptor. *Neuron*, 40(6):1161–1172.

Grubb, M. S. and Thompson, I. D. (2003). Quantitative characterization of visual response properties in the mouse dorsal lateral geniculate nucleus. *Journal of Neurophysiology*, 90(6):3594–607.

Grubb, M. S. and Thompson, I. D. (2004). Biochemical and anatomical subdivision of the dorsal lateral geniculate nucleus in normal mice and in mice lacking the b 2 subunit of the nicotinic acetylcholine receptor. *Vision Research*, 44(28):3365–3376.

Grubb, M. S. and Thompson, I. D. (2005). Visual response properties of burst and tonic firing in the mouse dorsal lateral geniculate nucleus. *Journal of neurophysiology*, 93(6):3224–3247.

Gu, Y., Tran, T., Murase, S., Borrell, X. A., Kirkwood, A., and Quinlan, E. M. (2016). Neuregulin-Dependent Regulation of Fast-Spiking Interneuron Excitability Controls the Timing of the Critical Period. *The Journal of Neuroscience*, 36(40):10285–10295.

Guillery, R. W. and Sherman, S. M. (2002). Thalamic Relay Functions and Their Role in Corticocortical Communication : Generalizations from the Visual System. *Neuron*, 33(1):163–175.

Guillery, R. W. and Stelzner, D. J. (1970). The Differential Effects of Unilateral Lid Closure upon the Monocular and Binocular Segments of the Dorsal Lateral Geniculate Nucleus in the Cat. *Journal of Comparative Neurology*, 139(4):413–422.

Hamasaki, D. I., Rackensperger, W., and Vesper, J. (1972). Spatial organization of normal and visually deprived units in the lateral geniculate nucleus of the cat. *Vision Research*, 12(5):843–854.

Hammer, S., Monavarfeshani, A., Lemon, T., Su, J., and Fox, M. A. (2015). Multiple Retinal Axons Converge onto Relay Cells in the Adult Mouse Thalamus. *Cell Reports*, 12(10):1575–1583.

Harting, J. K., Huerta, M. F., Hashikawa, T., and van Lieshout, D. P. (1991). Projection of the mammalian superior colliculus upon the dorsal lateral geniculate nucleus: organization of tectogeniculate pathways in nineteen species. *Journal of Comparative Neurology*, 304(2):275–306.

Hartline, H. K. (1969). Visual receptors and retinal interaction. *Science*, 164(3877):270–278.

Hattar, S., Liao, H. W., Takao, M., Berson, D. M., and Yau, K. W. (2002). Melanopsin-containing retinal ganglion cells: architecture, projections, and intrinsic photosensitivity. *Science*, 295(5557):1065–70.

He, H.-Y. (2006). Visual Deprivation Reactivates Rapid Ocular Dominance Plasticity in Adult Visual Cortex. *Journal of Neuroscience*, 26(11):2951–2955.

Hebb, D. O. (1949). The first stage of perception: growth of the assembly. In *The Organization of Behavior*, number 4, pages 60–78. Wiley, New York.

Helmchen, F. and Denk, W. (2005). Deep tissue two-photon microscopy. *Nature*, 200(5):932–940.

Hengen, K. B., Lambo, M. E., Van Hooser, S. D., Katz, D. B., and Turrigiano, G. G. (2013). Firing rate homeostasis in visual cortex of freely behaving rodents. *Neuron*, 80(2):335–42.

Hensch, T. K., Fagiolini, M., Mataga, N., Stryker, M. P., Baekkeskov, S., and Kash, S. F. (1998). Local GABA Circuit Control of Experience-Dependent Plasticity in Developing Visual Cortex. *Science*, 282(5393):1504–1508.

Heynen, A. J., Yoon, B.-J., Liu, C.-H., Chung, H. J., Huganir, R. L., and Bear, M. F. (2003). Molecular mechanism for loss of visual cortical responsiveness following brief monocular deprivation. *Nature Neuroscience*, 6(8):854–862.

Hickey, T. L., Spear, P. D., and Kratz, K. E. (1977). Qualitative Studies of Cell Size in the Cat's Dorsal Lateral Geniculate Nucleus Following Visual Deprivation. *Journal of Comparative Neurology*, 172(2):265–281.

Hofbauer, a. and Dräger, U. C. (1985). Depth segregation of retinal ganglion cells projecting to mouse superior colliculus. *Journal of Comparative Neurology*, 234:465–474.

Hofer, S. B. and Bonhoeffer, T. (2010). Dendritic spines: the stuff that memories are made of? *Current Biology*, 20(4):157–9.

Hofer, S. B., Mrsic-Flogel, T. D., Bonhoeffer, T., and Hübener, M. (2006). Lifelong learning: ocular dominance plasticity in mouse visual cortex. *Current Opinion in Neurobiology*, 16(4):451–9.

Hofer, S. B., Mrsic-Flogel, T. D., Bonhoeffer, T., and Hübener, M. (2009). Experience leaves a lasting structural trace in cortical circuits. *Nature*, 457(7227):313–317.

Hoffman, K.-P. and Holländer, H. (1978). Physiological and Morphological Changes in Cells of the Lateral Geniculate Nucleus in Monocularly-deprived and Reverse-sutured Cats. *Journal of Comparative Neurology*, 177(1):145–158.

Holtmaat, A. and Svoboda, K. (2009). Experience-dependent structural synaptic plasticity in the mammalian brain. *Nature Reviews Neuroscience*, 10(9):647–58.

Hong, Y. K., Park, S. H., Litvina, E. Y., Morales, J., Sanes, J. R., and Chen, C. (2014). Refinement of the Retinogeniculate Synapse by Bouton Clustering. *Neuron*, 84(2):332–339.

Hooks, B. M. and Chen, C. (2006). Distinct Roles for Spontaneous and Visual Activity in Remodeling of the Retinogeniculate Synapse. *Neuron*, 52(2):281–291.

Hooks, B. M. and Chen, C. (2008). Vision triggers an experience-dependent sensitive period at the retinogeniculate synapse. *Journal of Neuroscience*, 28(18):4807–4817.

Hooks, B. M., Lin, X. J. Y., Guo, C., and Svoboda, K. (2015). Dual-Channel Circuit Mapping Reveals Sensorimotor Convergence in the Primary Motor Cortex. *Journal of Neuroscience*, 35(10):4418–4426.

Howarth, M., Walmsley, L., and Brown, T. M. (2014). Binocular integration in the mouse lateral geniculate nuclei. *Current Biology*, 24(11):1241–1247.

Huang, Z. J., Kirkwood, A., Pizzorusso, T., Porciatti, V., Morales, B., Bear, M. F., Maffei, L., and Tonegawa, S. (1999). BDNF regulates the maturation of inhibition and the critical period of plasticity in mouse visual cortex. *Cell*, 98(6):739–755.

Hubel, D. and Wiesel, T. (1962). Receptive fields, binocular interaction and functional architecture in the cat's visual cortex. *Journal of Physiology*, 160:106–154.

Hubel, D. and Wiesel, T. (1970). The period of susceptibility to the physiological effects of unilateral eye closure in kittens. *Journal of Physiology*, 206(2):419.

Hubel, D. H. and Wiesel, T. N. (1959). Receptive fields of single neurones in the cat's striate cortex. *Journal of Physiology*, 148:574–591.

Hubel, D. H. and Wiesel, T. N. (1961). Integrative action in the cat's lateral geniculate body. *Journal of Physiology*, 155:385–398.

Hubel, D. H. and Wiesel, T. N. (1972). Laminar and columnar distribution of geniculocortical fibers in the macaque monkey. *Journal of Comparative Neurology*, 146(4):421–450.

Hubel, D. H., Wiesel, T. N., and LeVay, S. (1977). Plasticity of ocular dominance columns in monkey striate cortex. *Philosophical transactions of the Royal Society of London. Series B, Biological sciences*, 278(961):377–409.

Huberman, A. D., Murray, K. D., Warland, D. K., Feldheim, D. a., and Chapman, B. (2005). Ephrin-As mediate targeting of eye-specific projections to the lateral geniculate nucleus. *Nature Neuroscience*, 8(8):1013–21.

Huberman, A. D., Wei, W., Elstrott, J., Stafford, B. K., Feller, M. B., and Barres, B. A. (2009). Genetic Identification of an On-Off Direction- Selective Retinal Ganglion Cell Subtype Reveals a Layer-Specific Subcortical Map of Posterior Motion. *Neuron*, 62(3):327–334.

Inoue, K.-I., Takada, M., and Matsumoto, M. (2015). Neuronal and behavioural modulations by pathway-selective optogenetic stimulation of the primate oculomotor system. *Nature Communications*, 6:8378.

Jahnsen, B. Y. H. and Llinas, R. (1984). Electrophysiological properties of guinea-pig thalamic neurones:. *Journal of Physiology*, 349:205–226.

Jaubert-Miazza, L., Green, E., Lo, F.-s., Bui, K., Mills, J., and Guido, W. (2005). Structural and functional composition of the developing retinogeniculate pathway in the mouse. *Visual Neuroscience*, 22(5):661–676.

Jeffries, A. M., Killian, N. J., and Pezaris, J. S. (2014). Mapping the primate lateral geniculate nucleus: A review of experiments and methods. *Journal of Physiology*, 108(1):3–10.

Ji, X.-y., Zingg, B., Mesik, L., Xiao, Z., Zhang, L. I., and Tao, H. W. (2016). Thalamocortical Innervation Pattern in Mouse Auditory and Visual Cortex: Laminar and Cell-Type Specificity. *Cerebral Cortex*, 26(6):2612–25.

Jiang, Y., Yampolsky, D., Purushothaman, G., and Casagrande, V. A. (2015). Perceptual decision related activity in the lateral geniculate nucleus. *Journal of Neurophysiology*, 114(1):717–735.

Jones, K. R. and Berkley, M. A. (1983). Loss of temporal sensitivity in dorsal lateral geniculate nucleus and area 18 of the cat following monocular deprivation. *Journal of Neurophysiology*, 49(1):254–268.

Kalil, R. (1980). Quantitative study of the effects of monocular enucleation and deprivation on cell growth in the dorsal lateral geniculate nucleus of the cat. *Journal of Comparative Neurology*, 189(3):483–524.

Kaneko, M., Stellwagen, D., Malenka, R. C., and Stryker, M. P. (2008). Tumor Necrosis Factor-alpha Mediates One Component of Competitive, Experience-Dependent Plasticity in Developing Visual Cortex. *Neuron*, 58(5):673–680.

Kasper, E. M., Larkman, A. U., Lubke, J., and Blakemore, C. (1994). Pyramidal neurons in layer 5 of the rat visual cortex. II. Development of electrophysiological properties. *Journal of Comparative Neurology*, 339(4):475–494.

Khibnik, L. a., Cho, K. K. a., and Bear, M. F. (2010). Relative contribution of feedforward excitatory connections to expression of ocular dominance plasticity in layer 4 of visual cortex. *Neuron*, 66(4):493–500.

Kim, I.-J., Zhang, Y., Meister, M., and Sanes, J. R. (2010). Laminar restriction of retinal ganglion cell dendrites and axons: subtype-specific developmental patterns revealed with transgenic markers. *Journal of Neuroscience*, 30(4):1452–62.

Klapoetke, N. C., Murata, Y., Kim, S. S., Pulver, S. R., Birdsey-Benson, A., Cho, Y. K., Morimoto, T. K., Chuong, A. S., Carpenter, E. J., Tian, Z., Wang, J., Xie, Y., Yan, Z., Zhang, Y., Chow, B. Y., Surek, B., Melkonian, M., Jayaraman, V., Constantine-Paton, M., Wong, G. K.-S., and Boyden, E. S. (2014). Independent optical excitation of distinct neural populations. *Nature Methods*, 11(3):338–46.

Kobayashi, Y., Ye, Z., and Hensch, T. (2015). Clock Genes Control Cortical Critical Period Timing. *Neuron*, 86(1):264–275.

Kondo, S. and Ohki, K. (2016). Laminar differences in the orientation selectivity of geniculate afferents in mouse primary visual cortex. *Nature Neuroscience*, 19(2):316–319.

Kondo, S., Yoshida, T., and Ohki, K. (2016). Mixed functional microarchitecture for orientation selectivity in the mouse primary visual cortex. *Nature Communications*, 7:13210.

Krahe, T. E., El-Danaf, R. N., Dilger, E. K., Henderson, S. C., and Guido, W. (2011). Morphologically Distinct Classes of Relay Cells Exhibit Regional Preferences in the Dorsal Lateral Geniculate Nucleus of the Mouse. *Journal of Neuroscience*, 31(48):17437–17448.

Krahe, T. E. and Guido, W. (2011). Homeostatic plasticity in the visual thalamus by monocular deprivation. *The Journal of Neuroscience*, 31(18):6842–6849.

Kratz, K. E., Mangel, S. C., Lehmkuhle, S., and Murray Sherman, S. (1979). Retina X- and Y-cells in monocularly lid-sutured cats: normality of spatial and temporal properties. *Brain Research*, 172(3):545–551.

Krauzlis, R. J., Lovejoy, L. P., and Zénon, A. (2013). Superior colliculus and visual spatial attention. *Annual Review of Neuroscience*, 36:165–82.

Kuffler, S. W. (1953). Discharge Patterns and Functional of Mammalian Retina. *Journal of Neurophysiology*, 16(1):37–68.

Kuhlman, S. J., Olivas, N. D., Tring, E., Ikrar, T., Xu, X., and Trachtenberg, J. T. (2013). A disinhibitory microcircuit initiates critical-period plasticity in the visual cortex. *Nature*, 501(7468):543–6.

Lawrence, P. M. and Studholme, K. M. (2014). Retinofugal projections in the mouse. *Journal of Comparative Neurology*, 522(16):3733–3753.

Lehmann, K. and Löwel, S. (2008). Age-dependent ocular dominance plasticity in adult mice. *PLoS ONE*, 3(9):e3120.

Lehmkuhle, S., Kratz, E., Mangel, S. C., and Sherman, S. M. (1980). Effects of Early Monocular Lid Suture on Spatial and Temporal Sensitivity of Neurons in Dorsal Lateral Geniculate Nucleus of the Cat. *Journal of Neurophysiology*, 43(2):542–56.

Leinweber, M., Zmarz, P., Buchmann, P., Argast, P., Hübener, M., Bonhoeffer, T., and Keller, G. B. (2014). Two-photon Calcium Imaging in Mice Navigating a Virtual Reality Environment. *Journal of Visualized Experiments*, page 50885.

LeVay, S. and Ferster, D. (1977). Relay Cell Classes in the Lateral Geniculate Nucleus of the Cat and the Effects of Visual Deprivation. *Journal of Comparative Neurology*, 172(4):563–584.

LeVay, S., Wiesel, T. N., and Hubel, D. H. (1980). The development of ocular dominance columns in normal and visually deprived monkeys. *Journal of Comparative Neurology*, 191(1):1–51.

Linden, D. C., Guillery, R. W., and Cucciaro, J. (1981). The dorsal lateral geniculate nucleus of the normal ferret and its postnatal development. *Journal of Comparative Neurology*, 203(2):189–211.

Linden, M. L. (2008). *LGN Activity Patterns during Ocular Dominance Plasticity in vivo*. PhD thesis, Massachusetts Institute of Technology.

Linden, M. L., Heynen, A. J., Haslinger, R. H., and Bear, M. F. (2009). Thalamic activity that drives visual cortical plasticity. *Nature Neuroscience*, 12(4):390–392.

Livingstone, M. S. and Hubel, D. H. (1981). Effects of sleep and arousal on the processing of visual information in the cat. *Nature*, 291(5816):554–561.

Lund, J. S. (1988). Anatomical organization of macaque monkey striate visual cortex. *Annual Review of Neuroscience*, 11:253–88.

Madisen, L., Zwingmann, T. A., Sunkin, S. M., Oh, S. W., Zariwala, H. a., Gu, H., Ng, L. L., Palmiter, R. D., Hawrylycz, M., Jones, A. R., Lein, E. S., and Zeng, H. (2010). A robust and high-throughput Cre reporting and characterization system for the whole mouse brain. *Nature Neuroscience*, 13(1):133–140.

Maffei, L. and Fiorentini, A. (1976). Monocular deprivation in kittens impairs the spatial resolution of geniculate neurones. *Nature*, 264(5588):754–55.

Mangel, S. C., Wilson, J. R., and Sherman, S. M. (1983). Development of neuronal response properties in the cat dorsal lateral geniculate nucleus during monocular deprivation. *Journal of Neurophysiology*, 50(1):240–64.

Mangini, N. and Pearlman, A. (1980). Laminar distribution of receptive field properties in the primary visual cortex of the mouse. *Journal of Comparative Neurology*, 193(1):203–222.

Mank, M., Santos, A., Direnberger, S., Mrsic-Flogel, T., Hofer, S., Stein, V., Hendel, T., Reiff, D., Levelt, C., Borst, A., and Others (2008). A genetically encoded calcium indicator for chronic in vivo two-photon imaging. *Nature Methods*, 5(9):805–811.

Markram, H., Toledo-Rodriguez, M., Wang, Y., Gupta, A., Silberberg, G., and Wu, C. (2004). Interneurons of the neocortical inhibitory system. *Nature Reviews Neuroscience*, 5(10):793–807.

Marrocco, R. T., McClurkin, J. W., and Young, R. A. (1982). Modulation of lateral geniculate nucleus cell responsiveness by visual activation of the corticogeniculate pathway. *Journal of Neuroscience*, 2(2):256–263.

Marshel, J. H., Garrett, M. E., Nauhaus, I., and Callaway, E. M. (2011). Functional Specialization of Seven Mouse Visual Cortical Areas. *Neuron*, 72(6):1040–1054.

Marshel, J. H., Kaye, A. P., Nauhaus, I., and Callaway, E. M. (2012). Anterior-posterior direction opponency in the superficial mouse lateral geniculate nucleus. *Neuron*, 76(4):713–20.

Martersteck, E. M., Hirokawa, K. E., Evarts, M., Zeng, H., Sanes, J. R., Harris, J. A., Martersteck, E. M., Hirokawa, K. E., Evarts, M., Bernard, A., Duan, X., Li, Y., Ng, L., Sanes, J. R., and Harris, J. A. (2017). Ganglion Cells Diverse Central Projection Patterns of Retinal Ganglion Cells. *CellReports*, 18(8):2058–2072.

Marvin, J. S., Borghuis, B. G., Tian, L., Cichon, J., Harnett, M. T., Akerboom, J., Gordus, A., Renninger, S. L., Chen, T.-W., Bargmann, C. I., Orger, M. B., Schreiter, E. R., Demb, J. B., Gan, W.-B., Hires, S. A., and Looger, L. L. (2013). An optimized fluorescent probe for visualizing glutamate neurotransmission. *Nature Methods*, 10(2):162–70.

Mataga, N., Mizuguchi, Y., and Hensch, T. K. (2004). Experience-dependent pruning of dendritic spines in visual cortex by tissue plasminogen activator. *Neuron*, 44(6):1031–41.

Matthies, U., Balog, J., and Lehmann, K. (2013). Temporally coherent visual stimuli boost ocular dominance plasticity. *Journal of Neuroscience*, 33(29):11774–8.

Mazurek, M., Kager, M., and Van Hooser, S. D. (2014). Robust quantification of orientation selectivity and direction selectivity. *Frontiers in Neural Circuits*, 8:1–17.

McCormick, D. A. and Bal, T. (1997). Sleep and Arousal: Thalamocortical Mechanisms. *Annual Review of Neuroscience*, 20(1):185–215.

Medini, P. (2011). Layer- and cell-type-specific subthreshold and suprathreshold effects of long-term monocular deprivation in rat visual cortex. *Journal of Neuroscience*, 31(47):17134–48.

Meister, M., Wong, R. L., Baylor, D. a., and Shatz, C. J. (1991). Synchronous Burst of Action Potentials in Ganglion Cells of the Developing Mammalian Retina. *Science*, 252(5008):939–943.

Métin, C., Godement, P., and Imbert, M. (1988). The primary visual cortex in the mouse: receptive field properties and functional organization. *Experimental Brain Research*, 69:476–482.

Mioche, L. and Singer, W. (1989). Chronic recordings from single sites of kitten striate cortex during experience-dependent modifications of receptive-field properties. *Journal of Neurophysiology*, 62(1):185–197.

Mitzdorf, U. and Neumann, G. (1980). Effects of monocular deprivation in the lateral geniculate nucleus of the cat: An analysis of evoked potentials. *Journal of Physiology*, 304:221–230.

Mooney, R., Penn, A. A., Gallego, R., and Shatz, C. J. (1996). Thalamic relay of spontaneous retinal activity prior to vision. *Neuron*, 17(5):863–874.

Moore, B. D., Kiley, C. W., Sun, C., and Usrey, W. M. (2011). Rapid plasticity of visual responses in the adult lateral geniculate nucleus. *Neuron*, 71(5):812–819.

Moore, R. Y. and Eichler, V. B. (1972). Loss of a circadian adrenal corticosterone rhythm following suprachiasmatic lesions in the rat. *Brain Research*, 42(1):201–206.

Morgan, J., Berger, D., Wetzel, A., and Lichtman, J. (2016). The Fuzzy Logic of Network Connectivity in Mouse Visual Thalamus. *Cell*, 165(1):192–206.

Morris, R. (1984). Developments of a water-maze procedure for studying spatial learning in the rat. *Journal of Neuroscience Methods*, 11(1):7336–7336.

Mower, G. D. (1991). The effect of dark rearing on the time course of the critical period in cat visual cortex. *Developmental Brain Research*, 58(2):151–158.

Mrsic-Flogel, T. D., Hofer, S. B., Creutzfeldt, C., Cloëz-Tayarani, I., Changeux, J.-P., Bonhoeffer, T., and Hübener, M. (2005). Altered map of visual space in the superior colliculus of mice lacking early retinal waves. *The Journal of Neuroscience*, 25(29):6921–6928.

Mrsic-Flogel, T. T. D., Hofer, S. S. B., Ohki, K., Reid, R. C., Bonhoeffer, T., Hubener, M., and Hübener, M. (2007). Homeostatic regulation of eye-specific responses in visual cortex during ocular dominance plasticity. *Neuron*, 54(6):961–972.

Niell, C. M. and Stryker, M. P. (2008). Highly selective receptive fields in mouse visual cortex. *Journal of Neuroscience*, 28(30):7520–36.

Niell, C. M. and Stryker, M. P. (2010). Modulation of visual responses by behavioral state in mouse visual cortex. *Neuron*, 65(4):472–9.

Nucci, C., Piccirilli, S., Rodinò, P., Nisticò, R., Grandinetti, M., Cerulli, L., Leist, M., Nicotera, P., and Bagetta, G. (2000). Apoptosis in the dorsal lateral geniculate nucleus after monocular deprivation involves glutamate signaling, NO production, and PARP activation. *Biochemical and Biophysical Research Communications*, 278(2):360–367.

Oberlaender, M., Ramirez, A., and Bruno, R. (2012). Sensory Experience Restructures Thalamocortical Axons during Adulthood. *Neuron*, 74(4):648–655.

Ohki, K., Chung, S., Ch, Y. H., Kara, P., and Reid, R. C. (2005). Functional imaging with cellular resolution reveals precise micro- architecture in visual cortex. *Nature*, 433(7026):597–603.

Oray, S., Majewska, A., and Sur, M. (2004). Dendritic spine dynamics are regulated by monocular deprivation and extracellular matrix degradation. *Neuron*, 44(6):1021–1030.

O'Rourke, M., Gasperini, R., and Young, K. M. (2014). Adult myelination: Wrapping up neuronal plasticity. *Neural Regeneration Research*, 9(13):1261–1264.

Pelli, D. G. (1997). The VideoToolbox software for visual psychophysics: transforming numbers into movies. *Spatial Vision*, 10(4):437–442.

Penn, A., Riquelme, P., Feller, M. B., and Shatz, C. J. (1998). Competition in Retinogeniculate Patterning Driven by Spontaneous Activity. *Science*, 279(5359):2108–2112.

Petreanu, L., Huber, D., Sobczyk, A., and Svoboda, K. (2007). Channelrhodopsin-2-assisted circuit mapping of long-range callosal projections. *Nature Neuroscience*, 10(5):663–8.

Petreanu, L., Mao, T., Sternson, S. M., and Svoboda, K. (2009). The subcellular organization of neocortical excitatory connections. *Nature*, 457(7233):1142–5.

Pfeiffenberger, C., Cutforth, T., Woods, G., Yamada, J., Rentería, R. C., Copenhagen, D. R., Flanagan, J. G., and Feldheim, D. A. (2005). Ephrin-As and neural activity are required for eye-specific patterning during retinogeniculate mapping. *Nature Neuroscience*, 8(8):1022–1027.

Pickard, G. E., Ralph, M. R., and Menaker, M. (1987). The intergeniculate leaflet partially mediates effects of light on circadian rhythms. *Neuroreport*, 5(16):2186–8.

Piscopo, D. M., El-Danaf, R. N., Huberman, a. D., and Niell, C. M. (2013). Diverse Visual Features Encoded in Mouse Lateral Geniculate Nucleus. *Journal of Neuroscience*, 33(11):4642–4656.

Pologruto, T. A., Sabatini, B. L., and Svoboda, K. (2003). ScanImage: flexible software for operating laser scanning microscopes. *Biomedical Engineering Online*, 2(1):13.

Prusky, G. T. and Douglas, R. M. (2003). Developmental plasticity of mouse visual acuity. *European Journal of Neuroscience*, 17(1):167–173.

Rafols, J. a. and Valverde, F. (1973). The structure of the dorsal lateral geniculate nucleus in the mouse. A Golgi and electron microscopic study. *Journal of Comparative Neurology*, 150(3):303–32.

Ranson, a., Cheetham, C. E. J., Fox, K., and Sengpiel, F. (2012). Homeostatic plasticity mechanisms are required for juvenile, but not adult, ocular dominance plasticity. *Proceedings of the National Academy of Sciences*, 2011:1–6.

Reese, B. E. (1988). Hidden lamination in the dorsal lateral geniculate nucleus : the functional organization of this thalamic region in the rat. *Brain Research*, 472(2):119–137.

Rittenhouse, C. D., Shouval, H. Z., Paradiso, M. a., and Bear, M. F. (1999). Monocular deprivation induces homosynaptic long-term depression in visual cortex. *Nature*, 397(6717):347–350.

Rochefort, N. L., Narushima, M., Grienberger, C., Marandi, N., Hill, D. N., and Konnerth, A. (2011). Development of direction selectivity in mouse cortical neurons. *Neuron*, 71(3):425–432.

Rompani, S. B., Müllner, F. E., Wanner, A., Zhang, C., Roth, C. N., Yonehara, K., and Roska, B. (2017). Different Modes of Visual Integration in the Lateral Geniculate Nucleus Revealed by Single-Cell-Initiated Transsynaptic Tracing. *Neuron*, 93(4):767–776.

Rose, T., Goltstein, P. M., Portugues, R., and Griesbeck, O. (2014). Putting a finishing touch on GECIs. *Frontiers in Molecular Neuroscience*, 7:88.

Rose, T., Jaepel, J., Hubener, M., and Bonhoeffer, T. (2016). Cell-specific restoration of stimulus preference after monocular deprivation in the visual cortex. *Science*, 352(6291):1319–1322.

Roth, M. M., Dahmen, J. C., Muir, D. R., Imhof, F., Martini, F. J., and Hofer, S. B. (2016). Thalamic nuclei convey diverse contextual information to layer 1 of visual cortex. *Nature Neuroscience*, 19(2):299–307.

Saiepour, M. H., Rajendran, R., Omrani, A., Ma, W. P., Tao, H. W., Heimel, J. A., and Levelt, C. N. (2015). Ocular dominance plasticity disrupts binocular inhibition-excitation matching in visual cortex. *Current Biology*, 25(6):713–721.

Sanes, J. R. and Masland, R. H. (2014). The Types of Retinal Ganglion Cells: Current Status and Implications for Neuronal Classification. *Annual Review of Neuroscience*, 38(1):150421150146009.

Sato, M. and Stryker, M. P. (2008). Distinctive features of adult ocular dominance plasticity. *The Journal of Neuroscience*, 28(41):10278–10286.

Sawtell, N., Frenkel, M., Philpot, B., Nakazawa, K., Tonegawa, S., and Bear, M. (2003). NMDA receptor-dependent ocular dominance plasticity in adult visual cortex. *Neuron*, 38(6):977–985.

Schuett, S., Bonhoeffer, T., and Hübener, M. (2002). Mapping retinotopic structure in mouse visual cortex with optical imaging. *Journal of Neuroscience*, 22(15):6549.

Shatz, C. and Stryker, M. (1978). Ocular dominance in layer IV of the cat's visual cortex and the effects of monocular deprivation. *Journal of Physiology*, 281(1):267–283.

Shatz, C. J. (1983). The prenatal development of the cat's retinogeniculate pathway. *Journal of Neuroscience*, 3(3):482–499.

Shatz, C. J., Lindström, S., and Wiesel, T. N. (1977). The distribution of afferents representing the right and left eyes in the cat's visual cortex. *Brain Research*, 131(1):103–116.

Sherk, H. (1979). A comparison of visual-response properties in cat's parabigeminal nucleus and superior colliculus. *Journal of Neurophysiology*, 42(6):1640–55.

Sherman, S. M. (2004). Interneurons and triadic circuitry of the thalamus. *Trends in Neurosciences*, 27(11):670–675.

Sherman, S. M. and Guillery, R. W. (1996). Functional organization of thalamocortical relays. *Journal of Neurophysiology*, 76(3):1367–1395.

Sherman, S. M. and Guillery, R. W. (1998). On the actions that one nerve cell can have on another: Distinguishing drivers from modulators. *Proceedings of the National Academy of Sciences*, 95(12):7121–7126.

Sherman, S. M., Hoffman, K.-P., and Stone, J. (1972). Loss of a Specific Cell Type From Dorsal Lateral Geniculate Nucleus in Visually Deprived Cats. *Journal of Neurophysiology*, 35(4):532–41.

Sherman, S. M. and Spear, P. D. (1982). Organization of visual pathways in normal and visually deprived cats. *Physiological Reviews*, 62(2):738–855.

Sherman, S. M. and Stone, J. (1973). Physiological normality of the retina in visually deprived cats. *Brain Research*, 60(1):224–230.

Sillito, A. M., Cudeiro, J., and Jones, H. E. (2006). Always returning: feedback and sensory processing in visual cortex and thalamus. *Trends in Neurosciences*, 29(6):307–316.

Sillito, A. M., Jones, H. E., Gerstein, G. L., and West, D. C. (1994). Feature-linked synchronization of thalamic relay cell firing induced by feedback from the visual cortex. *Nature*, 369(6480):479–482.

Sinex, D. G., Burdette, L. J., and Pearlman, A. L. (1979). A psychophysical investigation of spatial vision in the normal and reeler mutant mouse. *Vision Research*, 19(8):853–857.

Smith, G. B., Heynen, A. J., and Bear, M. F. (2009). Bidirectional synaptic mechanisms of ocular dominance plasticity in visual cortex. *Philosophical Transactions of the Royal Society Series B: Biological Sciences*, 364(1515):357.

Southwell, D. G., Froemke, R. C., Alvarez-Buylla, A., Stryker, M. P., and Gandhi, S. P. (2010). Cortical plasticity induced by inhibitory neuron transplantation. *Science*, 327(5969):1145–8.

Spear, P. D., Mccall, M. A., and Tumosa, N. (1989). W-and Y-cells in the C layers of the cat's lateral geniculate nucleus: normal properties and effects of monocular deprivation. *Journal of Neurophysiology*, 61(1):58–73.

Sretavan, D. W. and Shatz, C. J. (1986). Prenatal development of cat retinogeniculate axon arbors in the absence of binocular interactions. *Journal of Neuroscience*, 6(4):990–1003.

Stephany, C.-E., Ikrar, T., Nguyen, C., Xu, X., and McGee, A. W. (2016). Nogo Receptor 1 Confines a Disinhibitory Microcircuit to the Critical Period in Visual Cortex. *Journal of Neuroscience*, 36(43):11006–11012.

Stodieck, S. K., Greifzu, F., Goetze, B., Schmidt, K. F., and Löwel, S. (2014). Brief dark exposure restored ocular dominance plasticity in aging mice and after a cortical stroke. *Experimental Gerontology*, 60:1–11.

Stosiek, C., Garaschuk, O., Holthoff, K., and Konnerth, A. (2003). In vivo two-photon calcium imaging of neuronal networks. *Proceedings of the National Academy of Sciences*, 100(12):7319–7324.

Sun, W., Tan, Z., Mensh, B. D., and Ji, N. (2016a). Thalamus provides layer 4 of primary visual cortex with orientation- and direction-tuned inputs. *Nature Neuroscience*, 19(2):308–15.

Sun, Y., Ikrar, T., Davis, M. F., Holmes, T. C., Gandhi, S. P., Xu, X., Holmes, T. C., Gandhi, S. P., and Xu, X. (2016b). Neuregulin-1/ErbB4 Signialing Regulates Visual Cortical Plasticity. *Neuron*, 92(1):160–173.

Sur, M., Humphrey, a. L., and Sherman, S. M. (1982). Monocular deprivation affects X- and Y-cell retinogeniculate terminations in cats. *Nature*, 300(5888):183–185.

Sur, M., Weller, R. E., and Sherman, S. M. (1984). Development of X- and Y-cell retinogeniculate terminations in kitten. *Nature*, 310(5974):246–249.

Svoboda, K., Denk, W., Kleinfeld, D., and Tank, D. W. (1997). In vivo dendritic calcium dynamics in neocortical pyramidal neurons. *Nature*, 385(6612):161–65.

Swadlow, H. A. (1983). Efferent systems of primary visual cortex: a review of structure and function. *Brain Research*, 287(1):1–24.

Swindale, N. V., Matsubara, J. A., and Cynader, M. S. (1987). Surface organization of orientation and direction selectivity in cat area 18. *Journal of Neuroscience*, 7(5):1414–1427.

Tagawa, Y., Kanold, P. P. O., Majdan, M., and Shatz, C. J. C. (2005). Multiple periods of functional ocular dominance plasticity in mouse visual cortex. *Nature Neuroscience*, 8(3):380–388.

Tailby, C., Cheong, S. K., Pietersen, a. N., Solomon, S. G., and Martin, P. R. (2012). Colour and pattern selectivity of receptive fields in superior colliculus of marmoset monkeys. *Journal of Physiology*, 590(16):4061–4077.

Thestrup, T., Litzlbauer, J., Bartholomäus, I., Mues, M., Russo, L., Dana, H., Kovalchuk, Y., Liang, Y., Kalamakis, G., Laukat, Y., Becker, S., Witte, G., Geiger, A., Allen, T., Rome, L. C., Chen, T.-W., Kim, D. S., Garaschuk, O., Griesinger, C., and Griesbeck, O. (2014). Optimized ratiometric calcium sensors for functional in vivo imaging of neurons and T lymphocytes. *Nature Methods*, 11(2):175–82.

Thompson, A. D., Picard, N., Min, L., Fagiolini, M., and Chen, C. (2016). Cortical Feedback Regulates Feedforward Retinogeniculate Refinement. *Neuron*, 91(5):1021–1033.

Thomson, A. M., West, D. C., Wang, Y., and Bannister, A. P. (2002). Synaptic connections and small circuits involving excitatory and inhibitory neurons in layers 2-5 of adult rat and cat neocortex: triple intracellular recordings and biocytin labelling in vitro. *Cerebral Cortex*, 12(9):936–953.

Tian, L., Hires, S. A., Mao, T., Huber, D., Chiappe, M. E., Chalasani, S. H. S., Petreanu, L., Akerboom, J., McKinney, S. a., Schreiter, E. R. E., Others, Bargmann, C. I., Jayaraman, V., Svoboda, K., and Looger, L. L. (2009). Imaging neural activity in worms, flies and mice with improved GCaMP calcium indicators. *Nature Methods*, 6(12):875–881.

Tieman, S. B. (1984). Effects of monocular deprivation on geniculocortical synapses in the cat. *The Journal of comparative neurology*, 222(2):166–176.

Tigges, M. and Tigges, J. (1970). The retinofugal fibers and their terminal nuclei in Galago crassicaudatus (primates). *Journal of Comparative Neurology*, 138(1):87–101.

Tsumoto, T. and Suda, K. (1981). Effects of Early Monocular Deprivation on Development of Cortico-geniculate Projections in the Cat. *Experimental Brain Research*, 43(3-4):451–454.

Vastola, E. F. (1967). Steady-State on Effects of Visual Cortex on Geniculate Cells. *Vision Research*, 7(7):599–609.

Vetencourt, J. F. M., Sale, A., Viegi, A., Baroncelli, L., Pasquale, R. D., O' Leary, O. F., Castrén, E., and Maffei, L. (2008). The antidepressant fluoxetine restores plasticity in the adult visual cortex. *Science*, 320(5874):385–388.

Volland, S., Esteve-rudd, J., Hoo, J., Yee, C., and Williams, D. S. (2015). A Comparison of Some Organizational Characteristics of the Mouse Central Retina and the Human Macula. *PLoS ONE*, 10(4):e0125631.

Wagner, E., McCaffery, P., and Dräger, U. C. (2000). Retinoic acid in the formation of the dorsoventral retina and its central projections. *Developmental Biology*, 222(2):460–70.

Wallace, D. J., Fitzpatrick, D., and Kerr, J. N. (2016). Primate Thalamus: More Than Meets an Eye. *Current Biology*, 26(2):R60–R61.

Wang, L., Fontanini, a., and Maffei, a. (2012). Experience-Dependent Switch in Sign and Mechanisms for Plasticity in Layer 4 of Primary Visual Cortex. *Journal of Neuroscience*, 32(31):10562–10573.

Wang, Q. and Burkhalter, A. (2007). Area Map of Mouse Visual Cortex. *Journal of Comparative Neurology*, 502(3):339–357.

Weyand, T. G., Boudreaux, M., and Guido, W. (2001). Burst and Tonic Response Modes in Thalamic Neurons During Sleep and Wakefulness. *Journal of Neurophysiology*, 85(3):1107–1118.

Wiesel, T. and Hubel, D. (1965). Comparision of the effects of unilateral and bilateral eye closure on cortical unit responses in kittens. *Journal of Neurophysiology*, 28(6):1029 – 1040.

Wiesel, T. N. (1968). Receptive Fields and Functional Architecture. *Journal of Physiology*, 195(1):215–243.

Wiesel, T. N. and Hubel, D. H. (1963a). Effects of visual deprivation on morphology and physiology of cells in the cat's lateral geniculate body. *Journal of Neurophysiology*, 26:978–93.

Wiesel, T. N. and Hubel, D. H. (1963b). Single-cell responses in striate cortex of kittens deprived of vision in one eye. *Journal of Neurophysiology*, 26:1003–1017.

Wiesel, T. N., Hubel, D. H., and Lam, D. M. K. (1974). Autoradiographic demonstration of ocular-dominance columns in the monkey striate cortex by means of transneuronal transport. *Brain Research*, 79(2):273–279.

Wiesenfeld, Z. and Kornel, E. E. (1975). Receptive fields of single cells in the visual cortex of the hooded rat. *Brain Research*, 94(3):401–412.

Williams, S. E., Mann, F., Erskine, L., Sakurai, T., Wei, S., Rossi, D. J., Gale, N. W., Holt, C. E., Mason, C. A., and Henkemeyer, M. (2003). Ephrin-B2 and EphB1 mediate retinal axon divergence at the optic chiasm. *Neuron*, 39(6):919–935.

Wilson, J. R. and Sherman, S. M. (1976). Receptive-field characteristics of neurons in cat striate cortex: Changes with visual field eccentricity. *Journal of Neurophysiology*, 39(3):512–33.

Wimmer, V. C., Broser, P. J., Kuner, T., and Bruno, R. M. (2010). Experience-induced plasticity of thalamocortical axons in both juveniles and adults. *Journal of Comparative Neurology*, 518(22):4629–4648.

Yazaki-Sugiyama, Y., Kang, S., Câteau, H., Fukai, T., and Hensch, T. K. (2009). Bidirectional plasticity in fast-spiking GABA circuits by visual experience. *Nature*, 462(7270):218–221.

Yu, X., Chung, S., Chen, D.-Y. Y., Wang, S., Dodd, S. J., Walters, J. R., Isaac, J. T. R., and Koretsky, A. P. (2012). Thalamocortical Inputs Show Post-Critical-Period Plasticity. *Neuron*, 74(4):731–742.

Yuste, R. and Denk, W. (1995). Dendritic spines as basic functional units of neuronal integration. *Nature*, 375(6533):682–84.

Zeater, N., Cheong, S. K., Solomon, S. G., Dreher, B., Martin, P. R., Zeater, N., Cheong, S. K., Solomon, S. G., Dreher, B., and Martin, P. R. (2015). Binocular Visual Responses in the Primate Lateral Geniculate Nucleus. *Current Biology*, 25(24):3190–3195.

Zhao, X., Chen, H., Liu, X., and Cang, J. (2013). Orientation-selective responses in the mouse lateral geniculate nucleus. *Journal of Neuroscience*, 33(31):12751–63.

Ziburkus, J. and Guido, W. (2006). Loss of Binocular Responses and Reduced Retinal Convergence During the Period of Retinogeniculate Axon Segregation. *Journal of Neurophysiology*, 96(5):2775–2784.

Acknowledgements

First of all, I would like to thank *Tobias Rose*, for his supervision of my thesis work, especially for all the time he took in the beginning to introduce me to two-photon microscopy and later for data analysis. With his great enthusiasm for science and his knowledge, he always provided good advice and discussions.

I am very grateful to *Tobias Bonhoeffer and Mark Hübener*, for giving me the opportunity to carry out my thesis in this lab, their helpful advice both during the development of the project and the preparation of the paper manuscript, and for making it possible for me to attend several conferences in the last years.

I am thankful to *Thomas Misgeld* for being a helpful member of my thesis advisor committee and to the members of my PhD thesis commitee, *Mark Hübener, Laura Busse, Rainer Uhl, Wolfgang Enard, Heinrich Jung and Benedikt Grothe*, for taking the time to evaluate my PhD thesis.

I thank *Volker Staiger, Max Sperling, Frank Voss, Claudia Huber and Helena Tultschin*, for their technical assistance, especially with histology and genotyping. Thanks to *Johanna Sigl-Glöckner*, who helped a lot with histology and with testing different functional indicators. I would like to thank *Pieter Goltstein* for sharing his MRP and code for analysis of retinotopic stimuli. Many thanks also to *Volker Staiger, Marcus Knopp, Onur Gökçe, Veronika Bednarova and diverse interns* for not only sharing an office with me, but also their refreshing conversations. I also want to thank *Volker Staiger, Mike Myoga and Joel Bauer*, for partly reading my thesis and providing useful comments.

For support, training and funding of conferences I thank the *IMPRS and its coordination team*. I am very thankful to *Boehringer Ingelheim Fonds* for two years of monetary and continued personal support. Thank you for all the special training, especially the funding of my participation in TENSS, and for the opportunity of meeting so many great scientists.

Special thanks goes to *all current and past members of the lab and the Grothe MPI "mini-group"* for advice, discussions, coffee breaks, support and enjoyable lunch times. But most of all for the experiences we shared in the last years: barbecues, climbing/gym times, the skiing weekend, parties, our special happy hours, brunch times and weekly TV evenings.

I would like to thank all my friends, far and close, who made the past years so much more enjoyable, especially in difficult times; all the knights of the order of the π, especially *Franziska, Kathy and Gertje*, who I can always count on to support me or to heighten my mood; all members of the *JGW-Schülerakademie-Team* and the various academies that I was part of, which was very rewarding throughout the years especially my interaction with all *'my' students*; and *Caro*.

Last, but not least, I am deeply grateful to my family: my parents, *Heike and Mario*, my sister, *Annalena*, and my brother, *Maximilian*. They always greatly support me throughout all ups and downs and give me the freedom to pursue my goals.

Curriculum vitae

Juliane Jäpel-Schael

Nationality	German
Lab Address	Max Planck Institute of Neurobiology
	Department: Synapses – Circuits – Behavior
	Am Klopferspitz 18, 82152 Martinsried, Germany
Lab Phone	+49 89 8578 3682
E-mail	jjaepel@neuro.mpg.de

Higher Education

Since Sept 2011	*PhD candidate*, Max Planck Institute of Neurobiology, Germany Thesis: Experience-dependent functional plasticity of eye-specific thalamocortical axons, Supervisor: Dr. Mark Hübener
Oct 2009 – May 2011	*Master of Biomedicine*, Julius Maximilians University of Würzburg Research project (9 months): Changes in neuronal Ca^{2+} homeostasis leading to Ca^{2+} induced ER stress response Institute of Clinical Neurobiology, Würzburg, Germany, Supervisor: Dr. Robert Blum
Oct 2006 – July 2009	*Bachelor of Biomedicine*, Julius Maximilians University of Würzburg Research project (3 months): Interaction of Mena and Spectrin in the mammalian heart Department of Physiology I, Würzburg, Germany, Supervisor: Prof. Kai Schuh

Additional Research Experience

May 2011 – Aug 2011	*Institute of Clinical Neurobiology*, Würzburg, Germany Student research assistant, Supervisor: Dr. Robert Blum
Apr 2010 – July 2010	*Bayer HealthCare*, Richmond, CA, USA Intern in the area of Immunology with focus on Multiple Sclerosis, Supervisor: Dr. Edward Croze
Feb 2010 – Apr 2010	*German Cancer Research Center*, Heidelberg, Germany Intern in the area of signaling and functional genomics, Supervisor: Prof. Michael Boutros

Publications

Rose, T., **Jaepel, J.**, Hübener, M., Bonhoeffer, T. (2016) Cell-specific restoration of stimulus preference after monocular deprivation in the visual cortex. Science 352 (6291) 1319-22

Samtleben, S., **Jaepel, J.**, Fecher C., Andreska T., Rehberg M., Blum R. (2013) Direct imaging of ER calcium with targeted-esterase induced dye loading (TED). J Vis Exp 7 (75)

Jaepel, J., Blum, R. (2011) Capturing ER Calcium dynamics. Eur J Cell Biol 90 (8) 613-9

Fellowships and Awards

Aug 2012 – July 2014	Two-years PhD Fellowship, Boehringer Ingelheim Fonds
June 2012	Travel Grant of Boehringer Ingelheim Fonds
Since 2011	Fellowship of the International Max Planck Research School for Molecular and Cellular Life Sciences
Feb 2007 – May 2011	Undergraduate Fellowship, German National Academic Merit Foundation
May 2006	Special prize of the UNESCO, Federal Competition "Jugend forscht"

Conferences Attended (selected)

March 22-25, 2017	12th Meeting of the German Neuroscience Society, Göttingen (Germany), Talk
July 1-6, 2016	FENS 10th Forum of Neuroscience, Copenhagen (Denmark), Poster
Oct 17-21, 2015	Neuroscience 2015, Chicago (USA), Poster
Sept 20-23, 2015	1st European Conference on Axon Guidance, Circuit Development and Regeneration, Vienna (Austria), Poster and Flash Talk
Aug 30 – Sept 2, 2015	5th European Visual Cortex Meeting, Seeon (Germany), Poster
June 28 – July 2, 2015	7th LMU-Harvard Young Scientist's Forum, Munich (Germany), Poster

Summer courses for high-school students

33 h – 38 h courses for 15-16 students given by two instructors: Course design, material preparation, lectures, student advisement

Aug 2015	Neurobiology of vision
Aug 2012	Neurological deficits
Aug 2011	Learning and memory

Workshops and Training Events

Method learning	Transylvanian Experimental Neuroscience Summer School, June 2012, 2 weeks Scientific Image Processing and Analysis, 2.5 days International Science and Engineering Camp 2006, Pohang, South Korea, 10 days
Lab management	Time and project management, 2 days
Scientific soft skills	Getting funded: Writing an Individual Fellowship Application, 2.5 days Scientific Writing, 3 days Scientific Communication Seminar, 3.5 days